ZnO nanowires for solar cells: a comprehensive review

Vincent Consonni, Joe Briscoe, Erki Kärber, Xuan Li, Thomas Cossuet

ZnO nanowires for solar cells: A comprehensive review

Vincent Consonni,[1*] Joe Briscoe,[2] E. Kärber,[3] Xuan Li,[2] Thomas Cossuet[1]

[1] Univ. Grenoble Alpes, CNRS, Grenoble INP, LMGP, F-38000 Grenoble, France

[2] School of Engineering and Materials Science and Materials Research Institute, Queen Mary University of London, Mile End Road, London, UK

[3] Laboratory of Thin Film Chemical Technologies, Department of Materials and Environmental Technology, Tallinn University of Technology, Ehitajate tee 5, Tallinn 19086, Estonia

Corresponding author:

E-mail : *vincent.consonni@grenoble-inp.fr*

Abstract

As an abundant and non-toxic wide band gap semiconductor with a high electron mobility, ZnO in the form of nanowires has emerged as an important electron transporting material in a vast number of nanostructured solar cells. ZnO nanowires are grown by low-cost chemical deposition techniques and their integration into solar cells presents, in principle, significant advantages including efficient optical absorption through light trapping phenomena and enhanced charge carrier separation and collection. However, they also raise some significant issues related to the control of the interface properties and to the technological integration. The present review is intended to report a detailed analysis of the state-of-the-art of all types of nanostructured solar cells integrating ZnO nanowires, including extremely thin absorber solar cells, quantum dot solar cells, dye-sensitized solar cells, organic and hybrid solar cells, as well as halide perovskite-based solar cells.

Keywords: ZnO nanowires, solar cells, extremely thin absorbers, quantum dots, polymers, chemical dyes, halide perovskites

1. Introduction

Zinc oxide (ZnO) has attracted much attention over the last two decades owing to its abundance, biocompatibility, and relative ease to grow it as nanostructures by a wide variety of deposition techniques [1] [2]. Owing to its highly anisotropic wurtzite structure, vertically aligned ZnO nanowires (NWs) can be formed within the self-induced and selective area growth approaches and act as building blocks in a wide variety of applications [3] [4]. As an n-type compound semiconductor with a wide band gap energy of 3.37 eV at room temperature and a high electron mobility, the integration of ZnO NWs as an electron transporting material (ETM) into a large number of photovoltaic (PV) cells is highly relevant [5] [6]. In all of these PV cells, a light absorber layer in the visible part of the electromagnetic spectrum is sandwiched between an ETM and a hole transporting material (HTM), which are in contact with a transparent electrode and a metallic electrode, respectively. The principle of this type of PV cells is the following: the visible photons, crossing the ETM / transparent electrode / glass substrate, are absorbed by the light absorber layer, in which electron-hole pairs are photo-generated. These charge carriers are subsequently separated as a result of type II band alignments on both ends, between the ETM and light absorber layer as well as the light absorber layer and HTM. Electrons propagate through the ETM and are collected by the front transparent electrode while holes propagate through the HTM and are collected by the back metallic electrode.

Basically, the ETM needs to be able to admit the electrons before Shockley-Read-Hall or interfacial recombination and trapping occur in the light absorber layer. Its introduction in the PV cell should not compromise the optimal electric continuity either. It also needs to be relatively transparent to allow the visible photons going through to the light absorber layer, capable of forming type II heterojunctions (*i.e.* of ensuring charge collection), capable of charge transport, and preferably low cost. The n-type ETM used during early stage research on these PV cells was mainly focused on anatase-TiO_2 owing to its non-toxicity, high stability, inexpensive manufacture, and wide band gap energy (*i.e.* 3.0-3.2 eV) [7]. Later, ZnO was brought into attention as an alternative for TiO_2. The main motivations behind this substitution were related to i) its ease to grow it as nanostructures with different shapes and sizes using low-temperature chemical synthesis [8] [4], ii) the related simpler, low-cost and low energy input manufacturing process, iii) the superior charge collection properties resulting from the oriented one-dimensional nanostructures such as vertically aligned NWs, iv) its higher electron mobility than TiO_2 (*i.e.* 200 cm^2/Vs for bulk ZnO and 1000 cm^2/Vs for single NW [1] as compared to 10 cm^2/Vs for TiO_2 [9]), v) its ease of coating the light absorber layer within the structure, as the precursor for the absorber layer can readily reach the

entire surface, which opens up innovative design of potential structures, and vi) the ability to tune the optical scattering regimes based on the ZnO NW size and aspect ratio (as compared to TiO_2). Many investigations have thus been reported concerning the use of ZnO NWs as the ETM, which plays an important role in extremely thin absorber solar cells (ETASCs) [10], quantum dot solar cells (QDSCs) [11], organic solar cells (OSCs) and hybrid solar cells (HSCs) [12], dye-sensitized solar cells (DSSCs) [13], and halide perovskite-based solar cells (HPSCs) in achieving high-efficiency photovoltaic (PV) cells. However, there is still limited data of the exact comparison of ZnO or TiO_2 as ETM on the performances of similar material systems.

In all of these PV cells, the architecture involving ZnO NW heterostructures is of radial type and involves either the core-shell or fully-impregnated configurations. In the core-shell configuration as presented in figure 1(a), the ZnO NW heterostructures consist of n-type ZnO NWs as a core, which are coated by a thin optical absorber shell in the visible part of the electromagnetic spectrum. The present core-shell NW heterostructures benefit from several valuable assets, such as efficient light trapping phenomena and charge carrier management. The light absorption is governed by specific optical modes while the separation of the charge carriers occurs over the short radial distance. The present core-shell configuration is involved in the so-called ETASCs (*i.e.* the absorber is an inorganic semiconductor) [14], quantum dot-sensitized solar cells (QDSSCs) (*i.e.* the absorber is a semiconducting quantum dot) [15], and DSSCs (*i.e.* the absorber is a chemical dye) [16] [17]. In contrast, in the fully-impregnated configuration as presented in figure 1(b), the ZnO NW heterostructures consist of n-type ZnO NWs, which are fully impregnated with a relatively thick optical absorber layer that also plays very often the role of the HTM. The present fully-impregnated configuration is involved in the so-called bulk heterojunction quantum dot solar cells (BHQDSCs) (*i.e.* the absorber is a quantum dot) [18] [19], inverted OSCs (*i*OSCs) (*i.e.* the absorber is a blend of organic semiconductors) [20], HSCs (*i.e.* the absorber is a single organic semiconductor) [20], and HPSCs (*i.e.* the absorber is a halide perovskite) [21]. In many optimized PV cells using both configurations, it should be noted that additional layers are introduced to enhance the properties at the different interfaces. Furthermore, depending on the number of light absorber materials in the stack, the active interfaces for charge carrier separation involve the ZnO NWs or not. Eventually, the performances of the solar cells integrating ZnO NWs are, to some extent, affected by the nature and density of intrinsic and extrinsic defects in their center and on their surfaces, such as oxygen and zinc vacancies, zinc interstitials or hydrogen related defects to name a few. The vast issue of the defects in ZnO

and its NW counterpart is beyond the scope of the present review article and one should refer to the following articles in Refs. [22] [23] [24] [25].

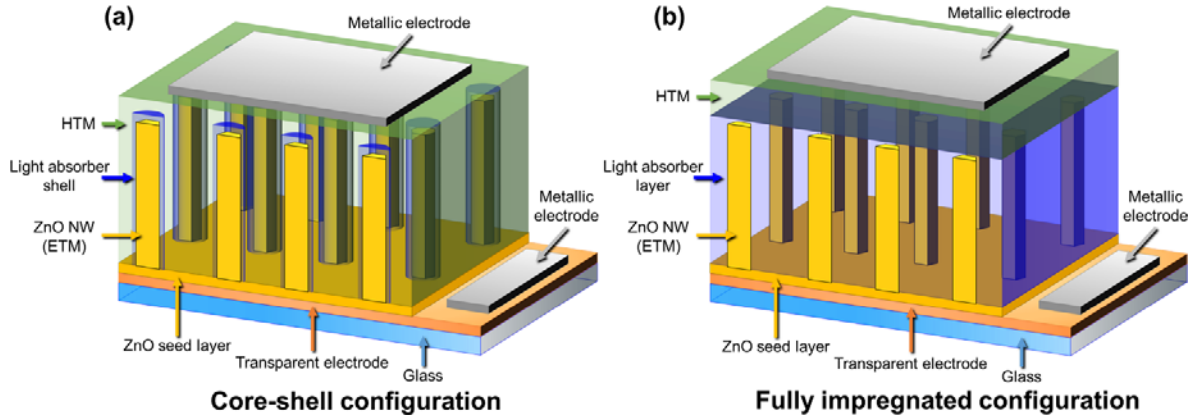

Figure 1. Schematic of the two typical configurations used for integrating ZnO NWs into solar cells. (a) Core-shell configuration as used in ETASCs, QDSSCs, and DSSCs. (b) Fully-impregnated configuration as used in BHQDSCs, *i*OSCs, HSCs, and HPSCs.

2. Extremely thin absorber solar cells

Background of extremely thin absorber solar cells

A patent released in 1978 entitled “solar cell comprising semiconductive whiskers” describes a solar cell design and its benefits which are achieved through using long vertical single crystal semiconductor arrays [26], resembling the ETASC design and rationale. In an ETASC, which is principally an all-solid-state sensitized solar cell, the optimum light absorber shell thickness may be around 10-200 nm, depending on the available gap size in the ZnO NW array and the quality of the absorber itself [27] [28] [29] [30] [31]. A thicker light absorber shell is preferred for added photon absorption; however, the performance is restrained on the thicker side by limited charge carrier transport properties in the absorber. The thickness of the whole ETASC is determined by the optimized length of ZnO NWs, which, in turn, is mostly a function of the capacity of the deposition techniques to allow the infiltration of the absorber and HTM into the dense forest of slim NWs. As a rule of thumb, an increase by a factor of x in the specific surface area of the substrate should allow the use of a thinner absorber by a factor of x, or more, while preserving the crucial volume for a complete light absorption [32]. In other words, as one sophisticated form of light trapping, the introduction of ZnO NWs leads to the increase in the internal reflections that, in turn, leads to an increase in the optical path length of the incident photons, and by that, to a rise of the probability of photon absorption in the absorber shell. However, this results in the likely sacrifice related to losses that may come along

owing to a larger interface area and a higher dark current. Remedies for suppressing surface recombination on the ZnO NW surfaces, but also for eliminating short circuits due to exposed electrode underneath the ETM, have been discussed through means such as compact oxide layers for surface passivation, insulating blocking layers, or sulfidic buffer layers [27] [32] [33]. There is still much debate along this line. Among other considerations, any chemical incompatibility for sequential deposition schemes may demand for an intermediate chemical blocking layer.

A thinner light absorber shell would allow to shorten the charge carrier transport length and by that to reduce the timescale before the charger carriers reach their respective electrodes. Theoretically, the ZnO NWs should be long enough to introduce a zero optical transmittance when coated with a light absorber shell. Notably, in the early patent from 1978, the single crystalline semiconductive whiskers are proposed to be up to several hundred micrometers long [26]. Uniform in thickness, it is also must for the light absorber shell to have continuous coverage on the ZnO NWs on the one hand, and, in turn, a continuous coverage by a HTM, on the other hand. In case the ZnO NWs are too narrowly spaced, the light absorber shell, if not the HTM as well, may have difficulties in penetrating the pores of the ZnO NWs. A number of suitable methods for infiltration of nanostructures have been identified including sol-gel, chemical spray pyrolysis (CSP), chemical bath deposition (CBD), ion-layer gas reaction (ILGAR), successive ionic layer adsorption and reaction (SILAR), solution casting, electrodeposition, and atomic layer deposition (ALD) [32]. Cost does matter as the criteria for qualification, as the ETASC rationale largely stems from the fact that lower quality semiconductors by inexpensive methods could be utilized [27] [10]. The use of longer ZnO NWs is especially useful to support absorption of photons, for which a lower absorption coefficient occurs in the particular absorber shell, and thus longer-wavelengths are targeted to be enhanced primarily as reported in a study with 0.5, 1.0, and 1.7 μm long ZnO NWs with a 100 nm diameter used, with some losses in the open-circuit voltage (V_{OC}) attributed to surface recombination [34]. However, as a key finding, by increasing the diameter of ZnO NWs from 105 to 330 nm while keeping their length similar as 1.5 μm, the short-circuit current density (J_{SC}), V_{OC}, and the resulting photo-conversion efficiency (PCE) are all increased [34]. For 20-110 nm-thick light absorber shells used, the thicknesses over 30 nm led to the deterioration of the J_{SC} primarily, with some accompanied losses in the V_{OC}, thus indicating the range of the diffusion lengths of the photo-generated carriers produced for the particular absorber used (*i.e.* CdSe) [34]. Absorber shell thicknesses lower than 30 nm, as an average estimate, resulted in a loss of V_{OC} attributed to tunneling recombination [34].

The earliest work in 2004 on modelling inorganic ETASCs based on p-i-n junction roughly predicted a PCE up to 15% for CdTe and $CuInS_2$ absorbers, without focusing on a special morphology in their calculations but rather on the nominal minority carrier diffusion length as shown in figure 2(a) [35]. Specifically for a ZnO NW based-ETASC, modelling and measurements *via* cell impedance has been explored by Bisquert *et al.* [36]. More recently, the effect of the geometrical dimensions on the light trapping phenomena in the ZnO NWs has been investigated, and the optimum diameter, length, NW to NW distance (*i.e.* period) and shell thicknesses, have been calculated by J. Michallon *et al.* following numerical simulations by rigorous coupled wave analysis of an ETASC with the focus on a CdTe shell, as seen in figure 2(b) [37] [38]. It was shown that optically radiated and guided modes are responsible for the large part of the absorption of the ETASC (see figure 2(c)), while Fabry-Perot resonances contribute to a negligible part [37]. The properties of the optically radiated modes are mostly dependent upon the NW to NW distance (*i.e.* period), while that of the optically guided modes depend on the NW diameter [38]. It is not trivial to precisely predict the highest PCE that limits any ETASCs due to the complexity and variance of the materials and morphologies involved. The effect of the limits that are set by Shockley-Read-Hall recombination and interfacial recombination, and the effect of the reduced electric field magnitude as a function of the length scale of the nanostructured p-n junction has been published [39]. A wider view on the ultimate limits of nanostructured solar cells has been explored, considering the presumption that nanostructures may carry unique properties that may reduce the entropy losses which are considered irredeemable for planar cells, and may ultimately allow to surpass the Shockley-Queisser limit which sets the highest PCE for single-bandgap planar solar cells [40].

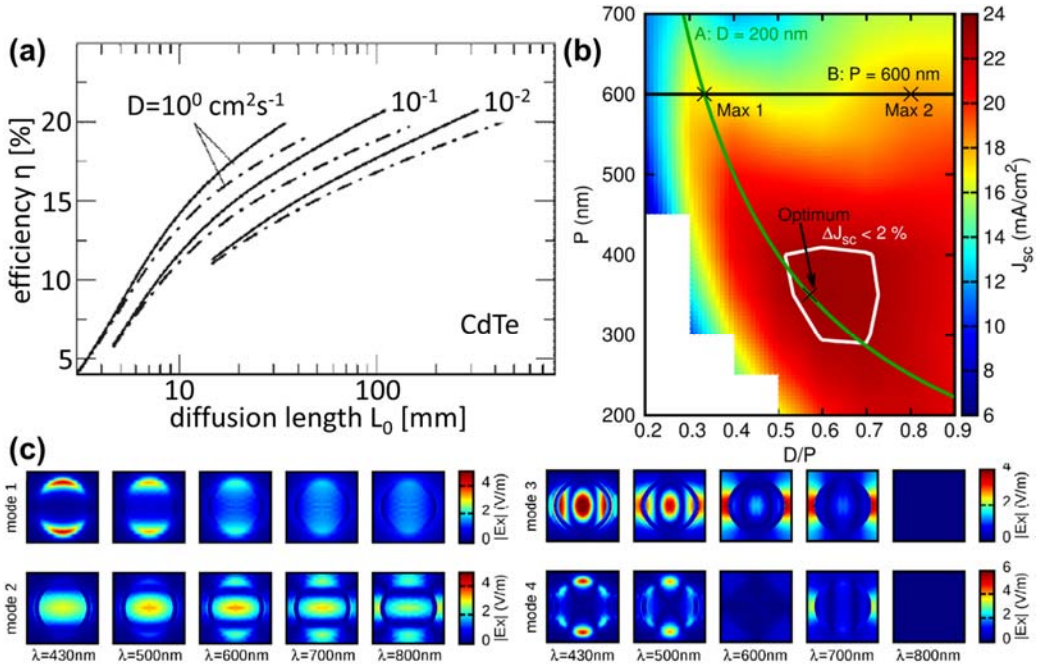

Figure 2. (a) Theoretical efficiency limit η for the ZnO NW/CdTe ETASC as a function of the nominal minority carrier diffusion length (L_0). The solid lines correspond to the case of an ideal light-trapping and no surface recombination, the dashed lines correspond to a surface recombination velocity of 10^7 cm/s. Reprinted with permission from [35]. Copyright 2004 Wiley & Sons. (b) Simulated ideal J_{SC} map for a ZnO NW/CdTe ETASC as a function of the ZnO NW period (P) and diameter over period ratio (D/P). (c) Corresponding maps of the modulus of the electric field (E_x) for the key optically guided modes corresponding to the geometrical dimensions with D = 480 nm and P = 600 nm, and represented for various wavelengths. Reprinted with permission from [37]. Copyright 2014 Optical Society of America.

In 2006, some of the main challenges with the ETASCs were articulated as follows [32]: interfacial recombinations, poor infiltration of the HTM and thus the lack of the intimate contact with the light absorber shell, low charge carrier mobility in the HTM, and tunneling-enhanced recombination at extremely low light absorber shell thicknesses. The efficiency of charge carrier separation seems to be the overarching point of concern for ETASCs. The magnitude of electron mobility in the ZnO NWs is less of a concern than hole mobility in the HTM [41].

Finally, one should keep in mind that, with the breath of investigations, scope of materials and a range of morphologies, the classification and labelling of the cells may vary slightly. A detailed chronological review describes the earliest of ETA solar cells attempts [10]. A selection of light absorber shells used to cover ZnO NWs is indicated in Table 1. The method for the absorber shell growth is indicated in Table 1, as both its excellent penetration and uniform coverage in the pores of the ZnO NWs is highly desired. The exact numbers in Table 1 are not normalized, per se, since record cells reported at the standard AM1.5 illumination conditions may still vary by area, but also, results are expected to be reported at various stages of cell development. The general trend is that

higher PCEs can be obtained from smaller areas, though linear correlation should not be assumed by default. Moreover, as the technology and thus the length/diameter/spacing/quality of the ZnO NWs vary, it may be difficult, if not impossible, to compare the results of PV studies based on criteria other than "feasibility and practicality" of the techniques used. The intrinsic stoichiometry of the ZnO NWs, and the resulting charge carrier concentration may vary as the deposition is made by a broad range of techniques under different conditions, including CBD [42] [43] [44] [45], electrodeposition [14] [46] [47], and CSP [48]. Thus, Table 1 mostly serves to inform about the scope of absorbing materials utilized on a ZnO NW core-shell heterostructure. An intrinsic parameter such as V_{OC} may mostly be assumed scale-invariant. The choice of the HTM have been CuSCN [36] [31] [14] [46], Cu_2O [49], among inorganic materials, and P3HT [50], spiro-MeOTAD [51], among organic ones, to bring a few examples for ZnO NW-based ETASCs. There are a number of studies that report successful deposition of light absorber shells on a ZnO NW array without demonstrating the performance of a completed ETASC. For the sake of brevity, these studies have been omitted, and generally also those that have reported solar cell performance at lower illuminations than that set with the standard of solar cell testing at AM1.5 illumination conditions. The discussion of studies with ZnO NWs used as the antireflective coating, on top of the absorber, or, buried into the absorber, have not been included [52] [53] [54]. A cell where the light absorber also acts as the HTM (see Figure 1b regarding the fully-impregnated configuration) could be referred to as a 3D cell [10] [32], or, as a two-component ETASC, though classification schemes may vary [32].

$CuInS_2$, CdTe, and CdSe extremely thin absorber solar cells

The first strong candidates among pioneering works of ETASCs were $CuInS_2$ [31] and CdTe [55] [56], based on a TiO_2 core, as proposed by Kaiser *et al.* and Ernst *et al.* in 2001 and 2003, where the porous TiO_2 film was found to outperform the planar film (see figure 3(a)) [56]. In 2005-2006, the use of a ZnO NW core was explored for the first time by Lévy-Clement *et al.* for its combination with the CdSe shell and CuSCN HTM, exhibiting a 2.3% PCE [14] [46]. Reports in 2008-2009 followed with the In_2S_3 shell and CuSCN HTM on top, whereas an intermixed layer formed at the interface of those shells was thought to be responsible for the absorption characteristics, presumably through Cu-diffusion related process during post-deposition annealing [43]. At that time, the NW length of 1.5 µm gave way to a PCE up to 2.8-3.4% by Beladi *et al.* and Dittrich *et al.* [43] [57] [58]. An optimal In_2S_3 shell thickness around 25 nm was further determined, as shown in figure 3(b) [57]. In 2013, Lévy-Clement *et*

al. reported a 3.2% ETASC with the ZnO / CdSe / CuSCN architecture through a systematic optimization procedure, as shown in figures 3(c) and 3(d) [34].

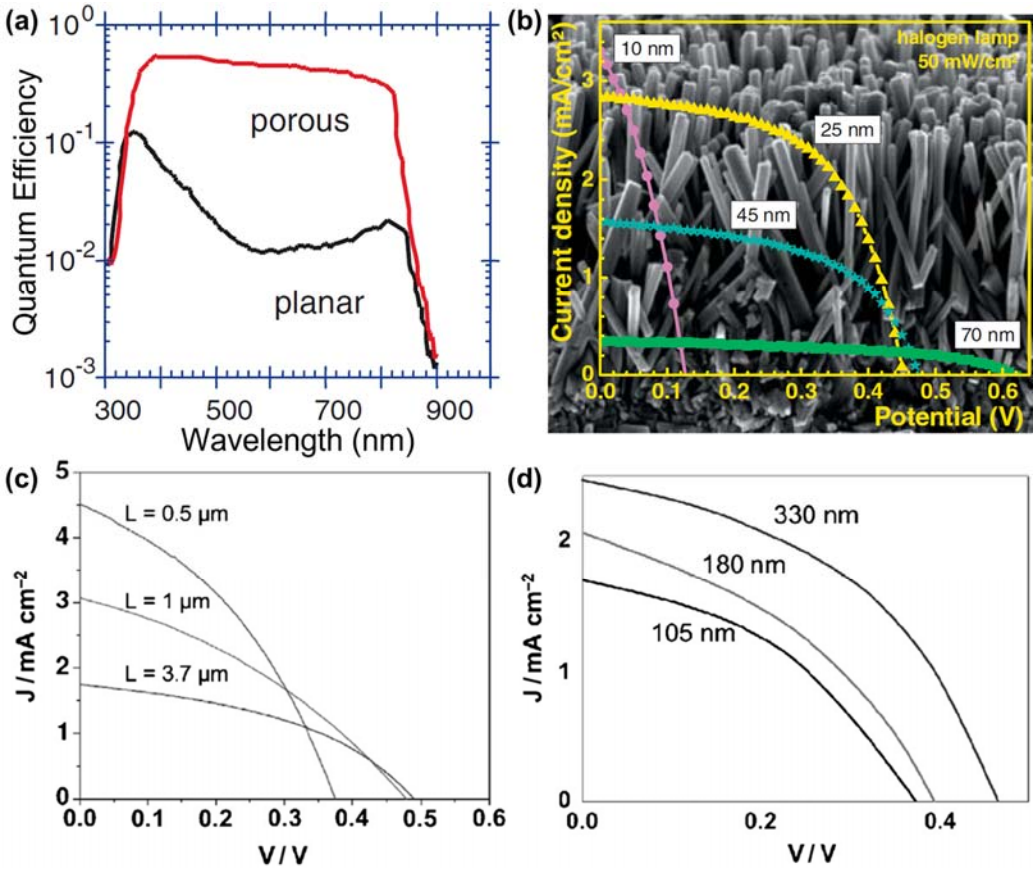

Figure 3. (a) Quantum efficiency versus photon energy for a planar TiO_2/CdTe solar cell and a highly porous-TiO_2/CdTe ETASC. Reprinted with permission from [56]. Copyright 2003 Institute Of Physics Publishing. (b) Cross-sectional SEM image of ZnO NWs, and J-V curves under illumination (AM 1.5G) of ZnO NW/In_2S_3 ETASCs with various local In_2S_3 absorber thickness. Reprinted with permission from [57]. Copyright 2008 Wiley & Sons. (c, d) J-V curves under illumination (500 W/m^2) of ZnO NW/CdTe/CuSCN ETASCs with various ZnO NW length and diameter, respectively. Reprinted with permission from [34]. Copyright 2013 Wiley & Sons.

For an ETASC integrating the $CuInS_2$ shell, the optimized absorber thickness was experimentally determined to be about 100 nm, as grown onto an In_2S_3 buffer layer deposited on ZnO NWs with a 600 nm height [48]. However, the folded curvature, *i.e.* the junction area of the absorber, is hardly what one would expect from an idealized ETASC depicted with an ultra-thin layer of absorber snaking in between the slim ETA and HTM that creates the junction. According to the ETASC, eight-times increase in the surface area of the absorber is needed for CdTe, while four-times increase might be sufficient for $CuInS_2$ due to a higher absorption coefficient when compared to that of CdTe, to reach a PCE of 15% as calculated for absorber thicknesses as low as 15-20 nm [35]. The optimized $CuInS_2$ based cell with 600 nm-long ZnO nanorods (Table 1) bears resemblance to a cell driven by

the ETA concept [48], but is still a far throw from the realization of the classically depicted ETASC sketch. A cell based on longer NWs up to 1000 nm, despite having excellent coverage by CSP, showed inferior performance with exact reasons that remained to be clarified [48].

The advancement on ZnO NW-based ETASC that use the CdTe absorber has not been too impressive despite a number of reports. In 2002, the first demonstration of achieving a conformal 40 nm-thick CdTe shell by the use of vapor phase epitaxy (VPE) on a ZnO NW core was reported by Lévy-Clement *et al.* [47]. In 2005, MOCVD was used to deposit a uniform CdTe shell onto ZnO NWs with height of 150 nm with short comments on the poor shape of the current-voltage measurements [59]. The same year, a report can be found to cover ZnO NWs by CdTe controllably by a cyclic manner though a negligible photocurrent and voltage was harvested from the respective solar cell. Close-spaced-sublimation has been used to deposit CdTe uniformly with slightly varying thickness onto long ZnO NW with 1 μm in length [60]; after thermal annealing of the shell, and light-soaking of the respective ETASC, up to 0.01% PCE was reported [61].

Only recently, in 2018, a 3.4% ETASC based on a CdTe shell and a 5.6% ETASC integrating a CdSe / CdTe shell were reported [62]. The benefit of the 10-15 nm thick intermediate CdSe buffer layer was attributed to the effect of surface passivation, while the duty of photon absorption - solely to the CdTe shell [62]. Nevertheless, the buffer layer can be expected to be photoactive and contribute to the photocurrent, as shown from the 10 nm thick CdS buffer layer used [63]. The CdTe shell seemed to be preferably agglomerated mostly on top of the densely packed ZnO NWs, as deposited by radio-frequency magnetron sputtering. The 10-15 nm-thick CdSe absorber shell on 9 μm-long ZnO NWs [44] when compared to the 10 nm-thick CdSe as the use of a buffer layer for CdTe layer of particles as the absorber shell on 4 μm-long ZnO NWs [62] show remarkably higher V_{OC} (580 vs 650 mV), a close-to comparable short-circuit current (twice longer rods used, at a slightly lower absorption edge), a considerably lower fill factor (FF) (40 vs 64%) and a somewhat lagging PCE (4.7 vs 5.6%). The longer NWs of 9 μm versus 4 μm seem to effectively assist the recovery from the disadvantage of having a higher absorption edge in CdSe when compared to the CdTe. However, the use of shorter ZnO NWs lessens the demands for the deposition methods, in particular to meet the strict requirement of full uniform coverage of the sidewalls of the ZnO NWs. ETASCs with up to a 3.2% PCE were reported in 2011 by using a CdSe shell with some tens of nanometers in thickness on 3μm-long ZnO NWs while using Cu_2O as the HTM (Table 1) [49]. Yet, as all layers were deposited by physical methods, the approach is somewhat less attractive when driven by the ETASC concept.

In an ETASC integrating a CdTe shell, the use of a 10 nm-thick CdS buffer layer showed much lower results (*i.e.* PCE of 1%) [63] when compared to the use of a 10 nm-thick CdSe buffer layer (*i.e.* PCE of 5.6%) [62]. In these studies, and in most cases not discussed, the ZnO / CdTe junction based cells [63] [62] are underperforming when compared to cells with an alternative absorber or an intermediate sulfidic layer, such as the ZnO / CdS [63], ZnO / CdS / CdTe [63], and ZnO / CdSe based ETASC [44]. A large lattice mismatch between ZnO and CdTe is likely to be one cause of such a discrepancy [64], even in the presence of a diffusion layer [65]. An alternative explanation may involve energy barriers at the ZnO NW / CdTe shell interface, which would be detrimental for charge carrier separation. Ultra-thin TiO_2 layer for surface passivation have been explored to mitigate the recombination losses at the ZnO NW / CdTe shell interface [66], although somewhat against the odds owing to a band mismatch at TiO_2 / CdTe interface itself [67]. Despite observed enhancement, the ETASC with the optimized TiO_2 layer thickness still exhibited a fairly low PCE of 1.4% [66]. For the purposes of comparison, in a QDSC as commented in Section 3, the use of a ZnO NW / CdS / CdSe QD configuration significantly outperformed when compared to the use of single CdSe, or CdS QDs alone, on top of the ZnO NWs [68]. A question arises as to whether a ZnO NW / CdS / CdSe / CdTe structure would show even higher performance, as results on the suitability of the closest partners therein seem to be encouraging.

CdS itself is a widely used buffer layer in thin film solar cells, and thus favorably combined with ZnO, although with an off-optimum bandgap energy for light absorption. The performance of ETASCs, using CdS as the light absorber shell on a ZnO NW core, have been reported. The cascade for band alignment and interface engineering were stressed as favorable in the study, in which the ETASC integrating the CdS shell, used as a reference structure, resulted in a 0.28% PCE [63], and, in a study, where an intermediate ZnS layer was used to increase the performance of the ZnO NW / CdS shell-based ETASC with a PCE increasing from 0.05% up to 0.37% in the case of the ZnO NW / ZnS / CdS shell-based ETASC [33]. The ZnS layer was speculated to lead to a homogeneous nucleation of the CdS shell on top of the ZnO NWs [33]. In 2009, a fairly high PCE of 3.5% was reported when using a CdSe shell (excluded from Table 1, for consistency, as liquid electrolyte was used in place of the HTM) with the success attributed to the steps taken to achieve a uniform 5 nm-thick CdS shell by SILAR onto ZnO NWs that were of 10 μm in length and of 100 nm in diameter [69].

Lastly, one of the highest PCE of a true ETASC (*i.e.* with the core-shell configuration) has been obtained by using the CdSe shell as grown onto ZnO NWs with a 9 μm length [44]. The 10 nm-thick CdSe shell showed the

highest performance in the explored $Zn_XCd_{1-X}Se$ system grown by ion-exchange [44]. Herein also, the crucial necessity for a continuous and uniform shell was once again reported [44]. The capacity of producing a J_{SC} of 18 mA/cm^2 by using a 10 nm-thick CdSe shell as the absorber is impressive [44] when compared to the 150 nm-thick $CuInS_2$ absorber exhibiting a J_{SC} of 16 mA/cm^2 (Table 1) [48]. With a factor of 15 increase in the NW length (9 µm vs 600 nm) and a factor of 15 decrease in the absorber thickness (Table 1), the effects due to the significantly increased interface have not deteriorated the cell as judged from the comparable J_{SC} (16 vs 18 mA/cm^2), even without considering the higher bandgap energy, and thus a lower absorption edge, at 1.6 eV for CdSe [44] when compared to 1.3 eV for $CuInS_2$ [70]. One cannot leave aside the crucial aspect of favorable band alignment of CdSe with respect to ZnO, thus promoting an efficient electron transfer to ZnO NWs [32]. Also, the fair PCEs obtained throughout the study give hope for a rise in further interest and active development of the somewhat underexplored ETASC concept based on ZnO NWs and more extensive use of chemical methods [42].

TiO_2/Sb_2S_3 and SnS extremely thin absorber solar cells

A "hybrid" ETASC based on ZnO NWs covered with a CdSe shell and a polymeric HTM (*i.e.* P3HT) was reported in 2008 with a PCE of 0.9% [71]. However, back in 2011, ETASCs with reasonable PCEs featured cells based mostly on the TiO_2 / Sb_2S_3 system as the window / absorber combination with the highest PCE of 5.1% when using P3HT as the HTM [27] [50]. In the same year, a comprehensive review of ETASCs underlined the obstacles and the need for fundamental research in the field of nanostructured inorganic solar cells [30]. From 2012 to 2015, the porous TiO_2 and CBD grown Sb_2S_3 system, by advancements through modified HTMs, and post-deposition treatments, showed PCEs up to 7.5% [72] [73] [74]. A nanocomposite cell that was based on very short (100 nm) ZnO NWs, subsequently gap-filled by Sb_2S_3 *via* a vacuum-based method, was reported in 2012 with a PCE of 2.9% [75]. In 2014, an ETASC integrating ZnO NWs covered with the ZnS / Sb_2S_3 shells by chemical methods demonstrated an enhancement of the PCE from 1.0 to 1.3%, when compared to the same ETASC based on the ZnO NWs covered with a single Sb_2S_3 shell, as a result of the introduction of the ZnS intermediate layer by ionic exchange [76]. An excellent ZnO NW core coverage by the ZnS and Sb_2S_3 shells was reported by using a chemical conversion process that uses ZnO and ZnS as the reactive templates, respectively. In 2017, another report on a core-shell heterostructure grown by chemical deposition techniques alone was based on the conformal coating of ZnO NW by the TiO_2 and Sb_2S_3 shells resulting in a 2.3% PCE of the respective ETASC, as shown in figure 4(d) [42]. In addition to a successful transfer of the TiO_2 / Sb_2S_3 based ETA photoactive structure onto a substrate of ZnO

NWs (also in Table 1), the deposition of the Sb_2S_3 shell by ultrasonic-CSP had thus shown good coverage on the CBD-grown ZnO NWs and excellent penetration into the gaps between the ZnO NWs (as seen in figures 4(a-c)) as required in an ETASC design [42]. Also, scaling up of the cell area does not seem to be an obstacle when CSP method is put to use, a cell area of 1 cm^2 in a planar configuration has been reported in the first study using ultrasonic spray pyrolysis for the growth of Sb_2S_3 for solar cell application in a TiO_2/Sb_2S_3 system [77]. For an ETASC, as well as for any nanostructured solar cells in general, excellent penetration of the HTM is a vital requirement for a successful charge carrier transport, and should be demonstrated whenever possible.

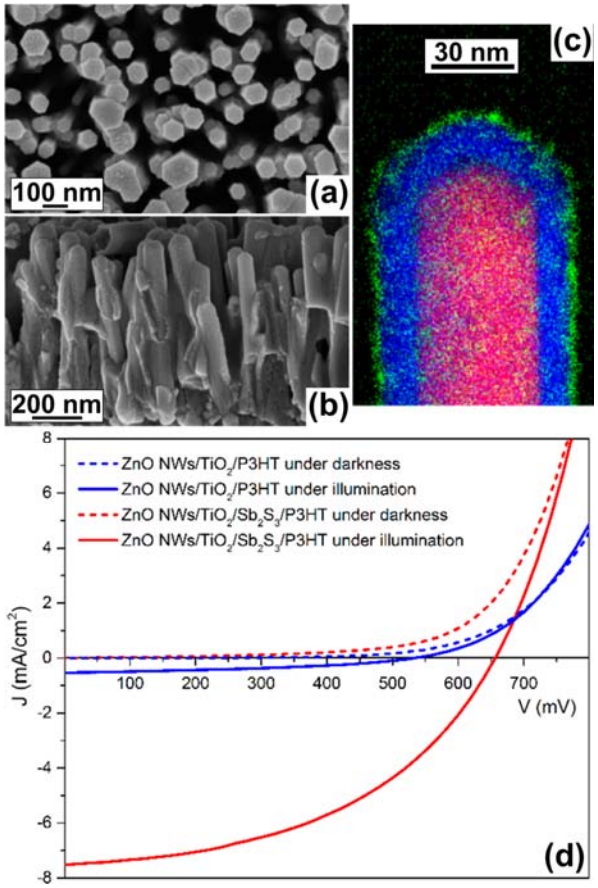

Figure 4. (a, b) Top-view and cross-sectional FESEM images, respectively, of $ZnO/TiO_2/Sb_2S_3$ core-shell NW heterostructures annealed at 300°C under N_2. (c) EDS-STEM elemental mapping superimposing the zinc, titanium, and antimony element signals of the $ZnO/TiO_2/Sb_2S_3$ core-shell NW heterostructures annealed at 300°C under N_2. (d) J-V curves of ZnO NW/TiO_2/P3HT and ZnO NW/TiO_2/Sb_2S_3/P3HT ETASCs in darkness and under illumination (AM 1.5G). Reprinted with permission from [42]. Copyright 2017 American Chemical Society.

As seen from Table 1, the 5-10 nm-thick Sb_2S_3 shell on 900 nm-long NWs compared to a 10 nm-thick shell of CdSe on 9 µm-long NWs (a factor of 10 higher) shows only two and a half times lower J_{SC} (7.5 vs 18 mA/cm^2) and twice lower performance in terms of the PCE (2.3 vs 4.7%) [42] [44]. Admittedly, face-to-face comparison is

unwarranted unless more parameters are alike. However, the lower amount of the absorber used (in thickness and in longitude), as well as the higher bandgap energy of 1.8 eV in Sb_2S_3 [42] when compared to 1.6 eV in CdSe [44], are the primary suspects for the differences, since the V_{OC}s are rather similar (650 vs 656 mV). However, the route towards higher currents by simply opting extremely long NWs seems to be limited. Lastly, all advances in the field of Sb_2S_3 solar cells, including semiconductor-sensitized nanostructured solar cells, have recently been reviewed [78].

A SnS shell based ETASC report that focused on investigating the effect of the magnitude of the piezoelectric effect originating from ZnO NWs on the performances of the respective solar cells, *via* the application of a moderate pressure resulted in a 37% improvement of the PCE from 1.2% up to 1.65% (Table 1 presents the former, for consistency) [79]. This demonstrated the yet untapped potential of the piezoelectric effect in the ZnO NW based PV devices *via* the so-called piezophototronics effects [79]. The somewhat low PCE may, for one, be due to a non-uniform SnS shell thickness that ranged from 0 to 500 nm, while the thicker part of the SnS shell was found on the top of the ZnO NWs [79].

Cu_2O extremely thin absorber solar cells

The PV absorber materials are not limited to the group of chalcogenides. All-oxide solar cells have more recently appeared as an attractive pursuit. In 2014, the immersion and full impregnation of the Cu_2O absorber by electrodeposition into the gaps, and on top, of the of 1.1μm-long ZnO NWs has opened the way to the fabrication of solar cells with a PCE up to 1.26%, whereas the necessity for a highly resistive layer on top of the ZnO NWs prior to the Cu_2O absorber deposition, to avoid short-circuiting through gaps in between ZnO NWs, was once again corroborated [80]. Herein, the ZnO NWs were fully impregnated by the Cu_2O absorber layer, which does not fit the ETASC description based on the core-shell configuration [80]. A similar, fully impregnated geometry was reported along with simulations on the propagation of light in the ZnO NWs in 2015 for an array of highly ordered ZnO NW covered by 1-2 μm thick Cu_2O using electrodeposition, with a resulting PCE of 1.52% [81]. When compared to the performances of the PV devices that achieve a 1.3-5.6% PCE while based on a ETASC integrating a binary sulfide shell of 5-15 nm in thickness (Table 1), the Cu_2O approach has yet to make steps to prove its capability. In 2016, mostly a topping of Cu_2O only, with little to no material on the sidewalls of ZnO NW, was reported [82]. In the future, it will be interesting to learn of the success in achieving a conformal absorber shell

coatings on top of ZnO NWs. Apart from the use as a light absorber layer, Cu_2O has also been utilized as the HTM, *e.g.* in a CdS-absorber based ZnO NW solar cells [49].

ZnSe, ZnS, and ZnTe extremely thin absorber solar cells

In the conventional ETASCs described before, the light absorption in the core-shell ZnO NW heterostructures is mostly achieved in the absorber shell, which exhibits a smaller bandgap energy that is relevant for absorption in the range of the solar spectrum. One decade ago, an alternative concept was developed by Zhang *et al.*, showing that the combination of two wide bandgap semiconductors (*e.g.* GaN and GaP) can create a new bandgap that is much smaller than any of the constituents [83]. This has led to the further development of the so-called ETASCs based on the type II interfacial transition, in which ZnO NWs are covered by an absorber shell with a wide bandgap energy (that is thus not supposed to absorb the light in the range of the solar spectrum when used alone). In this novel system, the conduction band minimum is located in the ZnO NW core while the valence band maximum is in the wide bandgap absorber shell. Basically, the light absorption is made through the type II transition at the interface between the ZnO NW core and the wide bandgap absorber shell: the photo-generated electrons and holes relax in the respective band edges and are thus spatially separated in the ZnO NW core and wide bandgap absorber shell, respectively. Interestingly, both photo-generated electrons and holes have a small probability to recombine through either a radiative or non-radiative process owing to the spatial separation of the wave functions, leading to typical long charge carrier lifetime (several tens of ns vs several hundreds of ps in the case of defects in the bulk). A critical issue is related to the magnitude of the light absorption through the type II interfacial transition, which may be somewhat weak.

This novel approach of the ETASCs based on the type II interfacial transition has been explored on a number of wide bandgap absorber shells combined with ZnO NWs, including ZnSe and ZnTe. The properties of the type II interfacial transition has been determined by theoretical computations in different cases [83] [84]. The unambiguous identification of the type II interfacial transition has been considered here as the key point to establish the present ETASCs as a promising approach. However, this identification is not straightforward and often questionable, requiring the use of a large number of characterization techniques including continuous and time-resolved photoluminescence as well as absorption and photocurrent measurements. Wang *et al.* showed in 2008 the formation of ZnO/ZnSe core-shell NW heterostructures by combining CVD and PLD techniques [85]. The 5-8nm thick epitaxial ZnSe shell was found to be crystallized according to the zinc blend structure to reduce the lattice

mismatch with ZnO NWs [85]. Later on, Wu *et al.* reported the formation of the same ZnO/ZnSe core-shell NW heterostructures by using a two-step CVD technique, but with the presence of a wurtzite transitional ZnSe layer [86]. More interestingly, the continuous photoluminescence and absorption measurements exhibited a strong line around 1.9 eV, as shown in figure 5(a), that could be attributed to the presence of the type II interfacial transition, while a significant photocurrent was shown in the same range by external quantum efficiency (EQE) measurements, as presented in figure 5(b) [86]. More importantly, time-resolved photoluminescence measurements as presented in figure 5(c,d) were reported one year later on the same heterostructure, showing that the 1.9 eV line has a slow decay time around 64 ns, which is an important additional finding to state that the type II interfacial transition has been shown [87]. A V_{OC} around 700 mV was further revealed at low power illumination conditions [87]. Additional reports investigating the ZnO/ZnSe core-shell NW heterostructures by other deposition techniques claimed that the type II interfacial transition has been demonstrated, but only by focusing on absorption measurements [88] [89]. More recently, Luo *et al.* also claimed the observation of the type II interfacial transition in ZnO/ZnTe core-shell NW heterostructures to account for the relatively high performances of the resulting ETASCs [90]. The ZnO/ZnS core-shell NW heterostructures have also been investigated quite intensively [91], but much more for the field of UV photodetectors [92].

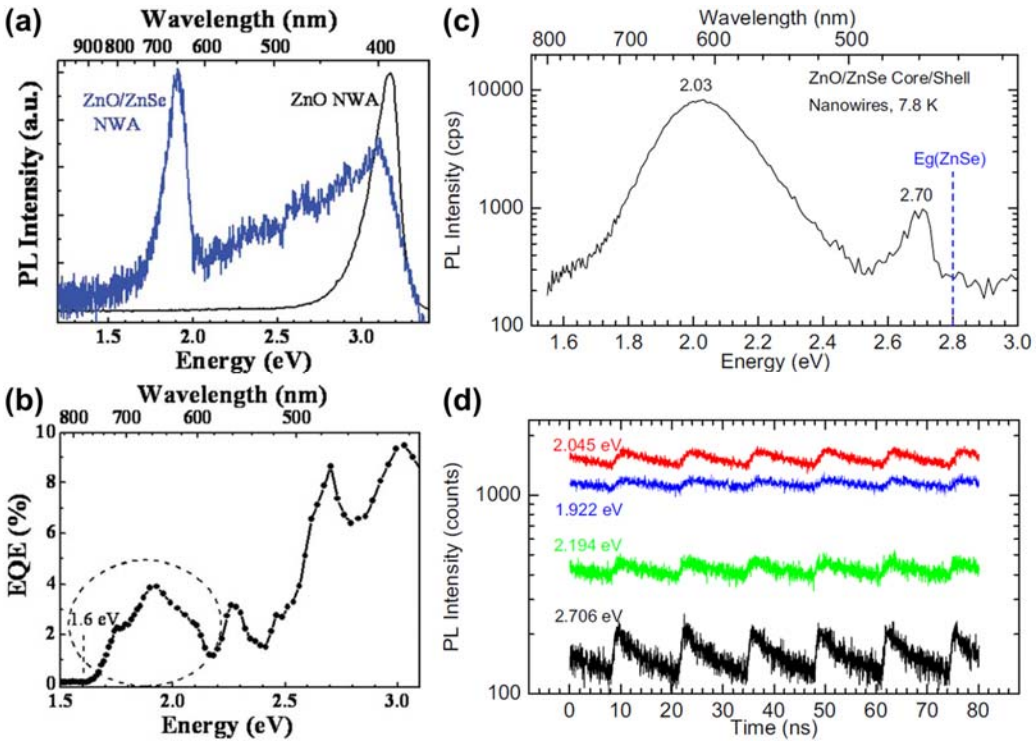

Figure 5. (a) Normalized photoluminescence spectra for ZnO NWs and ZnO/ZnSe core-shell NW heterostructures. (b) EQE of a ZnO NW/ZnSe ETASC. Reprinted with permission from [86]. Copyright 2011 Royal Society of Chemistry. (c, d) Time-

resolved photoluminescence of ZnO/ZnSe core-shell NW heterostructures measured at low temperature. (c) Time averaged spectrum and (d) decay curves monitored at different emission energies. Reprinted with permission from [87]. Copyright 2012 Elsevier.

ZnO nanowire core for amorphous silicon shells as an alternative 'extremely thin absorber solar cell'

Shells of amorphous silicon (a-Si) uniformly mounted on ZnO NWs, without reports on devices, were explored by Könenkamp *et al.* in 2000 [93]. Aluminum-doped ZnO NWs by hydrothermal growth, as the substrate for n-i-p shells of amorphous silicon was proposed in 2011 [94]. A conformal coating was achieved by plasma-enhanced chemical vapor deposition (PECVD). An increase in the absorber shell thickness from 25 nm up to 150 nm resulted in only a slight increase in the PCE from 3.92 to 4.27%, and the use of 2 μm instead of 1 μm long NWs resulted in a relatively insubstantial increase in the PCE from 4.27 up to 4.73% [94]. Another study in 2011 reported a PCE of 3.6% by using a 25 nm thick a-Si shell on 400 nm-long ZnO NWs [95]. When compared to the PCE of 3.92% obtained on the 1 μm-long ZnO NW [94], and a shell with similar thickness of 25 nm, one cannot help to notice that fairly large differences in NW height would be needed to further produce a substantial increase in the efficiencies based on a-Si absorber shells. In 2013, following an optimization routine by using 75 to 250 nm absorber shell thicknesses and NW lengths in the range of 600 to 1800 nm, the highest PCE of 6.07% was reported for 600 nm-long ZnO NWs with a 200 nm-thick absorber shell [45]. Thus, in terms of efficiency, a thick a-Si shell on short ZnO NWs provided the best results, despite longer NWs yielding more current. Although an ETA solar cell by nature asks for an absorber with strong absorption characteristics, interestingly, the cells based on chalcopyrite absorbers mostly fall behind in terms of the efficiency when compared to a-Si cell (Table 1), even at AM1.5 where the chalcopyrites ought to excel contrary to a-Si that has superior performance on low illumination intensities [96]. Then again, an ETA rationale is much about the cost-effectiveness. Thus, such a milestone on the use of a-Si brought to us by PECVD, although a good reference point, is somewhat out of scope of the ETASC.

Photoanode		Absorber shell			HTM	ETASCs				Ref.
Diameter (nm)	Height (μm)	Type	Thickness (nm)	Technique	Type	V_{OC} mV	J_{SC} mA/cm^2	FF	PCE %	
100-150	1-2	CdSe	30-40	Electrodeposition	CuSCN	500	4	-	2.3	[14]
100-330	0.5-3.7	CdSe	20-65	Electrodeposition	CuSCN	580	5.18	0.53	3.2	[34]
50-150	9	CdSe	10-15	Ion-exchange	Cu_2S	650	18	0.40	4.7	[44]
400	3.6	CdSe	20-35	RF MS	Cu_2O	670	11	0.45	3.2	[49]
70	4	CdSe/CdTe	10 / n.a.	RF MS	- (Ni/Au)	580	21	0.64	5.6	[62]
		CdTe	n.a.	RF MS		560	13	0.45	3.4	
200-300	0.6	$CuInS_2$	100	CSP	CuSCN	441	16	0.60	4.2	[48]

					or graphite					
100	1.5	In_2S_3:Cu*	(25)*	ILGAR	CuSCN	570	11	0.56	3.4	[57]
120**	1.4	ZnS/Sb_2S_3	15	Ion-exchange	P3HT	440	5.6	0.54	1.3	[76]
80	0.9	TiO_2/Sb_2S_3	5-10	ALD / CSP	P3HT	656	7.5	0.47	2.3	[42]
300	3	SnS	0-500	RF MS	- (Ag)	520	4.6	0.43	1.2	[79]
50-90	0.6	a-Si	200	PECVD	- (ITO)	840	11	0.63	6.1	[45]

*Absorption characteristic attributed to an interfacial layer in between the In_2S_3 and CuSCN, its formation being driven by Cu-diffusion [57] [58]

**Nanotubes.

Table 1. PV performances of the ETASCs integrating ZnO NWs. In some cases, numbers have been rounded owing to the sufficiently large contrast of the results, for the sake of comparability, and overview.

3. Quantum dot solar cells

Background of quantum dot solar cells

Semiconducting QDs have received increasing interest in the last two decades for their integration into next-generation solar cells owing to their strong assets and remarkable properties related to quantum confinement [97] [98] [99] [11]. First, by changing the size of QDs over a nanometer scale, the electronic energy levels are tunable. The variation of the band gap energy of QDs is achieved to maximize the absorption over the solar spectrum, while the shift of the electronic energy levels improves charge carrier transfer across the interfaces. The combination of QDs with different sizes over a broad range is of high potential for multi-junction solar cells. Second, QDs are known to generate multiple correlated electron hole pairs per absorbed photon through the so-called multiple exciton generation (MEG) process [100]. In bulk semiconductors, impact ionization predominates when the excitation energy equals a multitude of the band gap energy, such that its efficiency is very low over the solar spectrum [101]. In contrast, the inverse Auger process is greatly favored in QDs and approaches twice the threshold energy for absorption [102]. The MEG process can exist in QDs because its time scale is much shorter than the time scale required for hot exciton cooling produced by electron-phonon interactions [103]. The MEG process is thus expected to result in higher photocurrent, exceeding the standard Shockley-Queisser limit around 30% [102]. The direct extraction of hot electrons is also expected to generate a higher photo-voltage [104] [105]. Furthermore, QDs are integrated into QDSCs using low-cost and low-temperature chemical methods as well as relatively inexpensive solar cell manufacturing. Basically, there exists two different chemical routes for covering TiO_2 or ZnO materials acting as ETM with QDs, either by a direct attachment of QDs or by an attachment of molecules that are linked to QDs. In the former case, QDs are typically grown by the low-cost and low-temperature CBD and SILAR technique. This facilitates fast electron transfer at the QD / ZnO NW interface, depending on the density of

charge carrier trap and recombination centers, but detrimentally reduces the precise control over QD size. It should be noted here that the distinction between QDSCs and ETASCs is relatively tight and often based on the size of nanoparticles as well as on the continuity of the deposit. In the more widely used QDSCs, colloidal nanoparticles are pre-synthesized and dispersed in solution with surface passivating agents like oleic acid ligands using wet chemical methods. A key point consists in using the most appropriate bifunctional linker molecule binding the TiO_2 or ZnO materials (*e.g.* with a carboxylic group) on one side and QDs (*e.g.* with a thiol group) on the other side. A ligand exchange on the QD surface from the long organic oleic acid to a shorter organic ligand or to an inorganic molecule is typically achieved [106], which can additionally alter the electronic energy levels of QDs [107] and improve the stability of the related QDSCs [108]. The spacing between adjacent QDs is small enough to induce an efficient charge carrier transfer from QD to QD by hopping or tunneling processes, increasing in turn charge carrier mobility and diffusion length. Eventually, colloidal QDs are deposited by spin or dip coating, drop casting, simple immersion, or electrophoretic deposition.

The field of QDSCs integrating TiO_2 or ZnO materials is broad and involve many different architectures, mainly including QD-sensitized solar cells (QDSSCs) and bulk heterojunction QD solar cells (BHQDSCs). Semiconducting QDs belonging to the widely used chalcogenides group have intensively been developed in QDSCs in the 2000's [109] [110] [111] [18] [112]. They have initially been combined with mesoporous TiO_2 films and then progressively used with ZnO in the form of films. Robel *et al.* reported, for the first time, in 2006 the combination of CdSe QDs with mesoporous TiO_2 films, using three types of bifunctional linker molecules with carboxylic acid and thiol groups, and showed the fast electron injection from the excited state of CdSe QDs into TiO_2 particles [109]. Niitsoo *et al.* showed the combination of CdS and CdSe QDs using CBD for their direct attachment on nanoporous TiO_2 layers as well as a selenization process *via* selenosulphate conversion, reporting a PCE of 2.8% [110]. The combination of PbS and CdS QDs with mesoporous TiO_2 layers was then stated by Lee *et al.* using the SILAR technique for the direct attachment of QDs, leading to the fabrication of solid-state QDSSCs with a PCE of 1.46 and 0.8%, respectively, using spiro-OMeTAD as HTM [111]. Leschkies *et al.* showed that BHQDSCs integrating PbSe QDs with ZnO films within a linker mediated attachment exhibit a higher PCE of 1.6% than similar Schottky solar cells [18]. They further emphasized the significance of using an electron blocking layer like α-NPD between PbSe QDs and the top contact. Luther *et al.* revealed the combination of PbS QDs with ZnO nanocrystal films within a linker mediated attachment and the related BHQDSCs exhibited a PCE of 3% that is

stable over 1000 hours of continuous illumination in ambient air [112]. While much efforts have initially been dedicated to the issues of QD densification, passivation with ligands, and cross-linking, charge carrier transfer and extraction have more recently emerged as an important issue to be addressed by typically nanostructuring the photo-anode [113] [114]. ZnO NWs can be introduced in QDSCs to act as an efficient ETM, typically in i) QDSSCs where the NWs are covered with QDs as a shell to form core-shell heterostructures whereas a liquid electrolyte or a solid-state HTM are used together with a planar counter electrode, ii) BHQDSCs where the NWs are fully impregnated by QDs whereas a planar counter electrode is employed. The latter is expected to address some of the drawbacks of the planar depleted QD solar cells, where the thickness of the QD film is limited to a few hundred nanometers, as both the depletion region width and charge carrier diffusion length are small, strongly limiting in turn the optical absorption. A wide range of semiconducting QDs has thus been combined with ZnO NWs to fabricate both QDSSCs, including CdSe, CdS and CdTe, and BHQDSCs, including PbS and PbSe. The main advantages of using ZnO NWs are related to improved light trapping phenomena to increase optical absorption, increased interfacial area with QDs to favor exciton dissociation and electron transfer, as well as enhanced electron transport efficiency through the NWs directly contacted to TCO/glass substrate. The PV performances of the QDSCs incorporating ZnO NWs are gathered in Table 2-4 and commented in the following sections.

CdSe and CdSe/CdS quantum dot-sensitized solar cells

Leschkies *et al.* reported, for the first time, in 2007 the combination of CdSe QDs with ZnO NWs using bifunctional mercaptopropionic acid (MPA) as a linker molecule. Both sulfur and carboxylate terminations bind to CdSe QDs and ZnO NWs, respectively, while the short organic chain ensures efficient charge carrier transfer [15]. The resulting QDSSCs involving O_2-plasma treated ZnO NW and using liquid electrolyte as HTM exhibited a PCE of 0.4 % with a J_{SC} and V_{OC} in the ranges of 1–2 mA/cm^2 and 500–600 mV. By performing time-resolved photoluminescence measurements, Sun *et al.* revealed that the electron transfer from CdSe QDs to ZnO is faster and of the order of 10 ns using thioglycol acid (TGA) as a bifunctional linker molecule instead of MPA owing to its shorter organic chain length [115]. The resulting QDSSCs exhibited an increased PCE of 0.66% using TGA as compared to the PCE of 0.41% using MPA. Following those pioneering works, the group of Pullerits has intensively investigated the characteristics of the electron injection from CdSe QDs into ZnO NWs when capped with a bifunctional mercaptopropionic as a linker molecule [116] [117] [118] [119] [120] [121].The photo-degradation effects on charge carrier transfer from CdSe QDs to ZnO NWs under ambient and low-O_2 atmospheres were

assessed by transient absorption (TA) measurements, indicating that changes in TA dynamics are related to effective quenching of bigger QDs as well as the formation of electron and hole trap states [116]. The role of oxygen was then identified to generate trap states on the CdSe QD surface and to simultaneously passivate them by oxidation [117]. Correlatively, Hou *et al.* reported that the photoconductivity dynamics is controlled by the oxygen desorption on the surfaces of ZnO NWs and CdSe QDs in the cluster form [122]. Additionally, it was also found that the characteristics of the electron injection are dependent upon the morphology of ZnO, owing to dielectric permittivity change and different band-edge state densities [118]. Zidek *et al.* combined TA with time-resolved terahertz spectroscopy to track down excited electrons in CdSe QDs and ZnO NWs covered with CdSe QDs as seen in figure 6(a,b). They showed that the electron transfer occurs *via* a fast and slow component on a 3-12 ps and 60-102 ps time scale, as shown in figure 6(c) [119]. This was attributed to a two-step electron transfer from CdSe QDs directly attached as a monolayer onto ZnO NWs, through an intermediate charge transfer state. Later on, Zheng *et al.* showed that additional contributions occur when several layers of CdSe QDs are deposited on ZnO NWs, giving birth to the concept of indirectly and directly attached QDs, as presented in figure 6(d) [120]. An excitation depopulation process over a 4 ns time scale was revealed in indirectly attached QDs, originating from radiative electron hole pair recombination as well as non-radiative excitation-to-charge conversion associated *via* an energy transfer from the indirectly to directly attached QDs. Additionally, the surface chemistry of CdSe QDs through the selection of the most appropriate linker molecule was found to be of high significance in order to slow down charge carrier relaxation for the benefit of MEG and HET processes in QDSSCs [121]. By using several bifunctional ω-mercaptocarboxylic acids, Bley *et al.* further reported from time-resolved photoluminescence measurements, that the electron tunneling rate from the lowest excited states of CdSe QDs in the cluster form to the conduction band of ZnO NWs is increased by shortening the length of the linker molecule and by adding a thin ZnS passivating layer on the QDs [123]. However, the photoconductivity was increased by elongating the linker molecules, which was attributed to their role as diffusion barriers for oxygen. The present fundamental investigations have emphasized the importance of carefully addressing the issue of surface states in ZnO NWs and CdSe QDs, showing the need for combining ZnO NWs or CdSe QDs, or both of them, with a passivating layer.

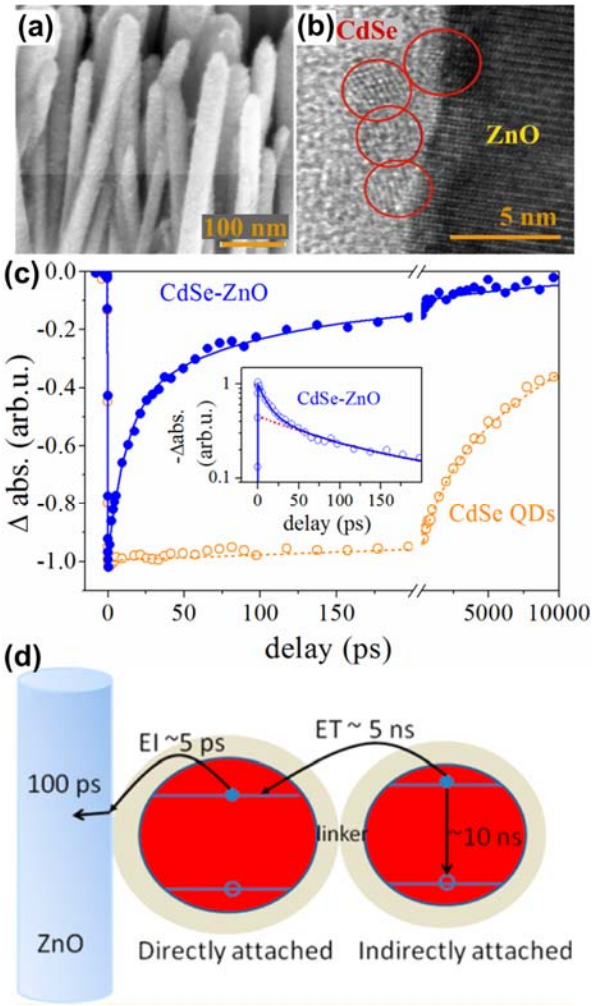

Figure 6. (a) SEM image of CdSe QD-sensitized ZnO NWs. (b) HRTEM image of CdSe QDs attached to a ZnO NW for sensitization. (c) Transient absorption kinetics of CdSe QDs (orange open circles) and CdSe QDs attached to ZnO surface (blue filled circles). The dashed orange line represents a two-exponential fit and the solid blue line represents a three-exponential fit. The inset illustrates the transient absorption kinetics of QD-sensitized ZnO (open circles) compared to the sum of nanosecond component and slow component only (dotted red line). Reprinted with permission from [119]. Copyright 2012 American Chemical Society. (d) Main photo-induced processes in CdSe QD-sensitized ZnO NW QDSSCs. Reprinted with permission from [120]. Copyright 2013 American Chemical Society.

A significant number of reports have then consisted of efforts in combining CdSe QDs with CdS in the form of a thin shell or of QDs to explore the performances of the related QDSSCs that incorporate ZnO NWs [68] [124] [125] [126] [127] [128] [129] [130]. Seol *et al.* reported, for the first time, in 2010 the combination of CdSe QDs grown by CBD with ZnO NW / CdS core-shell heterostructures using the SILAR technique, for which the morphology is revealed in figure 7(a,b). The resulting QDSSCs boosted the absorbance as shown in figure 7(c) as well as the J_{SC}, V_{OC}, and PCE to 17.3 mA/cm^2, 627 mV, and 4.15%, respectively [68], as compared to 2.4 mA/cm^2, 191 mV, and 0.17% when no thin CdS shell was deposited (see figure 7(d)). The boost clearly indicated that the

CdS interlayer drastically enhances the electron transfer from CdSe QDs to ZnO NWs and reduces interfacial recombination by passivating the surface states of ZnO NWs. Subsequently, ordered mesocellular carbon foam (MSU-F-C) was shown to be an efficient counter electrode by increasing surface area as compared to planar gold and platinum as well as by acting as a redox relay in the electrolyte lowering in turn charge transfer resistance as deduced by electrochemical impedance spectroscopy [124]. In contrast, Chen *et al.* reported a co-sensitization by CdS QDs grown by CBD and MPA-capped CdSe QDs by simple immersion, showing a PCE of 1.42% [125]. A similar approach was developed by Luan *et al.*, where both TGA-capped CdS and CdSe QDs were deposited by simple immersion on ZnO NWs [126]. The co-sensitization resulted in the fabrication of QDSSCs outperforming the performances of the QDSSCs with a single sensitization of either CdS or CdSe QDs. The Al_2O_3 thin shell over ZnO NWs was also shown as an efficient passivating layer increasing FF and PCE to 0.42 and 1%, respectively. A very similar approach was reported by Hui *et al.* using instead MPA-capped CdS and CdSe QDs grown by a single-step CBD technique [127]. Tian *et al.* also reported the deposition of TiO nanosheets (NS) on ZnO NWs for increasing surface area and forming an energy barrier that decreases electron recombination rate [128]. The resulting QDSSCs integrating CdS and CdSe QDs grown by the SILAR and CBD techniques, respectively, and covered with a conformal ZnS shell had an increased V_{OC} and PCE from 420 to 640 mV and from 1.19 to 2.72%, respectively, by adding the TiO_2 nanosheets. More recently, the doping of CdSe QDs with Mn has been found to be of high potential for enhancing light absorption and reducing charge carrier interfacial recombination with the formation of a thin Mn-doped CdSe shell over CdSe QDs [129]. The resulting QDSSCs integrating CdS and Mn-doped CdSe QDs and covered with a conformal ZnS shell following the same procedures exhibited a J_{SC}, V_{OC}, and PCE of 12.6 mA/cm^2, 740 mV, and 4.64%, respectively. Importantly, the same group reported the development of Ag nanoparticles favoring localized surface plasmon resonances in QDSSCs, which has been shown of high potential as well by strongly increasing light absorption and electron injection rate as well as by reducing charge carrier interfacial recombination [130]. The resulting QDSSCs involving ZnO / Ag / TiO_2 core-shell NW heterostructures covered with CdS and CdSe QDs showed a PCE of 5.92%.

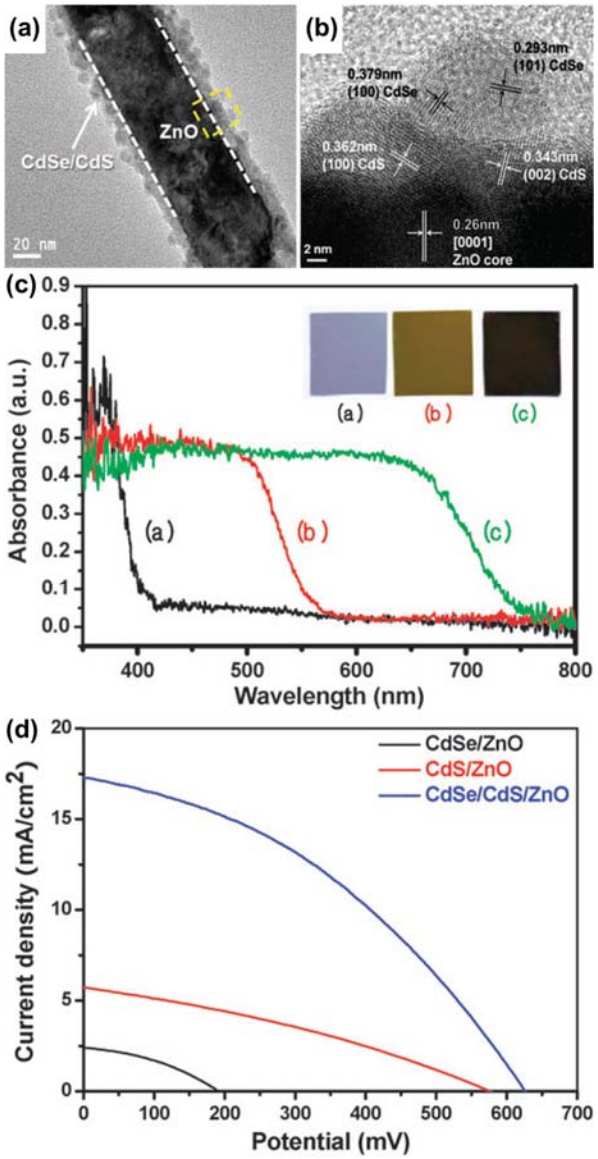

Figure 7. (a, b) TEM and HRTEM images of a CdS/CdSe QD-sensitized ZnO NW, respectively. (c) Absorbance spectra of ZnO NWs (denoted (a)), CdS QD-sensitized ZnO NWs (denoted (b)), and CdS/CdSe QD-sensitized ZnO NWs (denoted (c). The insets are photographs of the corresponding samples. (d) J-V curves under illumination (AM 1.5G) of CdSe, CdS and CdS/CdSe QD-sensitized ZnO NW QDSSCs. Reprinted with permission from [68]. Copyright 2010 Royal Society of Chemistry.

Alternatively, the combination of CdSe QDs with CdS in the form of a thin shell or of QDs has been explored using different types of hierarchical structures composed of ZnO NWs [131] [132] [133] [134]. Sudhagar *et al.* investigated the formation of Si NW / ZnO NW branched hierarchical structures to increase surface area and light scattering phenomena [131]. The combination of the branched NW underlay with a thin CdS shell grown by SILAR, CdSe QDs grown by CBD, and a thin shell of ZnS formed SILAR resulted in the fabrication of QDSSCs with a J_{SC}, V_{OC}, and PCE of 11 mA/cm^2, 710 mV, and 3%, respectively. For similar reasons, a hierarchical macro-porous

Zn_2SnO_4 / ZnO NW composite film was also developed as the photoanode and the effects of its thickness was reported on the performances of the related QDSSCs reaching a highest PCE of 2.08% [132]. In order to further increase the developed surface area and to favor the electron transportation in hierarchical structures, ZnO NWs can be covered by ZnO nanosheets, leading to the fabrication of QDSSCs with an improved J_{SC}, V_{OC}, FF and PCE of 10.74 mA/cm^2, 610 mV, 0.5, and 3.28%, respectively [133]. This was correlated with an increased electron lifetime associated with a decreased charge transfer resistance pointing out a decrease in charge carrier recombination. More recently, hierarchical structures including TiO_2 NWs covered with ZnO NWs on their sidewalls were also shown to significantly improve the performances of the related QDSSCs, which exhibit a J_{SC}, V_{OC}, and PCE of 12.49 mA/cm^2, 493 mV, and 3.20%, respectively [134].

Photoanode	QDs	Ligand	J_{SC} (mA/cm^2)	V_{OC} (mV)	FF	PCE (%)	Ref.
ZnO NWs	CdSe	MPA	2.1	~ 600	0.3	0.4	[15]
ZnO NWs	CdSe	TGA	2.8	580	0.404	0.66	[115]
ZnO NWs	CdSe/CdS	-	17.3	627	0.383	4.15	[68]
MSU-F-C…ZnO NWs	CdSe/CdS	-	12.6	685	0.42	3.6	[124]
ZnO NWs	CdSe/CdS	MPA	5.19	661	0.415	1.42	[125]
ZnO NWs / Al_2O_3	CdSe	TGA	2.72	660	0.55	0.99	[126]
ZnO NWs	CdSe/CdS	TGA	4.36	680	0.24	0.72	[126]
ZnO NWs	CdSe/CdS	MPA	6.61	560	0.34	1.29	[127]
ZnO NWs / TiO_2 NSs	CdSe/CdS/ZnS	-	8.17	640	0.52	2.72	[128]
ZnO NWs	CdSe:Mn/CdS/ZnS	-	12.6	740	0.44	4.64	[129]
ZnO NWs / Ag NPs / TiO_2	CdSe/CdS	-	15.65	744	0.508	5.92	[130]
Si NW / ZnO NWs	CdSe/CdS	-	11.00	710	0.38	3.00	[131]
ZnO NWs / Zn_2SnO_4	CdSe/CdS	-	11.32	492	0.37	2.08	[132]
ZnO NWs / ZnO NSs	CdSe/CdS	-	10.74	610	0.5	3.28	[133]
TiO_2 NWs / ZnO NWs	CdSe/CdS	-	12.49	493	0.52	3.20	[134]

Table 2. PV performances of the QDSSCs integrating ZnO NWs and the CdSe or CdSe/CdS QDs.

CdS, CdTe and alternative sulfides quantum dot-sensitized solar cells

The development of CdS and CdTe QDs with ZnO NWs has been much less pronounced and very often used in the form of direct attachment through the CBD and SILAR techniques in the case of CdS and the mediated attachment in the case of CdTe, respectively. Tak *et al.* reported the SILAR deposition of CdS QDs, for which the size was tuned over a broad range from 3 to 11 nm along with their absorption edge from 3.2 to 2.4 eV by varying the SILAR cycle number [69]. The most efficient QDSSCs exhibited a J_{SC} and PCE of 7.23 mA/cm^2 and 3.53%, respectively. Zhang *et al.* investigated, from continuous and transient photovoltage measurements, the charge

carrier separation and recombination processes in ZnO NWs covered with thin and thick CdS QD films grown by CBD [135]. The resulting QDSSCs exhibited a V_{OC}, J_{SC}, and PCE of 440 mV, 2.6 mA/cm^2 and 0.34%, respectively. A similar approach was carried out by Lee *et al.* reporting a PCE of 0.54% [136] as well as by Chou *et al.* using the SILAR technique for depositing CdS QDs on ZnO NWs / NPs heterostructures reporting a PCE of 0.24% [137]. Later on, Qi *et al.* investigated the effects of the temperature as the use of SILAR technique proceeded for depositing CdS QDs and optimized the V_{OC}, J_{SC}, and PCE to 550 mV, 3.1 mA/cm^2, and 0.72%, respectively, at 60°C for facilitating the penetration ability of ethanol at the bottom of ZnO NWs [138]. By passivating ZnO nanorods with a Zn_2SnO_4 shell, as well as the CdSe QDs deposited by the SILAR technique with a ZnS shell, the V_{OC}, J_{SC}, and PCE were increased to 760 mV, 3.68 mA/cm^2, and 1.24%, respectively, which was mainly attributed to lower charge carrier interfacial recombination [139]. The use of Ag nanoparticles to induce localized surface plasmon resonances was further reported by Eskandari *et al.*, leading to the fabrication of QDSSCs with an improved PCE [140]. Meanwhile, CdTe QDs were combined to ZnO NWs using pulsed-electron beam deposition, showing a significant photosensitization process [141]. Cao *et al.* further reported the combination of CdTe QDs with ZnO NWs using TGA as the linker molecule [142]. The resulting QDSSCs exhibited a V_{OC} and J_{SC} of 500-600 mV and 0.3 mA/cm^2, respectively, pointing out poor charge carrier collection while the optical absorptance was fairly high. A similar approach was achieved by Chen *et al.* using MPA as the linker molecule for photo-electrochemical solar cells with a PCE of 1.83% [143]. Briscoe *et al.* reported the layer-by-layer conformal deposition of TGA-capped CdTe QDs on ZnO NWs, showing a light harvesting efficiency around 80% with 50 layers [144]. However, the resulting QDSSCs using CuSCN as the HTM had a V_{OC} and J_{SC} of 120 mV and 0.19 mA/cm^2, respectively, revealing possible short-circuiting as well as poor charge carrier collection likely due to interfacial recombination. The extraction of charge carriers and specifically of holes appeared as the limiting process in both in ETA and QDSSCs integrating a CdTe shell. So far, the use of CdS and CdTe QDS is much less efficient than the use of CdSe QDs.

The alternative solutions to the group of binary sulfides to form QDSSCs are very scarce in the literature. Kuo *et al.* reported in 2009 the combination of Zn-doped $CuInS_2$ QDs, covered by a thin ZnS passivating shell and capped with MPA, with ZnO NWs [145]. The resulting QDSSCs showed a J_{SC}, V_{OC}, and PCE of 3.21 mA/cm^2, 450 mV, and 0.71%, respectively. More recently, the development of $CuSbS_2$ QDs on ZnO NWs was achieved by heating ZnO / CuS / Sb_2S_3 core-shell NW heterostructures initially deposited by the SILAR technique [146]. The

resulting QDSSCs integrating P3HT as the HTM exhibited a J_{SC}, V_{OC}, and PCE of 5.87 mA/cm^2, 491 mV, and 1.61%, respectively.

Photoanode	QDs	Ligand	J_{SC} (mA/cm^2)	V_{OC} (mV)	FF	PCE (%)	Ref.
ZnO NWs	CdS	-	7.23	-	-	3.53	[69]
ZnO NWs	CdS	-	2.6	440	-	0.34	[135]
ZnO NWs	CdS	-	4.3	330	0.3	0.54	[136]
ZnO NWs / ZnO NPs	CdS	-	4.49	156	0.34	0.24	[137]
ZnO NWs	CdS	-	3.08	550	-	0.72	[138]
ZnO NWs / Zn_2SnO_4	CdS/ZnS	-	3.68	760	0.443	1.24	[139]
ZnO NWs / Ag NPs	CdS	-	3.25	630	0.29	0.60	[140]
ZnO NWs	CdTe	TGA	0.3	~ 500	-	-	[142]
ZnO NWs	CdTe	TGA	0.19	120	0.29	-	[144]
ZnO NWs	$CuInS_2$/ZnS	MPA	3.21	450	0.49	0.71	[145]
ZnO NWs	$CuSbS_2$	-	5.87	491	0.56	1.61	[146]

Table 3. PV performances of the QDSSCs integrating ZnO NWs and the CdS, CdTe or alternative QDs.

PbS and binary sulfides bulk-heterojunction quantum dot solar cells

Leschkies *et al.* reported, for the first time, in 2009 the integration of ZnO NWs into BHQDSCs composed of PbSe QDs capped with 1,2-ethanedithiol (EDT) ligands as the linker molecule as well as a α-NPD and ZnO thin film acting as electron and hole blocking layers, respectively [147]. By fixing the amount of PbSe QDs, they showed a significant increase in the performances of the BHQDSCs when ZnO NWs are introduced as compared to planar ZnO film, resulting in a J_{SC}, V_{OC}, and PCE of 18.6 mA/cm^2, 420 mV, and 1.97%, respectively. Following that pioneering work, most of the efforts have been devoted to the development of PbS QDs combined with ZnO NWs. Jean *et al.* showed, for the first time, in 2013 the fabrication of BHQDSCs composed of PbS QDs capped with 1,3-benzenedithiol (BDT) ligands and integrating ZnO NWs [19]. By optimizing the thickness of a MoO_3 anode interlayer specifically hampering shorting, the resulting BHQDSCs had a J_{SC}, V_{OC}, and PCE of 17.9 mA/cm^2, 600 mV, and 4.3%, respectively, significantly outperforming the related BHQDSCs integrating planar ZnO film, as shown in figure 8(e).

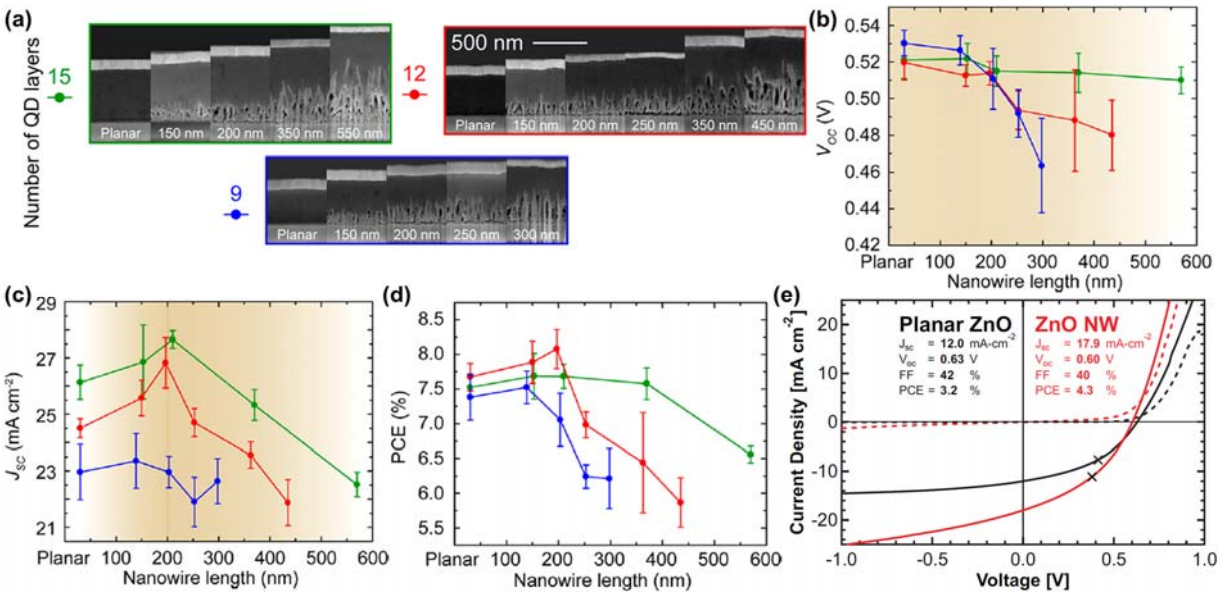

Figure 8. (a) Cross-sectional SEM images of PbS QD-sensitized ZnO/TiO_2 NW with varying ZnO NW length and number of QD layers. (b, c, d) Corresponding PbS QD-sensitized ZnO/TiO_2 NW BHQDSCs performances, (b) V_{OC}, (c) J_{SC}, and (d) PCE. Reprinted with permission from [148]. Copyright 2018 American Chemical Society. (e) J-V curves under darkness (dashed lines) and under illumination (AM 1.5G, solid lines) for a PbS QD-sensitized planar ZnO BHQDSC (dark lines) and a PbS QD-sensitized ZnO NW BHQDSC. The black crosses indicate the maximum power point for each device. Reprinted with permissions from [19]. Copyright 2013 Wiley & Sons.

By optimizing the thickness of PbS QDs capped with bromide anions as well as by densifying the ZnO NW arrays, Wang *et al.* showed the increases in the J_{SC}, V_{OC}, and PCE of the resulting BHQDSCs up to 34.47 mA/cm^2, 361 mV, and 6.07%, respectively [149]. The long-term stability of those BHQDSCs was further revealed under continuous light soaking, the PCE being around 90% of its maximum after 3000h [150]. An in-depth analysis of the charge carrier transport by impedance spectroscopy showed proof of the efficient charge carrier collection in the present BHQDSCs [151]. Additionally, the relatively low V_{OC} was related to the band bending at the surface of ZnO NWs. The issue of the passivation of the surfaces of ZnO NWs to reduce charge carrier interfacial recombination has thus emerged as critical. By coating ZnO NWs with a thin TiO_2 passivating layer as seen in figure 9, Chang *et al.* revealed, from transient photovoltage decay and impedance spectroscopy measurements, a significant decrease in charge carrier interfacial recombination, resulting in the improved performances of the BHQDSCs with a V_{OC} and PCE of 420 mV and 6.16%, respectively [152]. The use of an alternative ultrathin $Mg(OH)_2$ passivating layer was explored on ZnO NWs, leading to the fabrication of BHQDSCs with an improved V_{OC} and PCE of 520 mV and 5.04%, respectively [153]. The optimal thickness of both passivating layers has been selected as a good trade-off between a higher V_{OC} and a preserved J_{SC}.

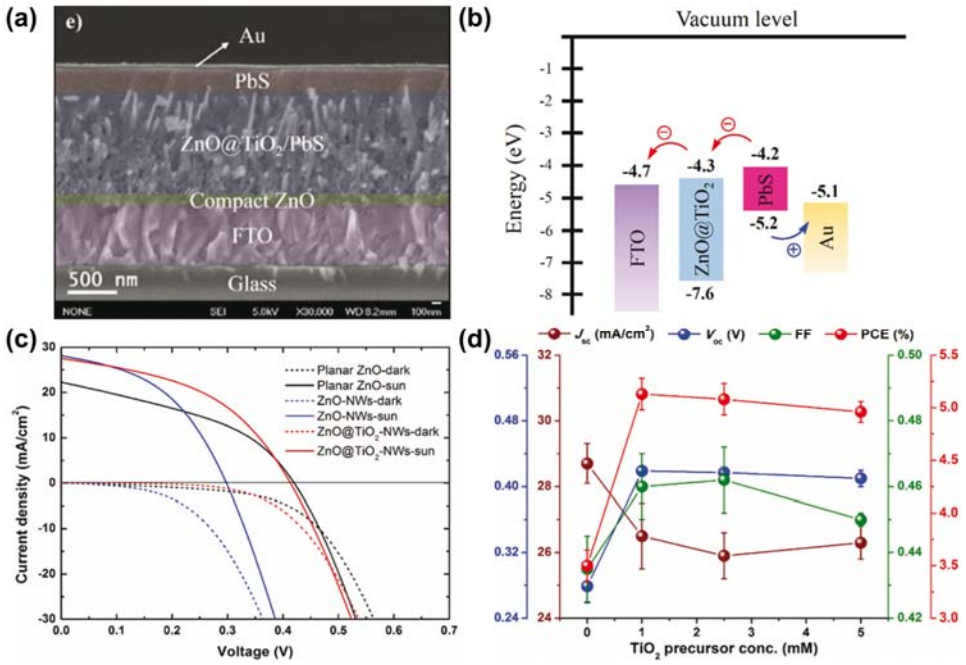

Figure 9. (a) Cross-sectional SEM image of a PbS QD sensitized-ZnO/TiO_2 NW BHQDSC. (b) Corresponding schematic energy band diagram. (c) J-V curves under darkness (dashed lines) and under illumination (AM 1.5G, solid lines) of PbS QD sensitized-planar ZnO, PbS QD sensitized-ZnO NW and PbS QD sensitized-ZnO/TiO_2 NW BHQDSCs. (d) Effects of the TiO_2 precursor concentration on the J_{SC}, V_{OC}, FF, and PCE values of the PbS QD sensitized-ZnO/TiO_2 NW BHQDSC. Reprinted with permission from [152]. Copyright 2015 Royal Society of Chemistry.

Interestingly, Rekemeyer *et al.* developed an efficient band alignment engineering approach in PbS QDs with a first exciton absorption peak at 1.3 eV, by using a multi-step ligand exchange process [154]. ZnO NWs were fully impregnated with PbS QDs capped with iodide anions while an upper layer composed of PbS QDs capped with 1,2-ethanedithiol (EDT) ligands forming a conduction band offset of 0.2 eV was formed on the top. The presence of both ligands permits the electronic energy levels of PbS QDs to be engineered forming a conduction band offset of 0.2 eV between the two types of QDs that is favorable for charge carrier collection. The resulting champion BHQDSCs exhibited a J_{SC}, V_{OC}, and PCE of 29.4 mA/cm^2, 570 mV, and 9.6%, respectively. More recently, the same group deeply optimized the dimensions of ZnO NWs (*i.e.* number density, diameter, length) for improving the performances of the resulting BHQDSCs as presented in figure 8(a-d), and also investigated the effects of the addition of a thin TiO_2 passivating layer over ZnO NWs [148]. The introduction of Ag nanocubes (NCs) with a side length around 80 nm was also achieved by Kawawaki *et al.* to benefit from strong optical far-field scattering and intense optical near-field at their edges and vertices [155]. The resulting BHQDSCs involving bromide anion-capped PbS QDs and ZnO NWs had an improved PCE of 6.03% with an increased external quantum efficiency in the wavelength range from 700 to 1200 nm. In order to open the way for the fabrication of multijunction solar cells

integrating BHQDSCs as the bottom subcells, Wang *et al.* tuned the size of PbS QDs capped with bromide anions over a broad range such that the first exciton absorption peak was varied from 1.32 to 0.67 eV [156]. The V_{OC} of 253 mV was reported for a photocurrent onset of 0.64 eV, which is as efficient as in germanium solar cells used in III-V semiconductor triple-junction solar cells. Eventually, the BHQDSCs were recently mounted on flexible PET substrates, further showing a good bending durability [157].

Photoanode	QDs	Ligand	J_{SC} (mA/cm^2)	V_{OC} (mV)	FF	PCE (%)	Ref.
ZnO NWs	PbSe	EDT	18.6	420	0.25	1.97	[147]
ZnO NWs	PbS	BDT	17.9	600	0.4	4.3	[19]
ZnO NWs	PbS	Br	34.47	361	0.488	6.076	[149]
ZnO NWs / TiO_2	PbS	Br	30.7	420	0.478	6.16	[152]
ZnO NWs / $Mg(OH)_2$	PbS	Br	21.51	520	0.450	5.04	[153]
ZnO NWs	PbS	EDT/TBAI	29.4	570	0.57	9.6	[154]
ZnO NWs / Ag NCs	PbS	Br				6.03	[155]
ZnO NWs	PbS (0.67eV)	Br	6.9	253	0.389	0.67	[156]
ZnO NWs*	PbS	EDT/TBAI	17.81	490	0.435	3.81	[157]

* Flexible BHQDSC

Table 4. PV performances of the BHQDSCs integrating ZnO NWs.

4. Organic / hybrid solar cells

Background of organic / hybrid solar cells

Many efforts have been devoted, over the last two decades, to developing organic solar cells (OSCs) based on π-conjugated polymers, owing to their low cost and potential compatibility with roll-to-roll processing using solution deposition techniques as well as with flexible substrates. The first demonstration of the generation of a significant photocurrent in an OSC made of a bilayer heterostructure was achieved by Tang *et al.* in 1986 [158]. The OSCs were then designed and optimized following the conventional bulk-heterojunction configuration introduced by Yu *et al.* [159] and Halls *et al.* [160] in 1995. The active layer, comprising a blend of p-type polymer donor and n-type fullerene-derivative acceptor deposited by spin coating, is sandwiched between a TCO / glass substrate acting as the anode and a low-work function metal (typically aluminum) as the cathode. It basically forms a percolated interpenetrating network following a post-deposition annealing: electron-hole pairs are photo-generated in the active layer to form tightly bound Frenkel excitons with a low diffusion length of 10 – 20 nm, which are further separated in the donor-acceptor interfacial area [161] [162]. Charge carrier transport subsequently occurs in

polymers with a low mobility, strongly limiting the optimal thickness of the active layer around 100 – 200 nm [161] [162]. Electrons and holes are eventually collected by the TCO and metal, respectively. Maximizing the interfacial area as well as improving the optical absorption in the active layer have thus been considered as some of the major issues. In this respect, many efforts have been devoted to narrowing the band gap energy of organic semiconductors [163] or using alternative approaches including tandem OSCs [164] [165] [166] and multiple polymer donors and fullerene derivative acceptors [167]. The highest PCE above 12% was reported in the conventional bulk-heterojunction configuration. However, the low long-term stability [168], originating from the aluminum oxidation when exposed to air and moisture as well as from the poor interface between the PEDOT:PSS layer acting as the anode buffer layer and ITO, has been a significant drawback [169] [170] [171]. This has resulted in the development of the OSCs in the inverted bulk-heterojunction configuration (*i*OSCs) which also uses a polymer blend (*i.e.* typically P3HT:PCBM) [172] [173] and of the hybrid solar cells (HSCs) when a single p-type polymer donor is employed (*i.e.* typically P3HT): the active layer is sandwiched between a TCO / glass substrate acting as the cathode and a high-work function metal (typically silver or gold) acting as the anode. An improved ambient stability of the OSCs resulted from the *i*OSCs, in which the vertical phase separation was also reported to be favorable to accumulate the p-type polymer electron donor and n-type fullerene-derivative electron acceptor at the top (close to the anode) and bottom (close to the cathode) of the active layer, respectively [173]. A cathode buffer layer between the TCO / glass substrate and the active layer has also emerged as an essential element in both *i*OSCs and HSCs i) to extract electrons and act as an efficient ETM while blocking the reverse hole flow, ii) to hamper any detrimental reactions between the active layer and the cathode, and, if possible, iii) to improve optical absorption using light trapping phenomena [174] [175] [176]. ZnO has rapidly appeared as a potential outstanding cathode buffer layer for both *i*OSCs and HSCs, further exhibiting highly appropriate energy level position and alignment with the active layer. From density-functional and hybrid-functional calculations, Noori *et al.* showed the large offset between the valence band maximum (VBM) of ZnO and the highest occupied molecular orbitals (HOMO) of P3HT, which is favorable to act as a large hole injection barrier [177]. This was confirmed by x-ray photoelectron spectroscopy measurements [178]. Also, it was stated that a band offset larger than 1.5 eV may be reached by carefully optimizing the ZnO / P3HT interface [177] [178]. From hard x-ray photoelectron spectroscopy measurements, the magnitude of the V_{OC} is also expected to depend on the polarity of ZnO, the Zn-polar ZnO / P3HT interface giving a larger V_{OC} than the O-polar ZnO / P3HT interface [179]. The description of the recombination kinetics is basically similar

in both *i*OSCs and HSCs integrating ZnO NWs [180]. Shirakawa *et al.* introduced, for the first time, a ZnO film grown by sputtering as the cathode buffer layer in an *i*OSC comprising the C_{60} and PAT6 bilayer heterostructure in 2004 [181]. White *et al.* then fabricated an *i*OSC comprising the standard bulk-heterojunction P3HT:PCBM blend and a ZnO film grown by the sol-gel process as the cathode buffer layer, exhibiting a PCE as high as 2.58% [182]. Additionally, the possibility to improve the performances and stability of *i*OSCs, when a ZnO film is incorporated and treated by fluorine plasma [183] or annealing under hydrogen atmosphere [184], or coated with dielectric ultrathin layers [185], also strengthens the need for investigating ZnO NW-based *i*OSCs and HSCs. In order to maximize optical absorption while allowing for efficient charge carrier management, Olson *et al.* showed, for the first time, the integration of ZnO NWs into *i*OSCs composed of the P3HT:PCBM blend and with no anode buffer layer, reporting a J_{SC}, V_{OC}, FF, and PCE of 10.0 mA/cm^2, 475 mV, 0.43, and 2.03%, respectively [20]. The same approach was used by the mentioned group to fabricate HSCs composed of ZnO NWs with the single P3HT polymer donor, leading to a J_{SC}, V_{OC}, FF, and PCE of 2.2 mA/cm^2, 440 mV, 0.56, and 0.53%, respectively [20]. From then on, the development of *i*OSCs and HSCs integrating ZnO NWs has received an increasing interest: a significant difference is that charge carrier separation occurs at the P3HT / PCBM interface for *i*OSCs and at the ZnO NW / P3HT interface for HSCs. The band alignment at the ZnO NW / P3HT and ZnO NW / PCBM interfaces was deeply investigated, as a pre-requisite to fabricate *i*OSCs and HSCs with a higher PCE [186]. A Fermi level pinning behavior at the ZnO NW / PCBM interface with a large interface dipole was revealed from x-ray and ultraviolet photoelectron spectroscopy measurements, which was in contrast to the Fermi level unpinning behavior at the ZnO NW / P3HT interface, as shown in figure 10 [186]. Additionally, the introduction of ZnO NWs increases the offset between the VBM of ZnO NWs and the HOMO of P3HT, namely the hole injection barrier from P3HT to ZnO NWs, which is in contrast to the ZnO NW / PCBM interface where the introduction of ZnO NWs has no effect. From photoluminescence measurements, Chan *et al.* showed the occurrence of a radiative emission around 1.3 eV, which was assigned to the type II radiative transition between electrons in the CBM of ZnO NWs that recombine with the holes in the HOMO of P3HT [187].

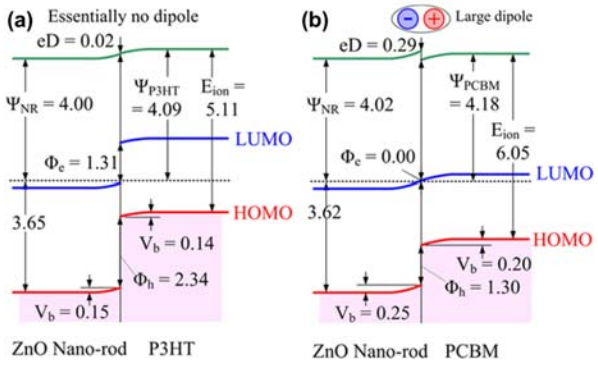

Figure 10. Energy band diagrams for (a) P3HT on ZnO NWs and (b) PCBM on ZnO NWs. Ψ is the work function, E_{ion} is the ionization energy, E_g is the band gap energy, eD is the interface dipole, V_b is the band bending, Φ_e is the electron barrier, and Φ_h is the hole barrier. Reprinted with permission from [186]. Copyright 2012 American Chemical Society.

The development of the *i*OSCs integrating ZnO NWs with the P3HT:PCBM blend have further been achieved using electrochemical [188] and electrospinning [189] deposition techniques. The use of a CuPc:C_{60} / CuPc blend with smaller molecules was also assessed in *i*OSCs, showing a J_{SC}, V_{OC}, FF, and PCE of 3.86 mA/cm^2, 460 mV, 0.30, and 0.53%, respectively [190]. Subsequently, the integration of ZnO NWs into *i*OSCs and HSCs have largely been investigated, by focusing on the contact issue, elucidation of the effects of the morphology and properties of ZnO NWs as well as on the optimization of the ZnO NW / active layer interface. The PV performances of both *i*OSCs and HSCs incorporating ZnO NWs are gathered in Tables 5 and 6 and commented in the following sections.

Effects of the anode and cathode

Some attention has been dedicated to optimizing the electron collection at the cathode. Instead of using ITO glass / substrate, Hu *et al.* and Reinhard *et al.* employed FTO / glass substrate [191] and PEDOT:PSS / glass substrate [192], respectively. A strong emphasis has been devoted to enhancing the hole collection by introducing an anode buffer layer between the bulk-heterojunction active layer and the anode, acting as an electron injection barrier as well as a protective layer. Kim *et al.* reported a strong improvement of the performances of the *i*OSCs involving ZnO NWs and the P3HT:PCBM blend by introducing a PEDOT:PSS anode buffer layer, resulting in a J_{SC}, V_{OC}, and PCE of 10.02 mA/cm^2, 550 mV, and 2.94%, respectively [193]. The V_2O_5 anode buffer layer can be grown by spin casting of a colloidal solution to strongly improve the performances of the related *i*OSCs, depending on its concentration as shown in figure 11(a) [194]. The use of a VO_x anode buffer layer grown by evaporation also enhances the performances of the *i*OSCs involving ZnO NWs and the P3HT:PCBM blend with a J_{SC}, V_{OC}, and PCE of 10.4 mA/cm^2, 580 mV, and 3.9%, respectively, as presented in figure 11(b) [195]. Wang *et al.* further investigated the use of a MoO_3 anode buffer layer and the effects of its thickness on the performances of the related

*i*OSCs [196]. An optimal thickness of 20 nm was determined, resulting in J_{SC}, V_{OC}, and PCE of 9.02 mA/cm^2, 550 mV, and 2.15%, respectively. Furthermore, Unalan *et al.* presented the fabrication of flexible HSCs incorporating ZnO NWs with a PCE of 0.6% by using single walled carbon nanotube / PET substrates [197]. Tong *et al.* also showed the fabrication of flexible *i*OSCs integrating ZnO NWs by using PET substrate, reporting a J_{SC}, V_{OC}, FF, and PCE of 9.82 mA/cm^2, 520 mV, 0.35, and 1.78%, respectively [198].

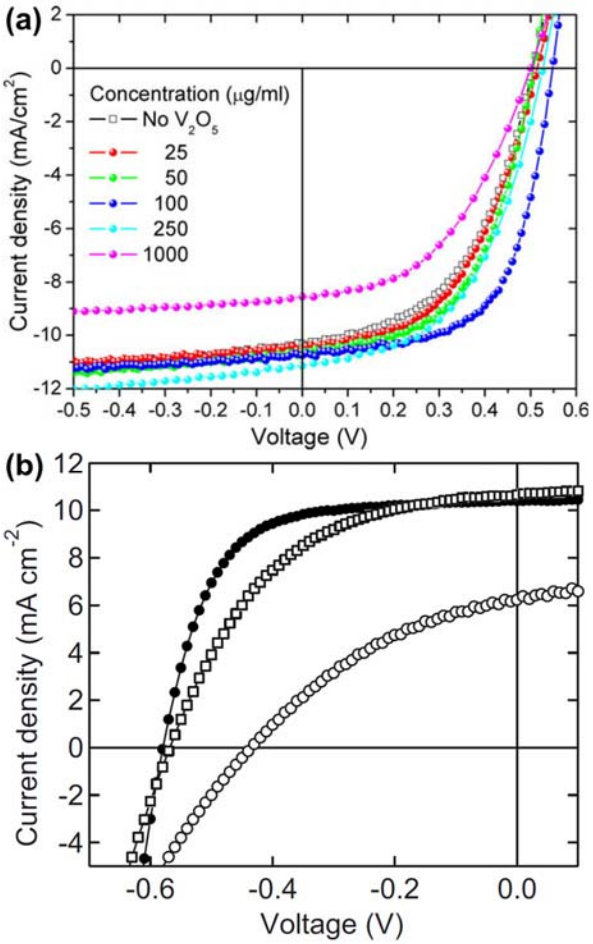

Figure 11. (a) J-V curves under illumination (AM1.5G) of Ag/V_2O_5/P3HT:PCBM/ZnONW/ITO *i*OSCs for various solution concentration for the V_2O_5 interlayer. Reprinted with permission from [194]. Copyright 2009 Elsevier. (b) J-V curves under illumination (AM 1.5G) of the Ag/P3HT:PCBM/planar-ZnO/ITO (open circles), Ag/VO_x/P3HT:PCBM/planar-ZnO/ITO (open squares), and Ag/VO_x/P3HT:PCBM/ZnONW/ITO (closed circles) *i*OSCs. Reprinted with permission from [195]. Copyright 2008 American Institute of Physics.

Effects of the morphology of ZnO nanowires

The morphology and properties of ZnO NWs in terms of dimensions (*i.e.* length, diameter, number density) and vertical alignment are typically tunable by either changing the morphology of the ZnO seed layer [199] [200] [201] or by changing the conditions used during the CBD [202] [203] [204]. There have been a lot of works tentatively

assessing the effects of the morphology and properties of ZnO NWs over the performances of the related *i*OSCs and HSCs.

Variation of the morphology of the ZnO seed layer

Peiró *et al.* investigated the effects of the chemical route (*i.e.* sol-gel dip coating and spin coating methods, spray pyrolysis) to prepare the ZnO seed layer acting as the hole blocking layer over the morphology of ZnO NWs and the performances of the resulting HSCs comprising MEH-PPV-based polymer and P3HT [205]. Baeten *et al.* tuned the diameter of ZnO NWs by varying the morphology of the ZnO seed layer grown in deionized water, resulting in the fabrication of HSCs comprising the P3HT polymer donor with a J_{SC}, V_{OC}, FF, and PCE of 2.64 mA/cm^2, 565 mV, 0.55, and 0.82%, respectively [206]. In contrast, Whittaker-Brooks *et al.* revealed the advantage of the sputtering technique over the standard sol-gel process to form compact ZnO seed layer perfectly oriented along the *c*-axis and thus favoring the morphology of ZnO NWs [207]. The PCE of the resulting HSCs comprising the P3HT polymer donor reached 1.64 %. Lee *et al.* varied the thickness of the ZnO seed layer while keeping constant the length of ZnO NWs to reveal its effect on the performances of the resulting flexible *i*OSCs [208]. They showed that an intermediate thickness is needed to get a good compromise between an efficient compactness (required to limit the shunt path between ITO and the P3HT:PCBM blend) and a limited series resistance. Later on, the vertical alignment and spacing of ZnO NWs was found to be critical to increase the interfacial area and to strongly affect the performances of the resulting *i*OSCs *via* the good infiltration of the P3HT:PCBM blend [209]. Even when the electrochemical deposition technique was used to form ZnO NWs on ITO / glass substrates, the presence of an optional ZnO seed layer was reported to be beneficial for improving their morphology [210].

Variation of the growth conditions of ZnO nanowires

Besides the variation of the morphology of the ZnO seed layer, the morphology of ZnO NWs has largely been tuned by changing the conditions used during the CBD in order to assess the effects on the performances of the resulting *i*OSCs and HSCs. These have, to some extent, been under debate for a long time and appear to strongly depend on the nature of the solar cells considered, either the *i*OSCS or HSCs integrating ZnO NWs.

By prolonging the growth time of ZnO NWs and hence by increasing their length up to 350 nm, Takanezawa *et al.* reported a correlated increase in the FF and PCE from 0.38 to 0.47 and 1.6 to 2.4%, respectively, in the *i*OSCs composed of the P3HT:PCBM blend, as shown in figure 12(a-g) [211]. The independence of the J_{SC} on the length of ZnO NWs was related to efficient charge carrier separation occurring at the P3HT / PCBM interface, rather than

proceeding at the minor ZnO NW / P3HT interface [212]. Correlatively, Gonzalez-Valls *et al.* showed that the performances of the *i*OSCs are degraded as the length of ZnO NWs is further increased from 0.4 to 5.2 µm, possibly due to a poorer infiltration of the P3HT:PCBM blend [213]. The correlation of the length of ZnO NWs with the PCE of the related *i*OSCs comprising the P3HT / PCBM blend was nevertheless questioned by Ogawa *et al.*, by compiling the experimental data reported in the literature [214]. In contrast to the *i*OSCs, Olson *et al.* reported that the J_{SC} (and related PCE) of the HSCs composed of the P3HT polymer donor is increased with the length of ZnO NWs from 250 to 500 nm [215]. Correlatively, Guo *et al.* stated that the J_{SC} of the HSCs comprising the MEH-PPV polymer donor is increased with the length of ZnO NWs from 170 to 400 nm while the electron lifetime is shorter [216]. A similar increase in the J_{SC} and PCE as the length of ZnO NWs is increased from 300 to 600 nm was reported by Baeten *et al.* in the performances of HSCs comprising the P3HT polymer donor as presented in figure 12(h), leading to a PCE of 0.76% by further optimizing the anode and buffer layer thicknesses [217]. However, as the length of ZnO NWs is further increased to 1000 µm, the PCE was found to strongly decrease. Interestingly, the diameter and vertical alignment of ZnO NWs was also found to strongly affect the performances of the HSCs comprising the P3HT polymer donor. By combining intensity modulated photocurrent spectroscopy measurements with theoretical computations, Wu *et al.* stated that the optimal length and technologically challenging spacing of ZnO NWs in the HSCs composed of the MEH-PPV polymer donor are about 500 nm and 5-10 nm, respectively, for favoring efficient exciton generation and dissociation along with charge carrier transport and collection [218].

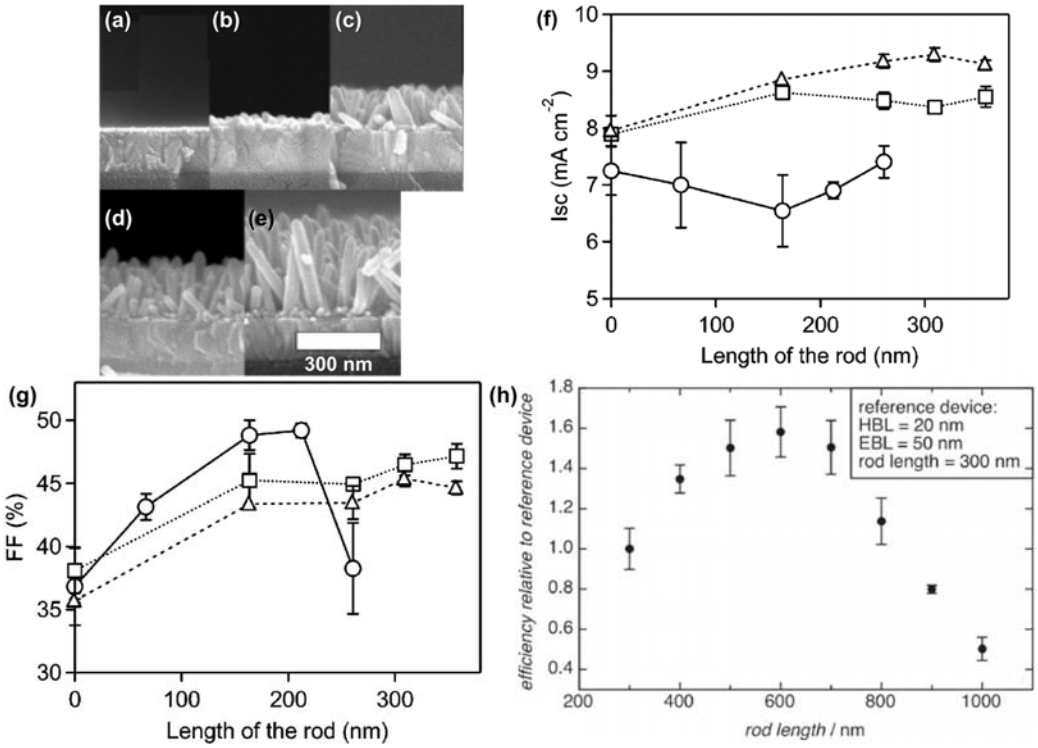

Figure 12. (a-e) Cross-sectional SEM images of ZnO nanostructures deposited by CBD on ITO layer for a growth time of (a) 0, (b) 40, (c) 60, (d) 80 and (e) 100 min. (f, g) I_{SC} and PCE, respectively, measured under AM 1.5G illumination of ZnO NW/P3HT:PCBM *i*OSCs as a function of the ZnO NW length. Optical densities of the films at 510 nm: 1.1 (circles), 1.3 (squares), and 1.6 (triangles). Reprinted with permission from [211]. Copyright 2007 American Chemical Society. (h) PCE relative to the reference device of ZnO NW/P3HT HSCs as a function of ZnO NW length. HBL and EBL stand for hole and electron blocking layers, respectively. Reprinted with permission from [217]. Copyright 2011 Wiley & Sons.

The variation of the interfacial area enhancement factor was revealed as the main morphological parameter to be considered in the case of HSCs, the morphology having negligible effects on the recombination kinetics [219]. Lee *et al.* further emphasized the significance of leaving enough spacing between ZnO NWs to improve the crystallinity of P3HT in HSCs, although being at the expense of the interfacial area [220]. Correlatively, Yun *et al.* showed the improvement of the infiltration of the P3HT:PCBM blend by using ZnO NWs with a low number density, resulting in a significant increase in the PCE of the related *i*OSCs from 2.8 to 4.07% [221]. Ho *et al.* performed a two-step hydrothermal growth of ZnO NWs in this respect: the first step was applied to define the density of ZnO NWs while the second step was used to lengthening the ZnO NWs while limiting their radial growth [222]. This approach led to a strong increase in the performances of the related *i*OSCs comprising the PBDTTT-C-T / $PC_{71}BM$ and PTB7 / $PC_{71}BM$ blends, resulting in the high PCE of 7.80 and 8.01 %, respectively.

Effects of the properties of ZnO nanowires

The effects of the properties of ZnO NWs on the performances of the related HSCs have more recently been pointed out, typically by introducing additional elements in the lattice of ZnO through extrinsic doping [223] [224] [225] [226] [227]. Li [223], Al [224], Mg [225], Ga [226], and Bi [227] dopants have been suggested to be incorporated in the lattice of ZnO NWs grown by CBD, further resulting in a strong effect on their morphology. Overall, an increase in the performances of the related HSCs has been reported with an optimal dopant content in the range of several percent. The modification of the barrier height between the ITO / glass substrate and the ZnO NWs was proposed following the Li doping to account for an increase in the V_{OC} while an oxygen-enrichment of the surface of ZnO NWs was suggested to explain the increase in the J_{SC} [223]. Both the morphology change of ZnO NWs due to doping for enhancing the interfacial area, and a modification of the nature and density of intrinsic and extrinsic point defects along with prolonged charge carrier recombination lifetime and reduced leakage current have been emphasized in the cases of Mg, Ga, and Bi doping to account for the increase in the V_{OC} and J_{SC} of the related HSCs involving the P3HT polymer donor [225] [226] [227].

Effects of the polymer preparation

A critical issue in both *i*OSCs and HSCs is related to the infiltration and self-ordering of the polymer into ZnO NW arrays and hence to the related efficient electron injection. In that respect, the polymer preparation has been reported to strongly affect the properties of that infiltration and self-ordering.

Olson *et al.* revealed that the use of dichlorobenzene, as a high boiling point and low pressure vapor solvent, instead of chloroform significantly improved the P3HT infiltration into the ZnO NWs and presumably its self-ordering [228]. They further showed that a post-deposition annealing at the melting temperature of 225 °C further enhances the P3HT infiltration, leading to a HSCs with a J_{SC}, V_{OC}, FF and PCE of 1.33 mA/cm^2, 443 mV, 0.484, and 0.28%, respectively. The corresponding EQE is shown in figure 13(a). Interestingly, the performances of the HSCs are also drastically improved by the storage in air for five days thanks to beneficial ageing effects. Baeten *et al.* stated that the HSCs comprising the pristine P3HT polymer donor showed a lower PCE than the HSCs with an annealed P3HT polymer donor for 1 min at the melting temperature of 225°C [217]. This was attributed to an improvement of the crystallinity of the polymer. A prolonged annealing time was found to be detrimental, likely because of the ordering of the polymer chains along the 10-10 direction. The same group then revealed that increasing the annealing time is responsible for a significant decrease in the charge carrier density and lifetime, further pointing out that the intimate contact between the ZnO NWs and P3HT polymer donor is crucial [219]. To

make the HSCs more eco-friendly, Baeten *et al.* further proposed a full water-processable HSCs by replacing chlorobenzene, chloroform and toluene solvents by water and using the P3PHT polymer donor [229].

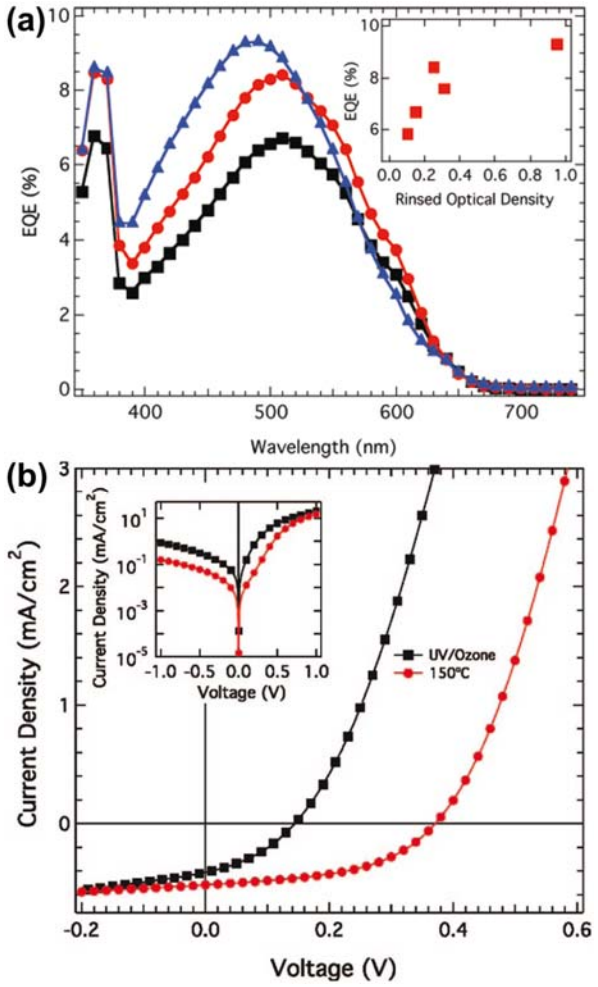

Figure 13. (a) EQE spectra of ITO/ZnO NW/P3HT/Ag HSCs: not annealed (black squares), annealed at 150°C (red circles), and annealed at 225°C (blue triangles). The inset shows the EQE as a function of optical density of the corresponding devices. Reprinted with permission from [228]. Copyright 2007 American Chemical Society. (b) J-V curves under illumination (AM 1.5G) of ITO/ZnO/P3HT/Ag bilayer HSCs. The ZnO layer is treated with UV/Ozone (black squares) or heated at 150°C (red circles) prior to depositing the P3HT. The inset shows the corresponding J-V curves under darkness. Reprinted with permission from [230]. Copyright 2008 American Chemical Society.

In the case of ZnO NW-based *i*OSCs, Takanezawa *et al.* revealed the dependence of the thickness of the P3HT:PCBM blend on the solution concentration ratio from 1.0:0.3 to 1.0:0.8, reporting an optimal ratio of 1.0:0.6 [211]. Chou *et al.* stated that the increase in the polymer solidification time, for instance by decreasing the spin-coating rate, can thicken the P3HT:PCBM blend as well and favor its self-organization and infiltration into ZnO NWs [231]. The PCE of the related *i*OSCs composed of the P3HT:PCBM blend was found to continuously increase from 1.58 to 3.58 % by prolonging the polymer drying time from 5 to 54 min. Gonzalez-Valls *et al.* moreover

investigated the effects of the solvents used on the polymer thickness and morphology, which are expected to induce ordering / disordering of the side-chains of the polymer involved [213]. Furthermore, the use of chemical additives in the P3HT:PCBM blend has been developed to improve the stability of the related ZnO NW-based HSCs. Sung *et al.* showed that the addition of 3-hydroxyflavone (3-HF) with the appropriate concentration increases the J_{SC} of the related *i*OSCs composed of the P3HT:PCBM blend and correlatively the PCE from 2.57 to 3.05% [232]. The stability of the HSCs was also improved significantly, the PCE decreasing by only 15% over one month.

Effects of the interface quality between the ZnO nanowires and polymer

The interface quality between the ZnO NWs and polymer appears as one of the major and widely investigated issue for both *i*OSCs and HSCs. In order to i) passivate the surface defects of ZnO NWs and reduce the interfacial recombination, as well as to ii) favor the wettability of ZnO NWs by the polymer solution for improving the infiltration and facilitating an intimate contact between the ZnO NWs and polymer, both of them as a pre-requisite for the efficient electron injection from the polymer to the ZnO NWs, many investigations have reported the need for performing post-deposition treatments over ZnO NWs and/or forming core-shell like heterostructures.

Post-deposition heat treatments

Olson *et al.* investigated how two different post-deposition treatments of ZnO NWs affects their surface properties and the performances of the resulting HSCs comprising the P3HT polymer donor, as presented in figure 13(b) [230]. A UV/ozone post-deposition treatment to remove organic contaminations was found to strongly improve the wettability of the polymer solution, but with no effect on its crystallinity. In contrast, a significant difference in the contact potential of 0.4 ± 0.1 eV of the surface of ZnO NWs when processed under UV/ozone treatment as compared to the annealing at 150 °C for 20 min was attributed to a surface dipole change that, in turn, affects the interfacial band alignment between the ZnO NW and P3HT polymer donor. This had a highly detrimental effect on the V_{OC} and PCE of the resulting HSCs where ZnO NWs were exposed to the UV/ozone treatment. The same approach was used by Leow *et al.* by varying the UV irradiation time at room temperature from 15 to 60 min to activate the photocatalytic reaction required to decompose organic contaminants [233]. It was revealed that the J_{SC} of the HSCs composed of the P3HT polymer donor continuously increases with the irradiation time while the V_{OC} first decreased strongly and then continuously increases as well. A deep investigation of the defects in ZnO NWs, namely oxygen and zinc vacancies, and their relationship with the annealing in air and under zinc vapor atmosphere was reported by Iza *et al.*, along with their effects on the performances of the resulting *i*OSCs [234]. It was shown

that the V_{OC} and PCE of the *i*OSCs are strongly increased from 20 to 450 mV and 0.04 to 1.34%, respectively, by raising the annealing temperature from 100 to 400 °C in air as a result of the vanishing of the zinc hydroxide layer on the surface of ZnO NWs, but no correlation with the density of surface defects like vacancies was carried out.

Inorganic core-shell heterostructures

An alternative approach for passivating surface defects consists in depositing an inorganic semiconducting shell, such as TiO_2 [220] [235] [236] [237], ZnS [238], and ZnO [239]. Greene *et al.* covered the ZnO NWs with a TiO_2 shell in a thickness range of 1-28 nm using atomic layer deposition, as shown in figure 14(a) [235]. The V_{OC}, FF, and PCE of the related HSCs composed of the P3HT polymer donor were found to strongly increase following the addition the TiO_2 shell with a thickness in the optimal range of 5-10 nm, as revealed in figure 14(b,d). The deposition of the TiO_2 shell was also achieved by soaking the ZnO NWs in a $TiCl_4$ solution heated at 70 °C and by subsequent annealing at 400 °C, resulting in the increase the J_{SC} and FF of the related HSCs composed of the P3HT polymer donor [236]. From transient absorption measurements, the interfacial recombination was found to be slower when the ZnO NWs are covered with the TiO_2 shell, the latter further helping in the P3HT infiltration. The deposition of a TiO_x amorphous shell was made by Lee *et al.* using a spin coating method and the V_{OC} of the related HSCs comprising the P3HT polymer donor was also shown to continuously increase from 400 to 800 mV by thickening the shell up to 5 nm, in correlation with the significant decrease in the reverse-bias current density [237]. In contrast, the same exciton decay dynamics suggested here the passivation of the surface defects of ZnO NWs, rather than changes in the bulk recombination dynamics. A shell composed of ZnO nanoparticles deposited by spin coating over ZnO NWs was revealed, from transient photo-voltage measurements, to also slow down the interfacial recombination by increasing the electron lifetime [239]. The related *i*OSCs comprising the P3HT:PCBM blend reached a J_{SC}, V_{OC}, FF, and PCE of 13.75 mA/cm^2, 570 mV, 0.52, and 4.1%, respectively.

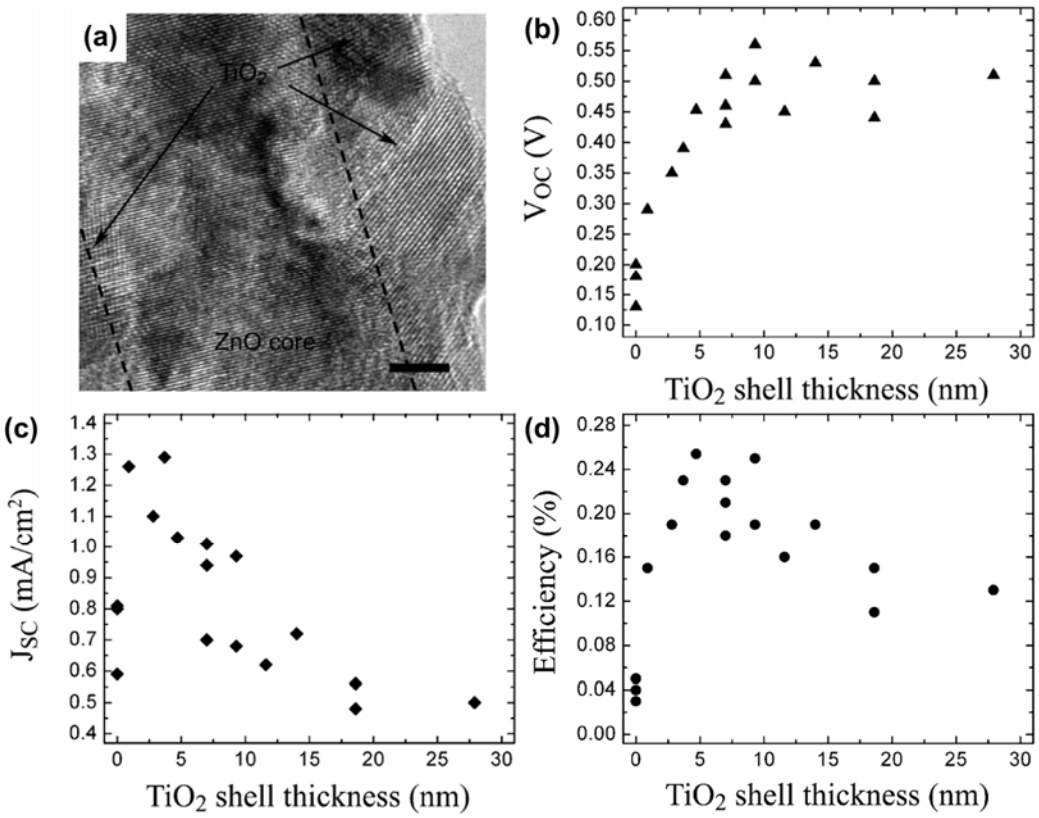

Figure 14. (a) HRTEM image of a ZnO/TiO_2 core-shell NW heterostructure. The ZnO core is outlined with dashed lines. Scale bar, 5 nm. (b, c, d) V_{OC}, J_{SC}, and PCE, respectively, of ZnO/TiO_2NW/P3HT HSCs as a function of the TiO_2 shell thickness. Reprinted with permission from [235]. Copyright 2007 American Chemical Society.

Hybrid core-shell heterostructures

A widely investigated approach further consists in modifying the surface properties of ZnO NWs by using chemical dyes (*i.e.* ruthenium based- and organic dyes) [205] [224] [240] [241] [242] [243] [244] [245], fullerene derivative-based interlayers [246] [247] [248] [249] or organic interlayers including the so-called self-assembled monolayers (SAMs) and small molecular layers (SMLs) [250] [251] [252] [253] [254] [94-99].

Ruthenium-based dyes including Z907 [205] [224] [240] and N719 [242] were used to modify the surface properties of ZnO NWs. In HSCs composed of either the P3HT [205] or MEH-PPV [240] polymer donor, the Z907 dye was found to improve the wettability of the ZnO NWs for better polymer infiltration and charge separation at the interface, but not to significantly contribute to the overall optical absorption. Similarly, the Rattanavoravipa *et al.* showed in *i*OSCs composed of the P3HT:PCBM blend that the N719 dye does not contribute to the photocurrent generation, but significantly increases the J_{SC} and V_{OC} by improving the electron transfer and transport [242]. Alternatively, organic dyes, including Eosin-Y [243] [244] [245], indoline D205 and squaraine [241] dyes, as eco-

friendly, easily purchased and inexpensive dyes have also been employed to alter the surface properties of ZnO NWs.

The introduction of a C_{60} interlayer on the top of ZnO NWs has also been investigated in relation to the performances of the resulting *i*OSCs [246] [247] [248] and HSCs [249]. The PCBM interlayer was found to improve the optical absorption of the *i*OSCS composed of the P3HT:PCBM blend by enhancing its self-organization and infiltration, resulting in an increase in the J_{SC} and PCE to 11.67 mA/cm^2 and 3.2%, respectively [246]. Chen *et al.* further revealed that the C_{60} interlayer assists the exciton separation at the interface and passivates the defect states on the surface of ZnO NWs, enhancing in turn the performances of the *i*OSCs composed of the P3HT:PCBM blend [247]. An improvement was also stated by Riedel *et al.* by inserting a C_{60} interlayer in *i*OSCs composed of the ZnPc:C_{60} blend [248]. Recently, the passivation of the defect states on the surface of ZnO NWs by a C_{60} pyrrolidine tris-acid interlayer was shown to have beneficial effects on the performances of the HSCs comprising the P3HT polymer donor [249].

Chen *et al.* synthesized an amine and bromine terminated 3-hexyl thiophene oligomer with a dual function, the amine functional group having a good affinity to ZnO NWs while its structure being close to P3HT for better interfacial compatibility in *i*OSCs [251]. Whittaker-Brooks *et al.* developed the adsorption of SAMs *via* the use of arylphosphonic acid derivatives for modifying the surface properties of ZnO NWs [252]. The resulting passivation of the surface defects of ZnO NWs as well as the improvement of the wettability by P3HT led to an enhancement of charge carrier transfer and a reduction of charge carrier recombination. The related HSCs composed of the P3HT polymer donor exhibited an increased J_{SC} and PCE of 12.01 mA/cm^2 and 2.05%, respectively. Ben Dkhil *et al.* more recently reported the use of ligands over ZnO NWs to deposit the aggregate-free P3HT polymer donor, resulting in an improvement of the performances of the related HSCs [254].

Advanced properties and alternative architectures

Charge carrier photo-generation and separation at the interface between the ZnO NWs and polymer have appeared as a major issue in both *i*OSCs and HSCs. Alternative ways to improve the management of charge carriers at the interface has recently arisen from the exploitation of the piezoelectric and pyroelectric properties of ZnO NWs crystallizing into the wurtzite structure. By contacting a P3HT polymer donor on the top of a single ZnO NW deposited on a flexible PDMS substrate, Yang *et al.* explored the effects of introducing strain on the performances of the related HSC [255]. It was shown that the band structure between ZnO and P3HT can be modified by the

piezo-potential induced by the externally applied strain, favoring in turn the management of charge carriers and hence maximizing the output voltage of the HSC. Shoaee *et al.* reported the enhancement of the J_{SC} and V_{OC} of the HSCs composed of either a P3HT or PCDTBT polymer donor by applying acoustic vibrations using a loudspeaker (75 dB at 1-50 kHz) [256]. The enhancement was shown at the given resonance frequency of ZnO NWs around 10 kHz, improving the PCE from 1.35 to 1.75% as shown in figure 15(a), and attributed to reduced charge carrier recombination losses. A model yielding the modification of the band structure at the interface was proposed as a consequence of applying acoustic vibrations, moving away the ZnO electrons or P3HT holes from the interface as a function of the ZnO polarization, as presented in figure 15(c). More recently, indoor light illumination and temperature were also used to improve the performances of the HSCs composed of the P3HT polymer donor by activating pyro-phototronic effects in ZnO NWs [257].

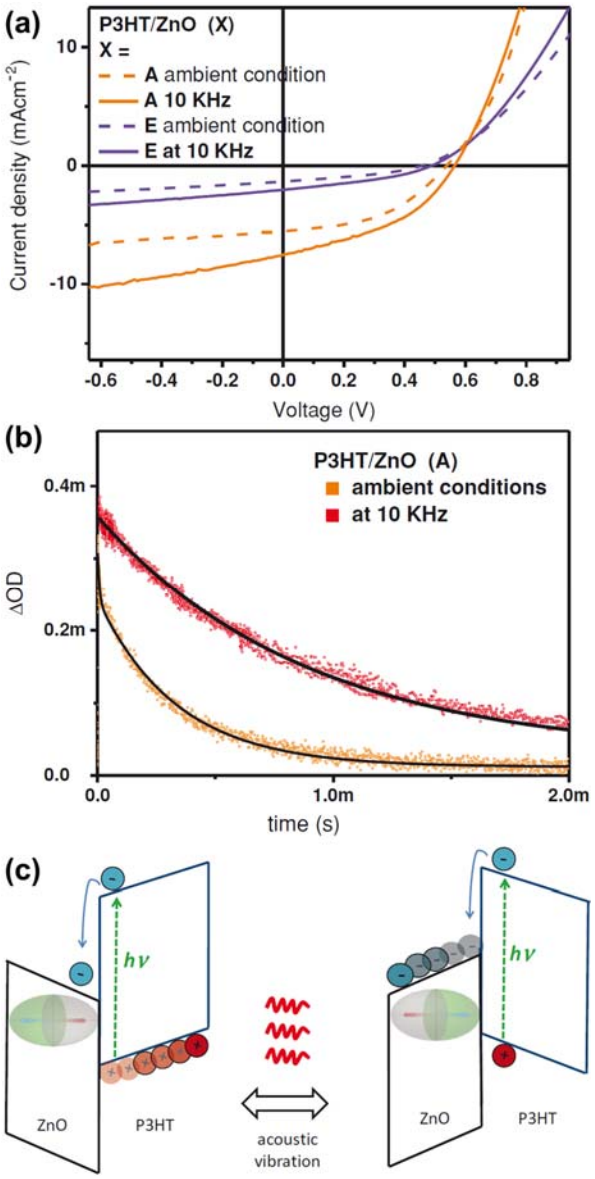

Figure 15. (a) J-V curves under illumination (AM 1.5G) of ZnO NW/P3HT HSCs measured in ambient conditions or under external vibration with a frequency of 10 Hz at 75 dB. The ZnO NWs have an aspect ratio of 38 (A) or 5 (E). (b) Transient absorption signals of ZnO/P3HT HSCs (A) measured in ambient conditions or under external vibration with a frequency of 10 Hz at 75 dB. (c) Schematic of the potential impact of an oscillating acoustic vibration upon photo-induced charge carrier dynamics in the ZnO NW/P3HT HSC in its two opposite/extreme states of polarization. Reprinted with permission from [256]. Copyright 2014 Wiley & Sons.

While most of the *i*OSCs and HSCs integrating ZnO NWs have employed a polymer blend or single polymer in a fully-impregnated configuration for a simple planar back-contact approach, alternative approaches involving the core-shell configuration have been explored as well [258] [259]. Briseno *et al.* reported the fabrication of ZnO / P3HT and ZnO / didodecylquaterthiophene (QT) core-shell NW heterostructures using a self-assembled technique in chlorobenzene solutions [258]. The conformal deposition of the polymer shell all around the ZnO NWs led to the fabrication of single NW HSCs. Iza *et al.* showed the fabrication of *i*OSCs composed of the P3HT:PCBM blend conformally covering the ZnO NWs as a shell [259]. Both J_{SC} and FF were improved in the core-shell configuration with respect to the more standard fully-impregnated configuration, which was attributed to enhanced charge carrier extraction while maintaining the optical absorption at the same level. Alternatively, Ambade *et al.* developed the integration of ZnO NWs in a planar configuration (*i.e.* lying on the ITO / glass substrate) into HSCs and *i*OSCs [260] [261] [262]. The adsorption of SMLs through the use of cyanoacrylic acid derivatives was used for tuning the work function and surface energy of ZnO NWs from 4.40 to 3.98 eV and from 52.5 to 33 mN/m, respectively [262]. The decrease in the work function by thickening the SMLs was associated with the presence of a strong dipole moment pointing away from ZnO NWs, further upshifting the conduction band minimum. The resulting *i*OSCS composed of either the P3HT:PC_{60}BM blend or the PTB7:Th:PC_{71}BM had an increased PCE of 3.68 and 8.0%, respectively, which was mainly attributed to a strong increase in the J_{SC} resulting from the reduced surface energy and larger electron affinity induced by the covalent attachment of the electron withdrawing cyano moiety. In contrast, the resulting HSCs comprising the P3HT polymer donor exhibited an increased PCE of 0.79% originating from a large increase in the V_{OC} related to the reduced work function.

Photocathode	Organic absorbers	Anode	J_{SC} (mA/cm^2)	V_{OC} (mV)	FF	PCE (%)	Ref.
ZnO NWs	P3HT	Ag	2.2	440	0.56	0.53	[20]
ZnO NWs	P3HT	Ag	1.33	440	0.48	0.28	[228]
ZnO NWs	P3HT	Ag	1.24	438	0.47	0.25	[230]
ZnO NWs	P3HT	Ag	2.64	565	0.55	0.82	[206]

ZnO NWs	P3HT	Ag	2.73	544	0.548	0.814	[219]
ZnO NWs	P3HT	Au	9.39	440	0.402	1.64	[207]
ZnO NWs	P3HT	PEDOT:PSS / Ag	2.67	546	0.53	0.76	[217]
ZnO NWs	P3HT	MoO_3 / Ag	3.10	550	0.37	0.65	[233]
ZnO NWs	MEH-PPV	PEDOT:PSS / Au	7.417	162	0.2808	0.337	[216]
ZnO NWs	P3PHT	Ag	0.102	170	0.33	0.0059	[229]
ZnO:Li NWs	P3HT	Ag	1.41	480	0.55	0.37	[223]
ZnO:Al NWs / Z907	MEH-PPV	PEDOT:PSS / Au	5.32	195	0.2771	0.287	[224]
ZnO:Mg NWs	P3HT	Ag	1.57	490	0.47	0.36	[225]
ZnO:Ga NWs	P3HT	Ag	1.98	530	0.42	0.44	[226]
ZnO:Bi NWs	P3HT	Ag	2.87	440	0.47	0.59	[227]
ZnO NWs / TiO_2	P3HT	Au	1.14	500	0.50	0.29	[235]
ZnO NWs / TiO_2	P3HT	Ag	2.91	380	0.50	0.55	[220]
ZnO NWs / TiO_2	P3HT	PEDOT:PSS / Au	0.53	320	0.41	0.070	[236]
ZnO NWs / Z907	P3HT	PEDOT:PSS / Au	1.73	300	0.389	0.20	[205]
ZnO NWs / Z907	TPD(4M)-MEH-M3EH-PPV	PEDOT:PSS / Au	-	-	-	0.15	[205]
ZnO NWs / Z907	P3HT	PEDOT:PSS / Au	2	-	-	0.2	[240]
ZnO NWs / D205	P3HT	VO_x / Ag	1.75	505	0.614	0.546	[241]
ZnO NWs / squaraine	P3HT	VO_x / Ag	5.52	323	0.574	1.02	[241]
ZnO NWs / Eosin-Y	P3HT	Ag	2.30	350	0.49	0.39	[244]
ZnO NWs / C_{60}	P3HT	Ag	2.26	200	0.38	0.167	[249]
ZnO NWs / mercurochrome	P3HT:ZnO NPs	Au	2.51	440	0.41	0.45	[250]
ZnO NWs / CF_3PA	P3HT	Au	12.01	480	-	2.05	[252]
ZnO NWs / FPA	P3HT	Au	11.93	470	-	1.95	[252]
ZnO NWs / HPA	P3HT	Au	10.76	450	-	1.84	[252]
ZnO NWs / OMePA	P3HT	Au	10.41	445	-	1.72	[252]
ZnO NWs / F_2PA	P3HT	Au	9.97	440	-	1.66	[252]
ZnO NWs*	P3HT	PEDOT / Au	-	-	-	0.6	[197]
ZnO NWs	P3HT	Au	5.51	540	-	1.35	[256]
ZnO NWs** vib	P3HT	Au	7.52	570	-	1.75	[256]
ZnO NWs*** sinconf	P3HT	Au	0.32	400	0.28	0.036	[258]
ZnO NWs*** sinconf	QT	Au	0.29	350	0.32	0.033	[258]
ZnO NWs / cyanoacrylic acid****	P3HT	MoO_3 / Ag	1.85	720	0.6	0.79	[262]

* Flexible HSC
** HSC measured under acoustic vibrations at 10 kHz and 75 dB
*** HSC integrating one single ZnO NW in a planar configuration
**** HSC integrating ZnO NWs in a planar configuration

Table 5. PV performances of the HSCs integrating ZnO NWs.

Photocathode	Organic absorbers	Anode	J_{SC} (mA/cm^2)	V_{OC} (mV)	FF	PCE (%)	Ref.

ZnO NWs	P3HT:PCBM	Ag	10.0	475	0.43	2.03	[20]
ZnO NWs	P3HT:PCBM	Ag	9.6	570	0.5	2.7	[211]
ZnO NWs	P3HT:PCBM	Ag	11.7	530	0.58	3.58	[231]
ZnO NWs	P3HT:PCBM	Ag	14.99	480	0.34	2.44	[188]
ZnO NWs	P3HT:PCBM	Ag	7.29	400	0.35	1.02	[191]
ZnO NWs	P3HT:PCBM	Ag	7.28	450	0.4096	1.34	[234]
ZnO NWs	P3HT:PCBM	PEDOT:PSS / Ag	10.02	550	0.53	2.94	[193]
ZnO NWs	P3HT:PCBM	PEDOT:PSS / Ag	11.63	490	0.35	1.96	[213]
ZnO NWs	P3HT:PCBM	MoO_3 / Al	9.02	550	0.44	2.15	[196]
ZnO NWs	P3HT:PCBM	MoO_3 / Ag	8.55	440	0.45	1.71	[209]
ZnO NWs	P3HT:PCBM	MoO_3 / Ag	14.9	560	0.487	4.07	[221]
ZnO NWs	P3HT:PCBM	MoO_3 / Ag	9.4	550	0.661	3.5	[189]
ZnO NWs	P3HT:PCBM	MoO_3 / Al	7.9	580	0.49	2.3	[192]
ZnO NWs	P3HT:PCBM	VO_x / Ag	10.4	580	0.65	3.9	[195]
ZnO NWs	P3HT:PCBM	VO_x / Ag	9.9	580	0.65	3.7	[212]
ZnO NWs	P3HT:PCBM	V_2O_5 / Ag	10.75	550	0.6021	3.56	[194]
ZnO NWs	CuPc:C_{60} : CuPc	PEDOT:PSS / Au	3.86	460	0.30	0.53	[190]
ZnO NWs	PBDTTT-C-T:$PC_{71}BM$	MoO_x / Ag	18.4	733	0.58	7.80	[222]
ZnO NWs	PTB7:$PC_{71}BM$	MoO_x / Ag	17.5	709	0.646	8.01	[222]
ZnO NWs	P3HT:PCBM:x-3-HF	Ag	11.56	590	0.4463	3.05	[232]
ZnO NWs / ZnO	P3HT:PCBM	MoO_3 / Ag	13.75	570	0.52	4.1	[239]
ZnO NWs / N719	P3HT:PCBM	Ag	8.89	570	0.41	2.00	[242]
ZnO NWs / Eosin-Y	MEH-PPV:PCBM	Ag	3.95	530	0.50	1.02	[243]
ZnO NWs / PCBM	P3HT:PCBM	Ag	11.67	550	0.5	3.2	[246]
ZnO NWs / C_{60}	P3HT:PCBM	Ag	11.6	530	0.34	2.09	[247]
ZnO NWs / C_{60}	ZnPc:C_{60}	MoO_3 / Ag	11.2	500	0.50	2.8	[248]
ZnO NWs / O3HT-NH_2	P3HT:PCBM	Ag	8.8	490	0.40	1.73	[251]
ZnO NWs / PSBTBT	P3HT:PCBM	Ag	13.23	547	0.28	2.02	[253]
ZnO NWs*	P3HT:PCBM	MoO_x / Au	9.917	266	0.37126	0.979	[208]
ZnO NWs*	P3HT:PCBM	Ag	9.82	520	0.35	1.78	[198]
ZnO NWs conf**	P3HT:PCBM	Ag	7.28	450	0.4096	1.34	[259]
ZnO NWs / cyanoacrylic acid***	P3HT:$PC_{60}BM$	MoO_3 / Ag	10.06	610	0.6	3.68	[262]
ZnO NWs / cyanoacrylic acid***	PTB7-Th:$PC_{71}BM$	MoO_3 / Ag	14.58	790	0.69	8.00	[262]

* Flexible *i*OSC
** *i*OSC integrating ZnO NWs in a conformal configuration
*** *i*OSC integrating ZnO NWs in a planar configuration

Table 6. PV performances of the *i*OSCs integrating ZnO NWs.

5. Dye-sensitized solar cells

Background of dye-sensitized solar cells

DSSCs are a type of photo-electrochemical system that utilize metal oxide semiconductors and organic/metalorganic-complex dyes. They traditionally incorporate a mesoporous oxide film with adsorbed dye molecules as the light absorbing layer, a liquid electrolyte that contains an I^-/I_3^- redox couple, and a platinized conductive substrate as counter electrode [263] [7]. Similar to the classic mesoporous TiO_2-based DSSC, a ZnO nanoparticle film was initially investigated early in the history of DSSCs, as it provides a large surface area. The pioneering work was performed by Redmond *et al*. in 1994 [264]. They fabricated transparent ZnO film using a sol-gel method and achieved 0.4% PCE. Later on, extensive research has been conducted in ZnO nanostructure-based DSSCs. For ZnO nanoparticles, the highest performances remain around 5% PCE with the record of 6.85% achieved by Saito and Fujihara in 2008 [265]. Percolation theory states that inter-particle hopping is considered to be the main effect to facilitate the electron transport process within a nanoparticle film [266]. An electron is estimated to cross 10^3-10^6 particles when travelling randomly within the network [266]. A lengthy electron-transport path correlates with the increase in the recombination processes between the electrons and the oxidized dye or redox medium in the electrolyte [267]. Thus, one-dimensional single-crystal nanostructured ZnO was proposed to provide a direct electron pathway from electron injection to electron collection, unlike the random transport pathways in nanoparticle films which leads to collisions and trappings at the grain boundary or at the semiconductor/electrolyte interface. Due to this potential benefit, and the ease of production of one-dimensional nanostructures of ZnO at low temperature [268], ZnO NWs have been of great research interest to act as the ETM of DSSCs and their PV performances are gathered in Table 7.

Single ZnO nanowire dye-sensitized solar cells

For the application of DSSCs, the adsorption of the dye to photo-anode and charge transfer between the dye and the photo-anode take place at the interface. It was found that increased active surface area leads to potentially higher degree of dye loading and thus increase of charge carrier generation [269]. It was also suggested that compared to non-nanostructured electrodes, semiconductors grown in the form of nanotubes or NWs, have a higher effective surface area in contact with the dye and electrolyte [7]. However, the specific surface area of ZnO NWs is still much less than that of a mesoporous structure. Lower dye loading causes poor light absorption. In order to achieve a higher degree of dye loading, a number of designs tuning the nanostructures have been demonstrated such as: elongated ZnO NWs [16] [270] or hierarchical structure using secondary growth [17] [271] [272]. For some time, the state-of-the-art performance of purely ZnO NW-based DSSCs (*i.e.* non-hierarchical) was 1.5% reported by Law

et al. [16]. In this work, polyethylenimine (PEI) was added to enhance anisotropic growth of the ZnO NWs to achieve high aspect ratio NWs. This could increase surface area and subsequent dye loading. The average length and diameter of the NWs were measured to be 16-17 μm and 130-200 nm, respectively [16]. Gao *et al*. also reported a similar approach using ammonium hydroxide to change the supersaturation degree of zinc precursors during the growth [273]. ZnO NWs with length of 14 μm and diameter of 120-150 nm were achieved, leading to a PCE of 1.7%. Other structures exceeding this efficiency have also been reported, however they mainly used hierarchical structures. Such structures include, on the one hand, ZnO NWs with a nanoparticle capping network, where the PCE was increased up to 1.75% [274], 1.77% [275], 2.2% [276], and 4.24% [277], and eventually reaches a maximum PCE of 4.74% [278] by engineering the interface with the dye by forming a zinc oxoacetate phase. Other hierarchical structures include as well ZnO NWs with outstretched branches (nanoflower/nanotree) overlayers (1.9% [271], 2.53% [279], 4.08% [280]). The main disadvantage of ZnO as the ETM in a DSSC is the chemical instability: dye precipitation was discovered in ZnO-based DSSCs [281]. Since the Ru complex-based dye was initially engineered for TiO_2 [282], dissolution of ZnO by the acidic carboxylic anchoring group of the sensitizer causes insoluble complexes and precipitation on the surface of ZnO [281]. The precipitates typically block the charge transfer between dye molecules and ZnO thus reducing the charge injection. They can also act as recombination sites leading to overall severe recombination.

Core-shell ZnO nanowire heterostructure dye-sensitized solar cells

To avoid a direct contact between dye molecules and ZnO NWs, core-shell heterostructures with combinations of different metal-oxides (ZnO, Al_2O_3, SiO_2, WO_3, MgO, TiO_2) have been reported [269] [283] [284] [285] [286]. Prior to their use in ZnO NW core-shell heterostructures, a number of metal-oxide combinations had been investigated. In 2003, Palomares *et al*. reported that dip-coated Al_2O_3 on TiO_2 nanocrystalline films led to an increase in V_{oc} up to 50 mV and 35% improvement in the PCE of the related DSSC [287]. In 2005, O'Regan *et al.* demonstrated an Al_2O_3 barrier layer coating on a TiO_2/dye/CuSCN solid-state solar cell [288]. It was reported that Al_2O_3 treated cells show improved V_{OC} and FF but lower J_{SC}. The Al_2O_3 layer was considered to act as a tunnel barrier, suppressing the recombination rate hence improving the photo-voltage [288]. These reports proposed a pioneering demonstration of decorating the n-type photo-anode by applying outer shell structure.

Core-shell ZnO / TiO_2 nanowire heterostructure dye-sensitized solar cells

In 2006, Law *et al.* reported enhanced DSSCs based on ZnO/Al_2O_3 and ZnO/TiO_2 NW core-shell heterostructures. The as-grown ZnO NWs had a length of 15 μm and a diameter of 150 nm [269]. ALD was used to deposit a thin shell of amorphous Al_2O_3 or anatase TiO_2. It was reported that the insulating Al_2O_3 shell increased the V_{OC}, but decreased the J_{SC} significantly, leading to decreased efficiency [269]. For TiO_2 shells, an optimal 10-25 nm in thickness increased both photo-voltage and FF, enhancing the performance up to 2.25% [269] compared to 1.5% for pure ZnO-based DSSC [16]. The structure of ZnO/TiO_2 is shown in Figure 16 below.

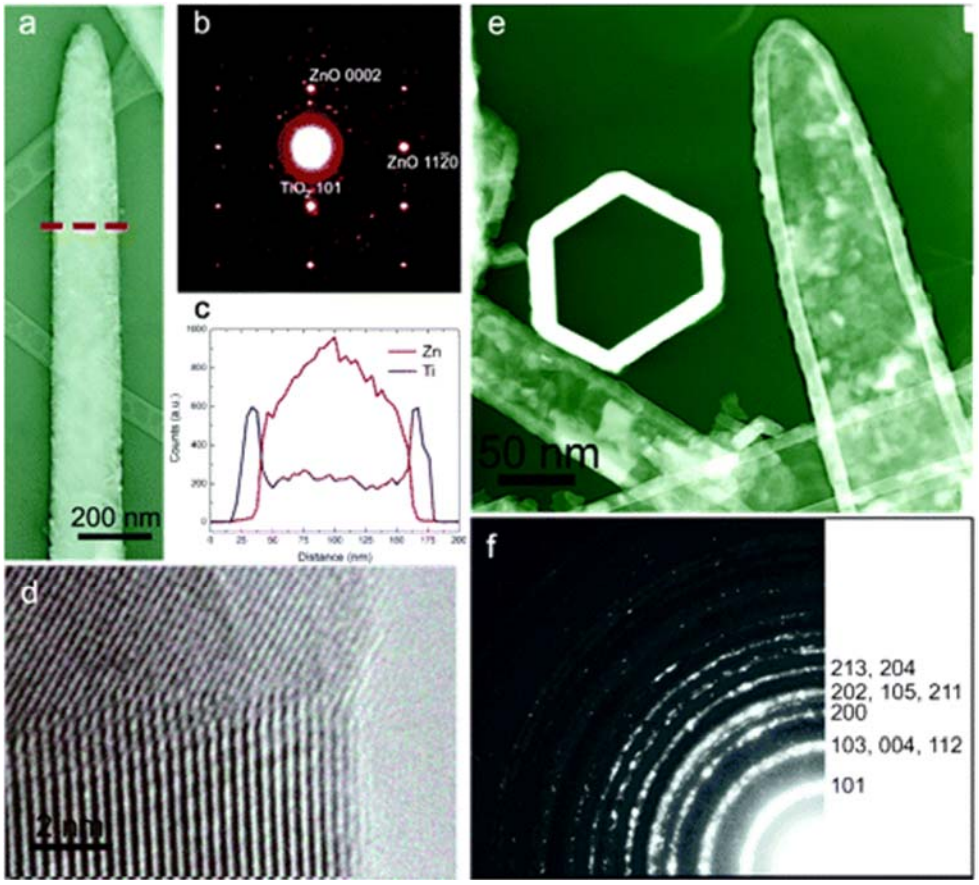

Figure 16. Characterization of ZnO/TiO_2 core−shell nanowires and TiO_2 nanotubes with a shell thickness of 13.5 ± 1 nm. (a) Dark-field TEM image of a core−shell wire. (b) Selected area electron diffraction pattern of a different core−shell wire, showing a polycrystalline anatase spot pattern superimposed on a single-crystalline ZnO spot pattern. The discontinuous anatase (101) ring is labelled. The continuous ring near centre is an artefact from the aperture. (c) EDS elemental profile along the dashed line in part (a). (d) High-resolution TEM image of the outer surface of a core−shell wire. (e) Dark-field TEM image of anatase nanotubes made by removing the ZnO wire cores in 1 M aqueous HCl. The tubes have hexagonal cross sections. (f) Electron diffraction of an ensemble of tubes. The 10 innermost rings are labelled (all rings are anatase). Reprinted with permissions from [269]. Copyright 2006 American Chemical Society.

It was suggested that the application of the shell would decrease the recombination rate possibly due to the passivation of surface recombination sites and build-up of a radial energy barrier that repels electrons from the

NWs to recombine [269]. Law *et al.* suggested that since the band gaps and band edge energies of bulk ZnO and anatase TiO_2 are equal to within about 50 mV, TiO_2 and ZnO can form an n-n^+ heterojunction free of band discontinuities and with a built-in potential, neglecting any difference in densities of states, of $\phi_{bi} \approx V_{th} \ln \frac{N_D^+}{N_D}$

Where V_{th} is the thermal voltage, N_D^+ and N_D are the donor concentrations in the heavily doped ZnO core and more lightly doped TiO_2 shell, respectively. As a result, an energy barrier of 75-150 mV is reasonable based on the doping difference between ZnO and TiO_2. This radial field would reduce the electron concentration at the NW surface by a factor of $\exp(-\phi_{bi} / KT)$, or roughly 20-300 times smaller than the concentration at the centre of a NW, leading to decreased recombination [269]. A schematic band diagram of the proposed situation is shown in Figure 17.

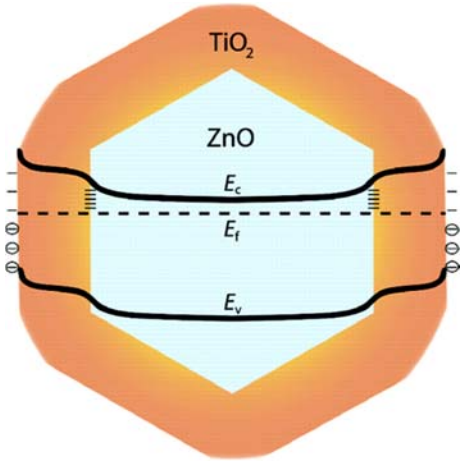

Figure 17. Schematic energy level diagram of a ZnO/TiO_2 core-shell structure in cross section and in equilibrium with the surrounding electrolyte. Reprinted with permissions from [269]. Copyright 2006 American Chemical Society.

Following this suggestion, a number of other ZnO/TiO_2 core-shell NW heterostructures were reported, including: a RF magnetron sputtered TiO_2 shell onto ZnO NWs with 2% PCE, compared to 1% for bare ZnO NWs [289]; sol-gel ZnO/TiO_2 structures, giving 3% PCE compared to 2.1% for bare NWs [285] [290]; atmospheric pressure CVD (APCVD) giving a 14 nm TiO_2 shell with 0.9% PCE, twice that of bare nanorods with V_{oc} increasing but J_{sc} and PCE decreasing with thicker shells [291]; dip-coating of TiO_2 on ZnO NWs with 3.8% PCE that was 2.6 higher than bare NWs [292]; solution-grown TiO_2 on ZnO NWs using ammonium hexafluorotitanate and H_3BO_3 giving ~3% PCE, around three times that of bare NWs [293]. In almost all cases, the main benefits of the ZnO/TiO_2 core-shell NW heterostructures is the preferential band alignment that drives strong charge separation, reducing recombination as well as promoting rapid charge transfer to ZnO NWs with the high charge carrier mobility. Reduced dye aggregations from the chemical stability of TiO_2 surface are also often-cited benefits. Importantly,

Xu *et al.* reported the formation of a multilayer assembly of core-shell ZnO/TiO_2 NW heterostructures up to a length larger than 40 μm, using alternate cycles of NW growth and self-assembled monolayer coating processes. By increasing the length of ZnO NWs, the PCE was enhanced up to 7.0 %, while continuously increasing the J_{SC} and decreasing the V_{OC} [294].

Alternative core-shell ZnO nanowire heterostructure dye-sensitized solar cells

Further metal-oxide shells have also been investigated for ZnO NW-based DSSCs. In 2008, Plank *et al.* reported hydrothermal synthesis of MgO shells onto ZnO NW arrays [295]. A solid-state DSSC was configured with spiro-OMeTAD as the HTM. The bare ZnO-based device showed only 0.072% PCE while the MgO shell coated device showed 0.33% PCE. The addition of MgO layer led to the J_{sc} improving from 0.8 to 2.3 mA/cm^2. V_{oc} was also improved by 70 mV from 280 to 350 mV. The improvement of photocurrent despite the insulating nature of MgO was attributed to enhanced dye loading, achieved by enhanced stability of ZnO in acidic dye solution and increased light scattering. It was also suggested that the physical separation induced by the insulating shell or coating between the electrons and holes reduce the charge recombination and promoted effective electron tunneling [295].

A ZnO/ZnS core-shell NW heterostructure was reported by Chung *et al.* in 2010 [296]. The ZnS shell was fabricated *via* solution growth using a $ZnSO_4$/thiourea/NH_4OH solution. The resulting structure achieved 2.72% PCE compared to 0.11% from bare NW device. The report suggested that the formation of a ZnS layer on the ZnO NWs reduced the density of surface defects, leading to improved DSSC performance [296].

In 2013, Guillen *et al.* reported a ZnO/ZnO core-shell NW heterostructure for DSSC application [297]. The shell was deposited from a ZnO colloidal suspension *via* spin coating at 2000 rpm for 30 s followed by thermal annealing of 100 °C for 5 mins. This was repeated 50 times to achieve an optimal coating which led to 2.1% PCE. Comparing to bare ZnO NW-based device, a significant 250 mV improvement of V_{oc} reaching 870 mV was observed. Electrochemical impedance spectroscopy and intensity-modulated photo-voltage spectroscopy showed a slowdown of the recombination dynamics [297].

In 2013, Zhou *et al.* reported ZnO/SnO_2 core-shell NW heterostructures for DSSCs [298]. The shell solution was a SnO_2 colloid prepared by refluxing a mixed solution of 0.5 M tin dichloride and dehydrate in 100 mL ethanol at 90 °C. The obtained colloid was then coated on ZnO *via* dip-coating. The film was finally annealed at 500 °C for 1 h. The structure led to a PCE of 4.71%, compared to 2.87 % from bare ZnO NW-based devices. From the result of UV-vis absorption on eluted dye concentrations, the application of shell was found to increase the surface

area leading to almost two times higher dye loading. On the other hand, the shell improved the stability by blocking the direct contact between ZnO and dye molecules [298].

In 2017, Jung *et al.* reported CuO-coated ZnO NWs for DSSCs, showing improved PCE from 0.032% (bare) to 0.11% (CuO-coated) [299]. The CuO shell was suggested to absorb more visible and NIR light, generating a larger number of excited electrons, improving the photocurrent. It could also behave as a blocking layer that reduces interfacial recombination by inhibiting electron back transfer [299].

Quality of the interface with the dye

In general, even though ZnO has a similar band gap and energy level position as TiO_2, high electron mobility and easy crystallization into various nanostructures at low temperature, the results of ZnO-based DSSCs still show lower PCE than that obtained with TiO_2. The best pure ZnO-based DSSC (6.58%) is still ZnO nanoporous film sensitized by N719 [265], exactly the same morphology as the pure nanoporous TiO_2-based DSSC. Other efforts utilizing different nanostructures (such as one-dimensional NWs for direct electron pathway) have all resulted in lower PCE. Building on these ZnO NWs using nanoparticle capping, nanoflower/tree decorating, dendritic NWs and core-shell coatings have all showed slight improvement as discussed above, but still with lower PCE than the nanoparticle-based devices. It is suggested that surface area is still the dominant factor that affects the performance of DSSCs by limiting the dye loading and therefore photo-current. From higher surface area (nanoparticles film) to intermedium surface area (complex nanostructure with ZnO backbone and additional particles/branches/dendrites) to low surface area (pure ZnO NWs) shows decreasing PCE. The performance of the ZnO-based DSSC is also suggested to be limited by the formation of Zn^{2+}/dye complex during direct use of N719, N3 and black dyes [300]. The dye molecules have carboxyl groups that leads to acidic nature of the dye solution, which is not compatible with ZnO surfaces. Reduced dye loading time (1-3 h compared to 12-24 h for TiO_2 based samples) have found to be beneficial to reduce the formation of Zn^{2+}/dye complex [301] [302]. Different dye such as D149 [303] and amphiphilic acid co-adsorbents [304] have also been reported to be able to reduce Zn^{2+}/dye complex. Since the Zn^{2+}/dye complex is caused by the dissolution of surface Zn atoms by the protons released from the dye molecules, the use of protective shells, resulting in core-shell NW heterostructures, has been extensively investigated and shows a promising path to improve the performance of ZnO NW-based DSSCs.

Photoanode	Technique	J_{SC} (mA/cm^2)	V_{OC} (mV)	FF	PCE (%)	Ref.

ZnO NWs	-	5.3-5.85	610-710	0.36-0.38	1.2-1.5	[16]
ZnO NWs	-	1.3	670	0.32	0.3	[270]
ZnO NWs	-	6.79	540	0.5	1.7	[273]
ZnO NWs / TiO_2	ALD	4.5	820	0.6	2.25	[269]
ZnO NWs / TiO_2 Solid state DSSC	ALD	1.14	500	0.5	0.29	[235]
ZnO NWs / MgO	Hydrothermal	2.3	350	0.42	0.33	[295]
ZnO NWs / TiO_2	RF MS	5.3	700	0.53	2.0	[289]
ZnO NWs / TiO_2	Sol-gel	6.3	760	0.6	3.1	[290]
ZnO NWs / ZnS	Solution growth	11.9	530	0.44	2.72	[296]
ZnO NWs / TiO_2	CVD	2.45	680	0.55	0.9	[291]
ZnO NWs / TiO_2	Solution dipping	10.6	590	0.61	3.8	[292]
ZnO NWs / TiO_2	Sol-gel spin coating	4.31	680	0.43	3	[285]
ZnO NWs / TiO_2	Solution growth	5.2	820	0.73	3.03	[293]
ZnO NWs / TiO_2	Solution growth	~ 15.5	~ 760	-	7.0	[294]
ZnO NWs / ZnO	Colloidal suspension spin coating	5.9	0.85	0.42	2.1	[297]
ZnO NWs / SnO_2	Colloidal suspension dip coating	9.8	0.59	0.57	4.71	[298]
ZnO NWs / CuO	E-beam evaporation	0.72	0.46	0.33	0.11	[299]

Table 7. PV performances of the DSSCs integrating ZnO NWs.

5. Halide perovskite-based solar cells

Background of halide perovskite-based solar cells

In 2009, Kojima *et al.* reported hybrid organic-inorganic metal halide perovskites (HPSCs) used as visible-light sensitizers for photovoltaic cells [305]. Organic-inorganic lead halide perovskite compounds such as $CH_3NH_3PbBr_3$ and $CH_3NH_3PbI_3$ were selected due to unique optical properties, excitonic properties, electrical conductivity [305] as well as large absorption coefficient, high charge carrier mobility and diffusion length [306]. The resulting 3.13% PCE with 960 mV V_{OC} showed the perovskite compounds to be a promising candidate towards high photo-voltage devices [305]. Here the device still resembled a liquid-state DSSC structure, with the perovskite replacing original dye molecules on a mesoporous TiO_2 scaffold [307]. The structure evolution of HPSCs is shown in Figure 18 [307].

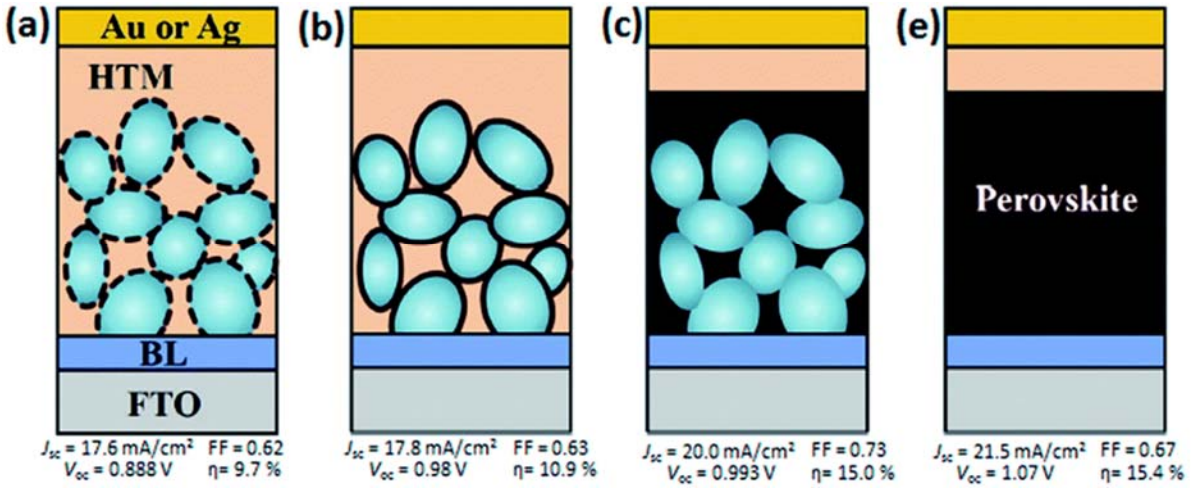

Figure 18. Structural evolution of HPSCs: (a) sensitized solar cell with nanodot perovskite, (b) meso-superstructured solar cell with a thin and continuous layer of perovskite, (c) perovskite-infiltrated solar cell with a capping layer of perovskite, and (d) planar heterojunction solar cell. Typical PV performance parameters are shown beneath each structure. Reprinted with permission from [307]. Copyright 2015 Royal Society of Chemistry.

Since then, the research on HPSCs has accelerated producing increasing PCEs, with record efficiency currently at 23.3% according to the National Renewable Energy Laboratory (NREL) [308]. Due to the higher absorption coefficient of perovskite materials than molecular dye sensitizers [21], high specific surface is not essential in the case of HPSCs comparing to DSSCs. Thus, one important factor of the ETM design is the overall thickness rather than high surface area-focused morphology.

It was suggested by Leijtens *et al.* that the different pore filling factor from different ETM thickness has a significant effect on the HPSC performance [309]. Thicker ETM films with lower pore filling fraction would form an ETM-perovskite mixture layer with the potential risk of HTM in contact with ETM, or even the conductive substrate. A thinner ETM film has the benefit of forming a perovskite-capping layer, meaning the full ETM film is embedded under perovskite layer. Photo-generated charges would be able to rapidly transfer into TiO_2 due to the high mobility of carriers within perovskite material [310]. It was also suggested that thinner ETM films with lower surface area would facilitate a faster charge collection at the conductive substrate. Lower surface area leads to lower amount of possible recombination sites, thinner film means charges would have a higher probability to be collected before recombination [309]. It was found that the efficiency of the TiO_2 based-HPSCs increased from 11.8% to 15.3% to 16.5% with decreased film thickness from 750 nm to 440 nm to 260 nm, respectively. It was later reported that 400 nm-thickness was around the optimal value for ETM in the framework of HPSCs [311] [312] [313].

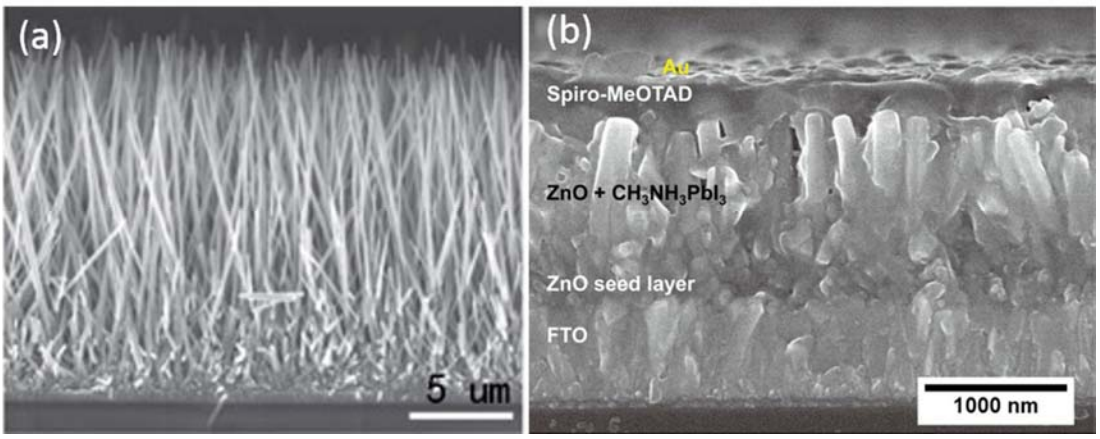

Figure 19. (a) ZnO NWs utilized in liquid-state DSSC with 16-17 μm lengths. Reprinted with permission from [16]. Copyright 2006 Nature Publishing. (b) ZnO NWs utilized in HPSC with 1 μm length. Reprinted with permission from [314]. Copyright 2014 American Chemical Society.

Figure 19 shows the comparison of structures for ZnO-based liquid-state DSSCs [16] and ZnO-based HPSCs [314], both optimized for improving the PCE. It can be seen that, as a result of the different surface area and overall thickness requirements, longer length is utilized for liquid state DSSCs while short length is optimal for HPSCs. Similar to the developing pathway in liquid-state DSSCs, ZnO was then selected as a substitute for TiO_2 in HPSCs. In 2013, Liu reported a HPSC based on a ZnO nanoparticle film. The PCE exceeded 10% on flexible substrates (ITO/PET) and 15% on rigid substrates (ITO/Glass) [313]. The PV performances of the HPSCs integrating ZnO NWs are gathered in Table 8.

ZnO nanowire halide perovskite-based solar cells

In the same year, Bi *et al.* reported enhanced light absorption using halide perovskites upon ZnO NWs. NWs with 1μm length achieved a 5.2% PCE using single-step deposited halide perovskites [21]. Kumar *et al.* reported 8.9% PCE combining electrodeposited ZnO seed layer and hydrothermally grown ZnO NWs [315]. The ZnO seed layer also acted as compact layer to block holes, preventing recombination with electrons within FTO and holes in the halide perovskite. A schematic of typical ZnO NW-based HPSCs is shown in Figure 1b.

In 2014, Son reported 11.13% PCE HPSCs based on ZnO NWs using two-step sequential method to deposit the halide perovskite [314]. The reported optimal length of ZnO NWs was also 1 μm. The author also fabricated 1 μm long TiO_2 NW based-HPSCs as comparison, achieving a slightly lower V_{oc} and 10% PCE. Time-limited photocurrent response under 530 and 700 nm monochromatic beams at 10 Hz showed that device signal amplitude, associated with charge collection, was rapidly saturated for the ZnO NW-based device whereas charge collection

was not fully detected for TiO_2 NW-based device due to slow collection rate. These results suggested that ZnO NW is an effective charge collection system in HPSCs [314]. The same group of authors showed one year later the effects of the seed layer on the morphology of ZnO NWs and the resulting performances of the HPSCs [316]. The ZnO seed layer grown by the sol-gel process was found to improve the verticality of ZnO NWs as well as the recombination resistances and ZnO NW-halide perovskite interface quality, leading to a larger V_{OC} reaching 956 mV. Additional surface modifications of ZnO NWs with $(NH_4)_2TiF_6$ treatment for forming a TiO_2 thin shell led to an increased PCE of 14.35% correlated with a further jump of V_{OC} and FF to 1055 mV and 0.698, respectively [316]. Similarly, Wang *et al.* showed the benefit of adding a TiO_2 thin shell on ZnO NWs *via* $TiCl_4$ treatment, increasing the PCE of the resulting HPSCs from 5.6 to 8.24% [317]. The improvement was presumably attributed to larger surface area, reduced electron recombination, and superior electron transport properties. In 2012, Dong *et al*. reported improved performance from 8.5% PCE for un-doped to 10.07% using aluminium-doped ZnO-coated ZnO NWs as ETM [318]. The aluminium-doped ZnO thin shell was deposited by spin-coating a mixed ethanolic solution of $Al(NO_3)_3$ and $Zn(Ac)_2$ onto the as-prepared ZnO NWs. The presence of the Al doping improved the V_{OC} and PCE due to reduced charge recombination in the device as the aluminium-doped ZnO shell has a higher conduction band than ZnO, larger electron mobility and higher electron density [318]. In contrast, Zhang *et al.* showed that the formation of an i-ZnO shell with a lower electron density on ZnO NWs is favorable for increasing the PCE of the resulting HPSCs up to 10.28% thanks to the reduction of charge carrier recombination [319].

In 2015, Mahmood *et al.* reported ZnO NW-based HPSCs achieving 16.19% PCE [320]. The synergistically improved ZnO NWs, with PEI coating and high aspect ratio (1 μm in length, 85 nm in diameter), were doped with nitrogen. Doping significantly improved electron density, leading to improved current and voltage. The ZnO NW array was coated with a thin layer of PEI *via* spin coating. Due to the strong interaction between the PEI and nonpolar surface of ZnO, a conformal coating of PEI can shift the work function of ZnO leading to increased photo-current (17.3 to 18.85 mA/cm^2). This was attributed to improved electron extraction and reduced series resistance with PEI coating [320]. Unlike the conventional metal-oxide shell utilized in DSSCs, a ZnO/PEI core-shell NW heterostructure showed interesting approach to improve ZnO-based HPSCs by passivating the surface trap states on ZnO. In general, while ZnO-DSSCs still shows low PCE, ZnO-HPSCs have already shown comparable results (20% PCE, 16.19% for NWs) with TiO_2-based HPSCs. As a promising candidate next to the widely used TiO_2,

ZnO shows promising results benefiting from low-cost and low energy manufacture processing. The higher electron mobility is also adding the advantage over TiO_2 especially in HPSC research.

Stability issue in ZnO-based halide perovskite-based solar cells

Similar to DSSCs, a major limitation of ZnO-based PSCs is also the stability. After the deposition of perovskite precursor solution onto the film, a post-annealing step is required to evaporate the solvent and crystalize the perovskite film at around 100 °C. However, prolonged thermal annealing can also degrade $CH_3NH_3PbI_3$ perovskite film, generating HI and CH_3NH_2, both evaporating at 100 °C. It was found that this degradation was catalysed and accelerated on ZnO films (2 mins) compared to TiO_2 films (40 mins) [321]. It was suggested that the basic nature of ZnO surface would lead to proton-transfer reactions at the ZnO/$CH_3NH_3PbI_3$ interface, which leads to decomposition of the perovskite film [322]. It was also suggested that low temperature solution-processed ZnO film has surface groups of hydroxide and acetate, and reaction of methyl ammonium iodide (MAI) and ZnO film would accelerate under moisture in ambient air, causing poor stability of ZnO based perovskite solar cells [323]. To solve the instability issue, surface passivation has been proposed to be effective similar to the core-shell approach in DSSCs. In 2017, Song *et al*. demonstrated a triple-cation perovskite structure ($Cs_x(MA_{0.1}7FA_{0.83})_{(100-x)}Pb(I_{0.83}Br_{0.17})_3$) on ZnO nanoparticle film using a one-step deposition method [324]. A stabilized performance of 18.9% was achieved, which was attributed to Cs doping and remnant PbI_2 passivation. Guo *et al*. reported a carefully engineered combination of ultrasonic assisted method and a two-step sequential spin-coating deposition technique onto ZnO nanoparticle films in 2018 [325]. The resultant compact and pinhole-free ZnO-HPSC achieved 14.52% and maintained 86.25% of its initial PCE though air exposure for 45 days In 2018, Cao *et al*. reported efficient (21.1%), hysteresis-free and stable (300 h) ZnO compact layer based HPSCs *via* successful surface passivation [326]. The passivation was achieved *via* depositing thin layer of MgO and protonated ethanolamine. MgO was suggested to inhibit the interfacial charge recombination while the protonated ethanolamine promotes the effective electron transport from perovskite to ZnO [326]. MgO was proven to be a successful shell material both in DSSC and HPSC application for ZnO. Although not performed on ZnO NW structure, these results show promising stabilised ZnO/perovskite interface *via* carefully doping design.

Chemical instability towards dye molecules and halide perovskites thus remains a major issue limiting the performance of the devices. One approach is to develop ZnO-suited light absorb layer such as D149 dye and mixed cation perovskite layers. Another approach is to design and develop surface decoration *via* core-shell NW

heterostructures. Through this, it seems possible that ZnO will remain of great interest in the area of solar cell research.

Photoanode	HP	Technique	J_{SC} (mA/cm^2)	V_{OC} (mV)	FF	PCE (%)	Ref.
ZnO NWs	$CH_3NH_3PbI_3$	One step	12.7	680	0.58	5.2	[21]
ZnO NWs	$CH_3NH_3PbI_3$	Two step	16.98	1020	0.51	8.9	[315]
ZnO NWs	$CH_3NH_3PbI_3$	Two step	19.77	900	0.6	10.7	[318]
ZnO NWs	$CH_3NH_3PbI_3$	Two step	20.08	990	0.56	11.13	[314]
ZnO NWs	$CH_3NH_3PbI_3$	Two step	21.7	970	0.7	16.19	[320]
ZnO NWs / TiO_2	$CH_3NH_3PbI_3$	Two step	19.44	1055	0.698	14.35	[316]
ZnO NWs / TiO_2	$CH_3NH_3PbI_3$	Two step	14.82	960.4	0.58	8.24	[317]
ZnO NWs / ZnO	$CH_3NH_3PbI_3$	Two step	21.9	990	0.473	10.28	[319]

Table 8. PV performances of the HPSCs integrating ZnO NWs.

6. Conclusions

The integration of ZnO NWs into nanostructured solar cells offers the outlook for a wide variety of advantages, including a reduced amount of high-cost raw matter in the final product, a potential low-cost using suitable chemical deposition techniques, light trapping phenomena, and possibly also a well-controlled charge carrier management through the efficient charge carrier separation ensured by the successive type II band alignments and the high crystalline quality of NWs. The fabrication, properties, and performances of a large number of ZnO NW-based nanostructured solar cells, such as ETASCs, QDSSCs, BHQDSCs, *i*OSCs, HSCs, DSSCs, and HPSCs, have been reviewed in details. Overall, the fabrication and technological integration of these nanostructured solar cells have reached a certain degree of maturity over the last decade. However, the performances of the ZnO NW-based solar cells are still inferior to the performances of the related planar solar cells using the same stack. The typical increase of the optical absorption in these nanostructured solar cells is basically counterbalanced by the charge carrier management issue. The large interfacial area in these nanostructured solar cells have appeared as a potential limitation requiring innovative solutions. In that respect, post-deposition treatment, annealing, and passivation layers, to name a few, have emerged as essential to address the charge carrier extraction ability. The use of ZnO NWs is also of high significance when combined with new inorganic or organic absorbers exhibiting limited physical properties that are not compatible with the planar solar cell architecture. In a more and more eco-friendly society, ZnO, as an abundant and biocompatible material, and in the form of NWs, is still highly promising as a building block for next-generation solar cells.

7. Acknowledgements

VC acknowledges the financial support by the French Research National Agency through the project DOSETTE (ANR-17-CE24-0003). This work has further been partially supported by the CDP Eco-SESA (ANR-15-IDEX-02) and by the LabEx CEMAM (ANR-10-LABX-44-01) funded by the French Research National Agency in the framework of the “Investissements d’avenir” program. Funding by the Carnot Institute ‘Energies du Futur’ through the project ‘CLAPE’ and by the Nanoscience Foundation of Grenoble though the project ‘II-VI Photovoltaic’ are also acknowledged. EK acknowledge Estonian Research Council project IUT19-4 “Thin films and nanomaterials by wet-chemical methods for next-generation photovoltaics” and European Regional Development Fund project TK141 “Advanced materials and high-technology devices for sustainable energetics, sensorics and nanoelectronics”.

REFERENCES

[1] Ozgur U, Alivov Y I, Liu C, Teke A, Reshchikov M A, Dogan S, Avrutin V, Cho S J and Morkoc H 2005 A comprehensive review of ZnO materials and devices *J. Appl. Phys.* **98** 041301

[2] Schmidt-Mende L and MacManus-Driscoll J L 2007 ZnO - nanostructures, defects, and devices *Mater. Today* **10** 40-8

[3] Ozgur U, Hofstetter D and Morkoc H 2010 ZnO Devices and Applications: A Review of Current Status and Future Prospects *Proc. IEEE* **98** 1255-68

[4] Xu S and Wang Z L 2011 One-dimensional ZnO nanostructures: Solution growth and functional properties *Nano Res.* **4** 1013-98

[5] Hochbaum A I and Yang P D 2010 Semiconductor Nanowires for Energy Conversion *Chem. Rev.* **110** 527-46

[6] Garnett E C, Brongersma M L, Cui Y and McGehee M D 2011 *Annu. Rev. Mater. Res.* **41** 269-95

[7] Hagfeldt A, Boschloo G, Sun L C, Kloo L and Pettersson H 2010 Dye-Sensitized Solar Cells *Chem. Rev.* **110** 6595-663

[8] Vayssieres L 2003 Growth of arrayed nanorods and nanowires of ZnO from aqueous solutions *Adv. Mater.* **15** 464-6

[9] O'Regan B, Schwartz D T, Zakeeruddin S M and Gratzel M 2000 Electrodeposited nanocomposite n-p heterojunctions for solid-state dye-sensitized photovoltaics *Adv. Mater.* **12** 1263-7

[10] Briscoe J and Dunn S 2011 Extremely thin absorber solar cells based on nanostructured semiconductors *Mater. Sci. Technol.* **27** 1741-56

[11] Kamat P V 2013 Quantum Dot Solar Cells. The Next Big Thing in Photovoltaics *J. Phys. Chem. Lett.* **4** 908-18

[12] Weickert J, Dunbar R B, Hesse H C, Wiedemann W and Schmidt-Mende L 2011 Nanostructured Organic and Hybrid Solar Cells *Adv. Mater.* **23** 1810-28

[13] Zhang Q F, Dandeneau C S, Zhou X Y and Cao G Z 2009 ZnO Nanostructures for Dye-Sensitized Solar Cells *Adv. Mater.* **21** 4087-108

[14] Levy-Clement C, Tena-Zaera R, Ryan M A, Katty A and Hodes G 2005 CdSe-Sensitized p-CuSCN/nanowire n-ZnO heterojunctions *Adv. Mater.* **17** 1512-5

[15] Leschkies K S, Divakar R, Basu J, Enache-Pommer E, Boercker J E, Carter C B, Kortshagen U R, Norris D J and Aydil E S 2007 Photosensitization of ZnO nanowires with CdSe quantum dots for photovoltaic devices *Nano Lett.* **7** 1793-8

[16] Law M, Greene L E, Johnson J C, Saykally R and Yang P D 2005 Nanowire dye-sensitized solar cells *Nat. Mater.* **4** 455-9

[17] Baxter J B and Aydil E S 2005 Nanowire-based dye-sensitized solar cells *Appl. Phys. Lett.* **86** 053114

[18] Leschkies K S, Beatty T J, Kang M S, Norris D J and Aydil E S 2009 Solar Cells Based on Junctions between Colloidal PbSe Nanocrystals and Thin ZnO Films *ACS Nano* **3** 3638-48

[19] Jean J, Chang S, Brown P R, Cheng J J, Rekemeyer P H, Bawendi M G, Gradecak S and Bulovic V 2013 ZnO Nanowire Arrays for Enhanced Photocurrent in PbS Quantum Dot Solar Cells *Adv. Mater.* **25** 2790-6

[20] Olson D C, Piris J, Collins R T, Shaheen S E and Ginley D S 2006 Hybrid photovoltaic devices of polymer and ZnO nanofiber composites *Thin Solid Films* **496** 26-9

[21] Bi D Q, Boschloo G, Schwarzmuller S, Yang L, Johansson E M J and Hagfeldt A 2013 Efficient and stable $CH_3NH_3PbI_3$-sensitized ZnO nanorod array solid-state solar cells *Nanoscale* **5** 11686-91

[22] Janotti A and Van de Walle C G 2007 Native point defects in ZnO *Phys. Rev. B* **76** 165202

[23] Van de Walle C G 2000 Hydrogen as a cause of doping in zinc oxide *Phys. Rev. Lett.* **85** 1012-5

[24] McCluskey M D and Jokela S J 2009 Defects in ZnO *J. Appl. Phys.* **106** 071101

[25] Tam K H, Cheung C K, Leung Y H, Djurisic A B, Ling C C, Beling C D, Fung S, Kwok W M, Chan W K, Phillips D L, Ding L and Ge W K 2006 Defects in ZnO nanorods prepared by a hydrothermal method *J. Phys. Chem. B* **110** 20865-71

[26] Diepers H 1978 Solar cell comprising semiconductive whiskers *United States Patents* **4,099,986**

[27] Hodes G and Cahen D 2012 All-Solid-State, Semiconductor-Sensitized Nanoporous Solar Cells *Accounts Chem. Res.* **45** 705-13

[28] Hodes G 2008 Comparison of Dye- and Semiconductor-Sensitized Porous Nanocrystalline Liquid Junction Solar Cells *J. Phys. Chem. C* **112** 17778-87
[29] Mora-Sero I and Bisquert J 2010 Breakthroughs in the Development of Semiconductor-Sensitized Solar Cells *J. Phys. Chem. Lett.* **1** 3046-52
[30] Dittrich T, Belaidi A and Ennaoui A 2011 Concepts of inorganic solid-state nanostructured solar cells *Sol. Energy Mater. Sol. Cells* **95** 1527-36
[31] Kaiser I, Ernst K, Fischer C H, Konenkamp R, Rost C, Sieber I and Lux-Steiner M C 2001 The eta-solar cell with CuInS2: A photovoltaic cell concept using an extremely thin absorber (eta) *Sol. Energy Mater. Sol. Cells* **67** 89-96
[32] Soga T 2006 Nanostructured Materials for Solar Energy Conversion *Elsevier*
[33] Edri E, Rabinovich E, Niitsoo O, Cohen H, Bendikov T and Hodes G 2010 Uniform Coating of Light-Absorbing Semiconductors by Chemical Bath Deposition on Sulfide-Treated ZnO Nanorods *J. Phys. Chem. C* **114** 13092-7
[34] Levy-Clement C and Elias J 2013 Optimization of the Design of Extremely Thin Absorber Solar Cells Based on Electrodeposited ZnO Nanowires *ChemPhysChem* **14** 2321-30
[35] Taretto K and Rau U 2004 Modeling extremely thin absorber solar cells for optimized design *Prog. Photovoltaics* **12** 573-91
[36] Mora-Sero I, Gimenez S, Fabregat-Santiago F, Azaceta E, Tena-Zaera R and Bisquert J 2011 Modeling and characterization of extremely thin absorber (eta) solar cells based on ZnO nanowires *Phys. Chem. Chem. Phys.* **13** 7162-9
[37] Michallon J, Bucci D, Morand A, Zanuccoli M, Consonni V and Kaminski-Cachopo A 2014 Light trapping in ZnO nanowire arrays covered with an absorbing shell for solar cells *Opt. Express* **22** A1174-A89
[38] Michallon J, Bucci D, Morand A, Zanuccoli M, Consonni V and Kaminski-Cachopo A 2015 Light absorption processes and optimization of ZnO/CdTe core-shell nanowire arrays for nanostructured solar cells *Nanotechnology* **26** 075401
[39] McCarthy R F, Hillhouse H W and Ieee 2012 *The Shockley-Queisser Limit and Practical Limits of Nanostructured Photovoltaics* (New York: Ieee)
[40] Xu Y L, Gong T and Munday J N 2015 The generalized Shockley-Queisser limit for nanostructured solar cells *Scientific Reports* **5** 13536
[41] Liu R C 2014 Hybrid Organic/Inorganic Nanocomposites for Photovoltaic Cells *Materials* **7** 2747-71
[42] Parize R, Katerski A, Gromyko I, Rapenne L, Roussel H, Karber E, Appert E, Krunks M and Consonni V 2017 $ZnO/TiO_2/Sb_2S_3$ Core-Shell Nanowire Heterostructure for Extremely Thin Absorber Solar Cells *J. Phys. Chem. C* **121** 9672-80
[43] Belaidi A, Dittrich T, Kieven D, Tornow J, Schwarzburg K, Kunst M, Allsop N, Lux-Steiner M C and Gavrilov S 2009 ZnO-nanorod arrays for solar cells with extremely thin sulfidic absorber *Sol. Energy Mater. Sol. Cells* **93** 1033-6
[44] Xu J, Yang X, Wang H K, Chen X, Luan C Y, Xu Z X, Lu Z Z, Roy V A L, Zhang W J and Lee C S 2011 Arrays of ZnO/ZnxCd1-xSe Nanocables: Band Gap Engineering and Photovoltaic Applications *Nano Lett.* **11** 4138-43
[45] Ho C I, Liang W C, Yeh D J, Su V C, Yang P C, Chen S Y, Yang T T, Lee J H, Kuan C H, Cheng I C and Lee S C 2013 Influence of the absorber layer thickness and rod length on the performance of three-dimensional nanorods thin film hydrogenated amorphous silicon solar cells *J. Appl. Phys.* **113** 163106
[46] Tena-Zaera R, Ryan M A, Katty A, Hodes G, Bastide S and Levy-Clement C 2006 Fabrication and characterization of ZnO nanowires/CdSe/CuSCN eta-solar cell *C. R. Chim.* **9** 717-29
[47] Levy-Clement C, Katty A, Bastide S, Zenia F, Mora I and Munoz-Sanjose V 2002 A new CdTe/ZnO columnar composite film for Eta-solar cells *Physica E* **14** 229-32
[48] Krunks M, Karber E, Katerski A, Otto K, Acik I O, Dedova T and Mere A 2010 Extremely thin absorber layer solar cells on zinc oxide nanorods by chemical spray *Sol. Energy Mater. Sol. Cells* **94** 1191-5
[49] Wang X H, Li R B and Fan D H 2011 Nanostructured Al-ZnO/CdSe/Cu_2O ETA solar cells on Al-ZnO film/quartz glass templates *Nanoscale Res. Lett.* **6** 614
[50] Chang J A, Rhee J H, Im S H, Lee Y H, Kim H J, Seok S I, Nazeeruddin M K and Gratzel M 2010 High-Performance Nanostructured Inorganic-Organic Heterojunction Solar Cells *Nano Lett.* **10** 2609-12
[51] Moon S J, Itzhaik Y, Yum J H, Zakeeruddin S M, Hodes G and Gratzel M 2010 Sb_2S_3-Based Mesoscopic Solar Cell using an Organic Hole Conductor *J. Phys. Chem. Lett.* **1** 1524-7

[52] Kartopu G, Turkay D, Ozcan C, Hadibrata W, Aurang P, Yerci S, Unalan H E, Barrioz V, Qu Y, Bowen L, Gurlek A K, Maiello P, Turan R and Irvine S J C 2018 Photovoltaic performance of CdS/CdTe junctions on ZnO nanorod arrays *Sol. Energy Mater. Sol. Cells* **176** 100-8
[53] Major J D, Tena-Zaera R, Azaceta E, Durose K and Ieee 2015 *2015 Ieee 42nd Photovoltaic Specialist Conference,* (New York: Ieee)
[54] Major J D, Tena-Zaera R, Azaceta E, Bowen L and Durose K 2017 Development of ZnO nanowire based CdTe thin film solar cells *Sol. Energy Mater. Sol. Cells* **160** 107-15
[55] Ernst K, Engelhardt R, Ellmer K, Kelch C, Muffler H J, Lux-Steiner M C and Konenkamp R 2001 Contacts to a solar cell with extremely thin CdTe absorber *Thin Solid Films* **387** 26-8
[56] Ernst K, Belaidi A and Konenkamp R 2003 Solar cell with extremely thin absorber on highly structured substrate *Semicond. Sci. Technol.* **18** 475-9
[57] Belaidi A, Dittrich T, Kieven D, Tornow J, Schwarzburg K and Lux-Steiner M 2008 Influence of the local absorber layer thickness on the performance of ZnO nanorod solar cells *Phys. Status Solidi-Rapid Res. Lett.* **2** 172-4
[58] Dittrich T, Kieven D, Rusu M, Belaidi A, Tornow J, Schwarzburg K and Lux-Steiner M 2008 Current-voltage characteristics and transport mechanism of solar cells based on ZnO nanorods/In(2)S(3)/CuSCN *Appl. Phys. Lett.* **93** 053113
[59] Tena-Zaera R, Katty A, Bastide S, Levy-Clement C, O'Regan B and Munoz-Sanjose V 2005 ZnO/CdTe/CuSCN, a promising heterostructure to act as inorganic eta-solar cell *Thin Solid Films* **483** 372-7
[60] Consonni V, Rey G, Bonaime J, Karst N, Doisneau B, Roussel H, Renet S and Bellet D 2011 Synthesis and physical properties of ZnO/CdTe core shell nanowires grown by low-cost deposition methods *Appl. Phys. Lett.* **98** 111906
[61] Consonni V, Renet S, Garnier J, Gergaud P, Artus L, Michallon J, Rapenne L, Appert E and Kaminski-Cachopo A 2014 Improvement of the physical properties of ZnO/CdTe core-shell nanowire arrays by $CdCl_2$ heat treatment for solar cells *Nanoscale Res. Lett.* **9** 222
[62] Akbarnejad E, Nayeri F D and Ghoranneviss M 2018 Core-shell solar cell fabrication using heterostructure of ZnO-nanowires arrays decorated with sputtered CdTe-nanoparticles *J. Phys. D-Appl. Phys.* **51** 095105
[63] Jin M J, Chen X Y, Gao Z M, Ling T and Du X W 2012 Improve photo-electron conversion efficiency of ZnO/CdS coaxial nanorods by p-type CdTe coating *Nanotechnology* **23** 485401
[64] Aranovich J A, Golmayo D, Fahrenbruch A L and Bube R H 1980 Photo-voltaic properties of ZnO-CdTe heterojunctions prepared by spray pyrolysis *J. Appl. Phys.* **51** 4260-8
[65] Khomyak V V, Ilashchuk M I, Parfenyuk O A and Shtepliuk, II 2013 Fabrication and electrical characterization of the anisotype n-ZnO/p-CdTe heterostructures for solar cell applications *J. Appl. Phys.* **114** 223715
[66] Zhang G H, Wu Y K, Ding H Y, Zhu Y S, Li J W, Lin Y, Jiang S L, Zhang Q, Pan N, Luo Y and Wang X P 2015 Remarkable enhancement of photovoltaic performance of ZnO/CdTe core-shell nanorod array solar cells through interface passivation with a TiO_2 layer *RSC Adv.* **5** 71883-9
[67] Tiefenbacher S, Pettenkofer C and Jaegermann W 2002 Ultrahigh vacuum preparation and characterization of TiO_2/CdTe interfaces: Electrical properties and implications for solar cells *J. Appl. Phys.* **91** 1984-7
[68] Seol M, Kim H, Tak Y and Yong K 2010 Novel nanowire array based highly efficient quantum dot sensitized solar cell *Chem. Commun.* **46** 5521-3
[69] Tak Y, Hong S J, Lee J S and Yong K 2009 Fabrication of ZnO/CdS core/shell nanowire arrays for efficient solar energy conversion *J. Mater. Chem.* **19** 5945-51
[70] Karber E, Abass A, Khelifi S, Burgelman M, Katerski A and Krunks M 2013 Electrical characterization of all-layers-sprayed solar cell based on ZnO nanorods and extremely thin CIS absorber *Sol. Energy* **91** 48-58
[71] Nadarajah A, Word R C, VanSant K and Konenkamp R 2008 Nanowire-quantum-dot-polymer solar cell *Phys. Status Solidi B* **245** 1834-7
[72] Chang J A, Im S H, Lee Y H, Kim H J, Lim C S, Heo J H and Seok S I 2012 Panchromatic Photon-Harvesting by Hole-Conducting Materials in Inorganic-Organic Heterojunction Sensitized-Solar Cell through the Formation of Nanostructured Electron Channels *Nano Lett.* **12** 1863-7
[73] Choi Y C, Lee D U, Noh J H, Kim E K and Seok S I 2014 Highly Improved Sb_2S_3 Sensitized-Inorganic-Organic Heterojunction Solar Cells and Quantification of Traps by Deep-Level Transient Spectroscopy *Adv. Funct. Mater.* **24** 3587-92

[74] Choi Y C and Seok S I 2015 Efficient Sb_2S_3-Sensitized Solar Cells Via Single-Step Deposition of Sb_2S_3 Using S/Sb-Ratio-Controlled $SbCl_3$-Thiourea Complex Solution *Adv. Funct. Mater.* **25** 2892-8
[75] Liu C P, Chen Z H, Wang H E, Jha S K, Zhang W J, Bello I and Zapien J A 2012 Enhanced performance by incorporation of zinc oxide nanowire array for organic-inorganic hybrid solar cells *Appl. Phys. Lett.* **100** 243102
[76] Han J H, Liu Z F, Zheng X R, Guo K Y, Zhang X Q, Hong T T, Wang B and Liu J Q 2014 Trilaminar ZnO/ZnS/Sb_2S_3 nanotube arrays for efficient inorganic-organic hybrid solar cells *RSC Adv.* **4** 23807-14
[77] Karber E, Katerski A, Acik I O, Mere A, Mikli V and Krunks M 2016 Sb_2S_3 grown by ultrasonic spray pyrolysis and its application in a hybrid solar cell *Beilstein J. Nanotechnol.* **7** 1662-73
[78] Kondrotas R, Chen C and Tang J 2018 Sb_2S_3 Solar Cells *Joule* **2** 857-78
[79] Zhu L P, Wang L F, Xue F, Chen L B, Fu J Q, Feng X L, Li T F and Wang Z L 2017 Piezo-Phototronic Effect Enhanced Flexible Solar Cells Based on n-ZnO/p-SnS Core-Shell Nanowire Array *Adv. Sci.* **4** 1600185
[80] Izaki M, Ohta T, Kondo M, Takahashi T, Mohamad F B, Zamzuri M, Sasano J, Shinagawa T and Pauporte T 2014 Electrodeposited ZnO-Nanowire/Cu_2O Photovoltaic Device with Highly Resistive ZnO Intermediate Layer *ACS Appl. Mater. Interfaces* **6** 13461-9
[81] Chen X, Lin P, Yan X Q, Bai Z M, Yuan H G, Shen Y W, Liu Y C, Zhang G J, Zhang Z and Zhang Y 2015 Three-Dimensional Ordered ZnO/Cu_2O Nanoheterojunctions for Efficient Metal-Oxide Solar Cells *ACS Appl. Mater. Interfaces* **7** 3216-23
[82] Panigrahi S, Calmeiro T, Martins R, Nunes D and Fortunato E 2016 Observation of Space Charge Dynamics Inside an All Oxide Based Solar Cell *ACS Nano* **10** 6139-46
[83] Zhang Y, Wang L W and Mascarenhas A 2007 "Quantum coaxial cables" for solar energy harvesting *Nano Lett.* **7** 1264-9
[84] Schrier J, Demchenko D O and Wang L W 2007 Optical properties of ZnO/ZnS and ZnO/ZnTe heterostructures for photovoltaic applications *Nano Lett.* **7** 2377-82
[85] Wang K, Chen J J, Zhou W L, Zhang Y, Yan Y F, Pern J and Mascarenhas A 2008 Direct growth of highly mismatched type II ZnO/ZnSe core/shell nanowire arrays on transparent conducting oxide substrates for solar cell applications *Adv. Mater.* **20** 3248-53
[86] Wu Z M, Zhang Y, Zheng J J, Lin X G, Chen X H, Huang B W, Wang H Q, Huang K, Li S P and Kang J Y 2011 An all-inorganic type-II heterojunction array with nearly full solar spectral response based on ZnO/ZnSe core/shell nanowires *J. Mater. Chem.* **21** 6020-6
[87] Zhang Y, Wu Z M, Zheng J J, Lin X A, Zhan H H, Li S P, Kang J Y, Bleuse J and Mariette H 2012 ZnO/ZnSe type II core-shell nanowire array solar cell *Sol. Energy Mater. Sol. Cells* **102** 15-8
[88] Amiri G, Souissi A, Haneche N, Vilar C, Lusson A, Sallet V and Galtier P 2013 Synthesis and characterization of core-shell ZnO/ZnSe nanowires grown by MOCVD *Phys. Status Solidi B* **250** 2132-6
[89] Ghoul M, Braiek Z, Brayek A, Ben Assaker I, Khalifa N, Ben Naceur J, Souissi A, Lamouchi A, Ammar S and Chtourou R 2015 Synthesis of core/shell ZnO/ZnSe nanowires using novel low cost two-steps electrochemical deposition technique *J. Alloy Compd* **647** 660-4
[90] Luo S P, He X O, Shen H P, Li J B, Yin X W, Oron D and Lin H 2017 Vertically aligned ZnO/ZnTe core/shell heterostructures on an AZO substrate for improved photovoltaic performance *RSC Adv.* **7** 14837-45
[91] Wang K, Chen J J, Zeng Z M, Tarr J, Zhou W L, Zhang Y, Yan Y F, Jiang C S, Pern J and Mascarenhas A 2010 Synthesis and photovoltaic effect of vertically aligned ZnO/ZnS core/shell nanowire arrays *Appl. Phys. Lett.* **96** 123105
[92] Rai S C, Wang K, Ding Y, Marmon J K, Bhatt M, Zhang Y, Zhou W L and Wang Z L 2015 Piezo-phototronic Effect Enhanced UV/Visible Photodetector Based on Fully Wide Band Gap Type-II ZnO/ZnS Core/Shell Nanowire Array *ACS Nano* **9** 6419-27
[93] Konenkamp R, Boedecker K, Lux-Steiner M C, Poschenrieder M, Zenia F, Levy-Clement C and Wagner S 2000 Thin film semiconductor deposition on free-standing ZnO columns *Appl. Phys. Lett.* **77** 2575-7
[94] Li H H, Yang P Y, Chiou S M, Liu H W and Cheng H C 2011 A Novel Coaxial-Structured Amorphous-Silicon p-i-n Solar Cell With Al-Doped ZnO Nanowires *IEEE Electron Device Lett.* **32** 928-30
[95] Kuang Y H, van der Werf K H M, Houweling Z S and Schropp R E I 2011 Nanorod solar cell with an ultrathin a-Si:H absorber layer *Appl. Phys. Lett.* **98** 113111
[96] Schubert M B and Werner J H 2006 Flexible solar cells for clothing *Mater. Today* **9** 42-50
[97] Kamat P V 2008 Quantum Dot Solar Cells. Semiconductor Nanocrystals as Light Harvesters *J. Phys. Chem. C* **112** 18737-53

[98] Nozik A J, Beard M C, Luther J M, Law M, Ellingson R J and Johnson J C 2010 Semiconductor Quantum Dots and Quantum Dot Arrays and Applications of Multiple Exciton Generation to Third-Generation Photovoltaic Solar Cells *Chem. Rev.* **110** 6873-90
[99] Kramer I J and Sargent E H 2011 Colloidal Quantum Dot Photovoltaics: A Path Forward *ACS Nano* **5** 8506-14
[100] Nozik A J 2002 Quantum dot solar cells *Physica E* **14** 115-20
[101] Bude J and Hess K 1992 Thresholds of impact ionizationin semiconductors *J. Appl. Phys.* **72** 3554-61
[102] Beard M C, Midgett A G, Hanna M C, Luther J M, Hughes B K and Nozik A J 2010 Comparing Multiple Exciton Generation in Quantum Dots To Impact Ionization in Bulk Semiconductors: Implications for Enhancement of Solar Energy Conversion *Nano Lett.* **10** 3019-27
[103] Ellingson R J, Beard M C, Johnson J C, Yu P R, Micic O I, Nozik A J, Shabaev A and Efros A L 2005 Highly efficient multiple exciton generation in colloidal PbSe and PbS quantum dots *Nano Lett.* **5** 865-71
[104] Ross R T and Nozik A J 1982 Efficiency of hot-carrier solar-energy converters *J. Appl. Phys.* **53** 3813-8
[105] Nozik A J 2001 Spectroscopy and hot electron relaxation dynamics in semiconductor quantum wells and quantum dots *Annu. Rev. Phys. Chem.* **52** 193-231
[106] Tang J, Kemp K W, Hoogland S, Jeong K S, Liu H, Levina L, Furukawa M, Wang X H, Debnath R, Cha D K, Chou K W, Fischer A, Amassian A, Asbury J B and Sargent E H 2011 Colloidal-quantum-dot photovoltaics using atomic-ligand passivation *Nat. Mater.* **10** 765-71
[107] Jasieniak J, Califano M and Watkins S E 2011 Size-Dependent Valence and Conduction Band-Edge Energies of Semiconductor Nanocrystals *ACS Nano* **5** 5888-902
[108] Chuang C H M, Brown P R, Bulovic V and Bawendi M G 2014 Improved performance and stability in quantum dot solar cells through band alignment engineering *Nat. Mater.* **13** 796-801
[109] Robel I, Subramanian V, Kuno M and Kamat P V 2006 Quantum dot solar cells. Harvesting light energy with CdSe nanocrystals molecularly linked to mesoscopic TiO_2 films *J. Am. Chem. Soc.* **128** 2385-93
[110] Niitsoo O, Sarkar S K, Pejoux C, Ruhle S, Cahen D and Hodes G 2006 Chemical bath deposited CdS/CdSe-sensitized porous TiO_2 solar cells *J. Photochem. Photobiol. A-Chem.* **181** 306-13
[111] Lee H, Leventis H C, Moon S J, Chen P, Ito S, Haque S A, Torres T, Nuesch F, Geiger T, Zakeeruddin S M, Gratzel M and Nazeeruddin M K 2009 PbS and US Quantum Dot-Sensitized Solid-State Solar Cells: "Old Concepts, New Results" *Adv. Funct. Mater.* **19** 2735-42
[112] Luther J M, Gao J B, Lloyd M T, Semonin O E, Beard M C and Nozik A J 2010 Stability Assessment on a 3% Bilayer PbS/ZnO Quantum Dot Heterojunction Solar Cell *Adv. Mater.* **22** 3704-7
[113] Tvrdy K, Frantsuzov P A and Kamat P V 2011 Photoinduced electron transfer from semiconductor quantum dots to metal oxide nanoparticles *Proc. Natl. Acad. Sci. U. S. A.* **108** 29-34
[114] Lan X Z, Masala S and Sargent E H 2014 Charge-extraction strategies for colloidal quantum dot photovoltaics *Nat. Mater.* **13** 233-40
[115] Sun X W, Chen J, Song J L, Zhao D W, Deng W Q and Lei W 2010 Ligand capping effect for dye solar cells with a CdSe quantum dot sensitized ZnO nanorod photoanode *Opt. Express* **18** 1296-301
[116] Zidek K, Zheng K, Chabera P, Abdellah M and Pullerits T 2012 Quantum dot photodegradation due to CdSe-ZnO charge transfer: Transient absorption study *Appl. Phys. Lett.* **100** 243111
[117] Zidek K, Zheng K, Abdellah M, Chabera P, Pullerits T and Tachyia M 2014 Simultaneous Creation and Recovery of Trap States on Quantum Dots in a Photoirradiated CdSe-ZnO System *J. Phys. Chem. C* **118** 27567-73
[118] Zheng K B, Zidek K, Abdellah M, Chabera P, Abd El-Sadek M S and Pullerits T 2013 Effect of metal oxide morphology on electron injection from CdSe quantum dots to ZnO *Appl. Phys. Lett.* **102** 163119
[119] Zidek K, Zheng K B, Ponseca C S, Messing M E, Wallenberg L R, Chabera P, Abdellah M, Sundstrom V and Pullerits T 2012 Electron Transfer in Quantum-Dot-Sensitized ZnO Nanowires: Ultrafast Time-Resolved Absorption and Terahertz Study *J. Am. Chem. Soc.* **134** 12110-7
[120] Zheng K B, Zidek K, Abdellah M, Torbjornsson M, Chabera P, Shao S Y, Zhang F L and Pullerits T 2013 Fast Monolayer Adsorption and Slow Energy Transfer in CdSe Quantum Dot Sensitized ZnO Nanowires *J. Phys. Chem. A* **117** 5919-25
[121] Zidek K, Abdellah M, Zheng K B and Pullerits T 2014 Electron relaxation in the CdSe quantum dot - ZnO composite: prospects for photovoltaic applications *Sci. Rep-UK* **4** 7244
[122] Hou D C, Dev A, Frank K, Rosenauer A and Voss T 2012 Oxygen-Controlled Photoconductivity in ZnO Nanowires Functionalized with Colloidal CdSe Quantum Dots *J. Phys. Chem. C* **116** 19604-10

[123] Bley S, Diez M, Albrecht F, Resch S, Waldvogel S R, Menzel A, Zacharias M, Gutowski J and Voss T 2015 Electron Tunneling from Colloidal CdSe Quantum Dots to ZnO Nanowires Studied by Time-Resolved Luminescence and Photoconductivity Experiments *J. Phys. Chem. C* **119** 15627-35
[124] Seol M, Ramasamy E, Lee J and Yong K 2011 Highly Efficient and Durable Quantum Dot Sensitized ZnO Nanowire Solar Cell Using Noble-Metal-Free Counter Electrode *J. Phys. Chem. C* **115** 22018-24
[125] Chen J, Wu J, Lei W, Song J L, Deng W Q and Sun X W 2010 Co-sensitized quantum dot solar cell based on ZnO nanowire *Appl. Surf. Sci.* **256** 7438-41
[126] Luan C Y, Vaneski A, Susha A S, Xu X Q, Wang H E, Chen X, Xu J, Zhang W J, Lee C S, Rogach A L and Zapien J A 2011 Facile solution growth of vertically aligned ZnO nanorods sensitized with aqueous CdS and CdSe quantum dots for photovoltaic applications *Nanoscale Res. Lett.* **6** 340
[127] Hui K N, Hui K S, Zhang X L, Mane R S and Naushad M 2016 Photosensitization of ZnO nanowire-based electrodes using one-step hydrothermally synthesized CdSe/CdS (core/shell) sensitizer *Sol. Energy* **125** 125-34
[128] Tian J J, Zhang Q F, Zhang L L, Gao R, Shen L F, Zhang S G, Qu X H and Cao G Z 2013 ZnO/TiO_2 nanocable structured photoelectrodes for CdS/CdSe quantum dot co-sensitized solar cells *Nanoscale* **5** 936-43
[129] Hou J, Zhao H F, Huang F, Jing Q, Cao H B, Wu Q, Peng S L and Cao G Z 2016 High performance of Mn-doped CdSe quantum dot sensitized solar cells based on the vertical ZnO nanorod arrays *J. Power Sources* **325** 438-45
[130] Zhao H F, Huang F, Hou J, Liu Z Y, Wu Q, Cao H B, Jing Q, Peng S L and Cao G Z 2016 Efficiency Enhancement of Quantum Dot Sensitized TiO_2/ZnO Nanorod Arrays Solar Cells by Plasmonic Ag Nanoparticles *ACS Appl. Mater. Interfaces* **8** 26675-82
[131] Sudhagar P, Song T, Lee D H, Mora-Sero I, Bisquert J, Laudenslager M, Sigmund W M, Park W I, Paik U and Kang Y S 2011 High Open Circuit Voltage Quantum Dot Sensitized Solar Cells Manufactured with ZnO Nanowire Arrays and Si/ZnO Branched Hierarchical Structures *J. Phys. Chem. Lett.* **2** 1984-90
[132] Li L B, Wang Y F, Rao H S, Wu W Q, Li K N, Su C Y and Kuang D B 2013 Hierarchical Macroporous Zn_2SnO_4-ZnO Nanorod Composite Photoelectrodes for Efficient CdS/CdSe Quantum Dot Co-Sensitized Solar Cells *ACS Appl. Mater. Interfaces* **5** 11865-71
[133] Tian J J, Uchaker E, Zhang Q F and Cao G Z 2014 Hierarchically Structured ZnO Nanorods-Nanosheets for Improved Quantum-Dot-Sensitized Solar Cells *ACS Appl. Mater. Interfaces* **6** 4466-72
[134] Feng H L, Wu W Q, Rao H S, Wan Q, Li L B, Kuang D B and Su C Y 2015 Three-Dimensional TiO_2/ZnO Hybrid Array as a Heterostructured Anode for Efficient Quantum-Dot-Sensitized Solar Cells *ACS Appl. Mater. Interfaces* **7** 5199-205
[135] Zhang Y, Xie T F, Jiang T F, Wei X, Pang S, Wang X and Wang D 2009 Surface photovoltage characterization of a ZnO nanowire array/CdS quantum dot heterogeneous film and its application for photovoltaic devices *Nanotechnology* **20** 155707
[136] Lee W, Min S K, Dhas V, Ogale S B and Han S H 2009 Chemical bath deposition of CdS quantum dots on vertically aligned ZnO nanorods for quantum dots-sensitized solar cells *Electrochem. Commun.* **11** 103-6
[137] Chou C Y, Li C T, Lee C P, Lin L Y, Yeh M H, Vittal R and Ho K C 2013 ZnO nanowire/nanoparticles composite films for the photoanodes of quantum dot-sensitized solar cells *Electrochim. Acta* **88** 35-43
[138] Qi J J, Liu W, Biswas C, Zhang G J, Sun L F, Wang Z Z, Hu X F and Zhang Y 2015 Enhanced power conversion efficiency of CdS quantum dot sensitized solar cells with ZnO nanowire arrays as the photoanodes *Opt. Commun.* **349** 198-202
[139] Bora T, Kyaw H H and Dutta J 2012 Zinc oxide-zinc stannate core-shell nanorod arrays for CdS quantum dot sensitized solar cells *Electrochim. Acta* **68** 141-5
[140] Eskandari M, Ahmadi V, Rad M Y and Kohnehpoushi S 2015 Plasmon enhanced CdS-quantum dot sensitized solar cell using ZnO nanorods array deposited with Ag nanoparticles as photoanode *Physica E* **68** 202-9
[141] Aga R S, Jowhar D, Ueda A, Pan Z, Collins W E, Mu R, Singer K D and Shen J 2007 Enhanced photoresponse in ZnO nanowires decorated with CdTe quantum dot *Appl. Phys. Lett.* **91** 232108
[142] Cao X B, Chen P and Guo Y 2008 Decoration of Textured ZnO Nanowires Array with CdTe Quantum Dots: Enhanced Light-Trapping Effect and Photogenerated Charge Separation *J. Phys. Chem. C* **112** 20560-6

[143] Chen H M, Chen C K, Chang Y C, Tsai C W, Liu R S, Hu S F, Chang W S and Chen K H 2010 Quantum Dot Monolayer Sensitized ZnO Nanowire-Array Photoelectrodes: True Efficiency for Water Splitting *Angew. Chem.-Int. Edit.* **49** 5966-9
[144] Briscoe J, Gallardo D E, Hatch S, Lesnyak V, Gaponik N and Dunn S 2011 Enhanced quantum dot deposition on ZnO nanorods for photovoltaics through layer-by-layer processing *J. Mater. Chem.* **21** 2517-23
[145] Kuo K T, Liu D M, Chen S Y and Lin C C 2009 Core-shell $CuInS_2$/ZnS quantum dots assembled on short ZnO nanowires with enhanced photo-conversion efficiency *J. Mater. Chem.* **19** 6780-8
[146] Liu Z F, Huang J J, Han J H, Hong T T, Zhang J and Liu Z H 2016 $CuSbS_2$: a promising semiconductor photo-absorber material for quantum dot sensitized solar cells *Phys. Chem. Chem. Phys.* **18** 16615-20
[147] Leschkies K S, Jacobs A G, Norris D J and Aydil E S 2009 Nanowire-quantum-dot solar cells and the influence of nanowire length on the charge collection efficiency *Appl. Phys. Lett.* **95** 193103
[148] Cheng J J, Chuang C H M, Hentz O, Rekemeyer P H, Bawendi M G and Gradecak S 2018 Dimension- and Surface-Tailored ZnO Nanowires Enhance Charge Collection in Quantum Dot Photovoltaic Devices *ACS Appl. Energy Mater. Interfaces* **1** 1815-22
[149] Wang H B, Kubo T, Nakazaki J, Kinoshita T and Segawa H 2013 PbS-Quantum-Dot-Based Heterojunction Solar Cells Utilizing ZnO Nanowires for High External Quantum Efficiency in the Near-Infrared Region *J. Phys. Chem. Lett.* **4** 2455-60
[150] Wang H, Kubo T, Nakazaki J and Segawa H 2014 PbS colloidal quantum dot/ZnO-based bulk-heterojunction solar cells with high stability under continuous light soaking *Phys. Status Solidi-Rapid Res. Lett.* **8** 961-5
[151] Wang H B, Gonzaez-Pedro V, Kubo T, Fabregat-Santiago F, Bisquert J, Sanehira Y, Nakazaki J and Segawa H 2015 Enhanced Carrier Transport Distance in Colloidal PbS Quantum-Dot-Based Solar Cells Using ZnO Nanowires *J. Phys. Chem. C* **119** 27265-74
[152] Chang J, Kuga Y, Mora-Sero I, Toyoda T, Ogomi Y, Hayase S, Bisquert J and Shen Q 2015 High reduction of interfacial charge recombination in colloidal quantum dot solar cells by metal oxide surface passivation *Nanoscale* **7** 5446-56
[153] Zang S P, Wang Y L, Su W, Zhu H C, Li G, Zhang X T and Liu Y C 2016 Increased open-circuit voltage of ZnO nanowire/PbS quantum dot bulk heterojunction solar cells with solution-deposited Mg(OH)(2) interlayer *Phys. Status Solidi-Rapid Res. Lett.* **10** 745-8
[154] Rekemeyer P H, Chang S, Chuang C H M, Hwang G W, Bawendi M G and Gradecak S 2016 Enhanced Photocurrent in PbS Quantum Dot Photovoltaics via ZnO Nanowires and Band Alignment Engineering *Adv. Energy Mater.* **6** 1600848
[155] Kawawaki T, Wang H B, Kubo T, Saito K, Nakazaki J, Segawa H and Tatsuma T 2015 Efficiency Enhancement of PbS Quantum Dot/ZnO Nanowire Bulk-Heterojunction Solar Cells by Plasmonic Silver Nanocubes *ACS Nano* **9** 4165-72
[156] Wang H B, Kubo T, Nakazaki J and Segawa H 2017 Solution-Processed Short-Wave Infrared PbS Colloidal Quantum Dot/ZnO Nanowire Solar Cells Giving High Open-Circuit Voltage *ACS Energy Lett.* **2** 2110-7
[157] Wang Y L, Su W, Zang S P, Li M Y, Zhang X T and Liu Y C 2017 Bending-durable colloidal quantum dot solar cell using a ZnO nanowire array as a three-dimensional electron transport layer *Appl. Phys. Lett.* **110** 163902
[158] Tang C 1986 Two-Layer Organic Photovoltaic Cell *Appl. Phys. Lett.* **48** 183-5
[159] Yu G, Gao J, Hummelen J C, Wudl F and Heeger A J 1995 Polymer photovoltaic cells - Enhanced efficiencies via a network of internal donor-acceptor heterojunctions *Science* **270** 1789-91
[160] Halls J J M, Walsh C A, Greenham N C, Marseglia E A, Friend R H, Moratti S C and Holmes A B 1995 Efficient photdiodes from interpenetrating polymer networks *Nature* **376** 498-500
[161] Menke S M and Holmes R J 2014 Exciton diffusion in organic photovoltaic cells *Energy Environ. Sci.* **7** 499-512
[162] Mikhnenko O V, Blom P W M and Nguyen T Q 2015 Exciton diffusion in organic semiconductors *Energy Environ. Sci.* **8** 1867-88
[163] Dou L T, Liu Y S, Hong Z R, Li G and Yang Y 2015 Low-Bandgap Near-IR Conjugated Polymers/Molecules for Organic Electronics *Chem. Rev.* **115** 12633-65
[164] You J B, Dou L T, Hong Z R, Li G and Yang Y 2013 Recent trends in polymer tandem solar cells research *Prog. Polym. Sci.* **38** 1909-28

[165] Chen C C, Chang W H, Yoshimura K, Ohya K, You J B, Gao J, Hong Z R and Yang Y 2014 An Efficient Triple-Junction Polymer Solar Cell Having a Power Conversion Efficiency Exceeding 11% *Adv. Mater.* **26** 5670-7
[166] Li M M, Gao K, Wan X J, Zhang Q, Kan B, Xia R X, Liu F, Yang X, Feng H R, Ni W, Wang Y C, Peng J J, Zhang H T, Liang Z Q, Yip H L, Peng X B, Cao Y and Chen Y S 2017 Solution-processed organic tandem solar cells with power conversion efficiencies >12% *Nat. Photonics* **11** 85-90
[167] Huang W C, Cheng P, Yang Y, Li G and Yang Y 2018 High-Performance Organic Bulk-Heterojunction Solar Cells Based on Multiple-Donor or Multiple-Acceptor Components *Adv. Mater.* **30** 1705706
[168] Cao H Q, He W D, Mao Y W, Lin X, Ishikawa K, Dickerson J H and Hess W P 2014 Recent progress in degradation and stabilization of organic solar cells *J. Power Sources* **264** 168-83
[169] de Jong M P, van Ijzendoorn L J and de Voigt M J A 2000 Stability of the interface between indium-tin-oxide and poly(3,4-ethylenedioxythiophene)/poly(styrenesulfonate) in polymer light-emitting diodes *Appl. Phys. Lett.* **77** 2255-7
[170] Wong K W, Yip H L, Luo Y, Wong K Y, Lau W M, Low K H, Chow H F, Gao Z Q, Yeung W L and Chang C C 2002 Blocking reactions between indium-tin oxide and poly (3,4-ethylene dioxythiophene): poly(styrene sulphonate) with a self-assembly monolayer *Appl. Phys. Lett.* **80** 2788-90
[171] Kawano K, Pacios R, Poplavskyy D, Nelson J, Bradley D D C and Durrant J R 2006 Degradation of organic solar cells due to air exposure *Sol. Energy Mater. Sol. Cells* **90** 3520-30
[172] Hau S K, Yip H L and Jen A K Y 2010 A Review on the Development of the Inverted Polymer Solar Cell Architecture *Polym. Rev.* **50** 474-510
[173] Chen L M, Hong Z R, Li G and Yang Y 2009 Recent Progress in Polymer Solar Cells: Manipulation of Polymer: Fullerene Morphology and the Formation of Efficient Inverted Polymer Solar Cells *Adv. Mater.* **21** 1434-49
[174] Huang J, Yin Z G and Zheng Q D 2011 Applications of ZnO in organic and hybrid solar cells *Energy Environ. Sci.* **4** 3861-77
[175] Li S S and Chen C W 2013 Polymer-metal-oxide hybrid solar cells *J. Mater. Chem. A* **1** 10574-91
[176] Liang Z Q, Zhang Q F, Jiang L and Cao G Z 2015 ZnO cathode buffer layers for inverted polymer solar cells *Energy Environ. Sci.* **8** 3442-76
[177] Noori K and Giustino F 2012 Ideal Energy-Level Alignment at the ZnO/P3HT Photovoltaic Interface *Adv. Funct. Mater.* **22** 5089-95
[178] Nagata T, Oh S, Yamashita Y, Yoshikawa H, Ikeno N, Kobayashi K, Chikyow T and Wakayama Y 2013 Photoelectron spectroscopic study of band alignment of polymer/ZnO photovoltaic device structure *Appl. Phys. Lett.* **102** 043302
[179] Nagata T, Oh S, Yamashita Y, Yoshikawa H, Ikeno N, Kobayashi K, Chikyow T and Wakayama Y 2014 Photoelectron spectroscopic study on band alignment of poly(3-hexylthiophene-2,5-diyl)/polar-ZnO heterointerface *Thin Solid Films* **554** 194-8
[180] Conings B, Baeten L, Boyen H G, Spoltore D, D'Haen J, Van Bael M K and Manca J V 2012 Generalized approach to the description of recombination kinetics in bulk heterojunction solar cells-extending from fully organic to hybrid solar cells *Appl. Phys. Lett.* **100** 203905
[181] Shirakawa T, Umeda T, Hashimoto Y, Fujii A and Yoshino K 2004 Effect of ZnO layer on characteristics of conducting polymer/C-60 photovoltaic cell *J. Phys. D-Appl. Phys.* **37** 847-50
[182] White M S, Olson D C, Shaheen S E, Kopidakis N and Ginley D S 2006 Inverted bulk-heterojunction organic photovoltaic device using a solution-derived ZnO underlayer *Appl. Phys. Lett.* **89** 143517
[183] Polydorou E, Zeniou A, Tsikritzis D, Soultati A, Sakellis I, Gardelis S, Papadopoulos T A, Briscoe J, Palilis L C, Kennou S, Gogolides E, Argitis P, Davazoglou D and Vasilopoulou M 2016 Surface passivation effect by fluorine plasma treatment on ZnO for efficiency and lifetime improvement of inverted polymer solar cells *J. Mater. Chem. A* **4** 11844-58
[184] Polydorou E, Sakellis I, Soultati A, Kaltzoglou A, Papadopoulos T A, Briscoe J, Tsikritzis D, Fakis M, Palilis L C, Kennou S, Argitis P, Falaras P, Davazoglou D and Vasilopoulou M 2017 Avoiding ambient air and light induced degradation in high-efficiency polymer solar cells by the use of hydrogen-doped zinc oxide as electron extraction material *Nano Energy* **34** 500-14
[185] Polydorou E, Botzakaki M A, Sakellis I, Soultati A, Kaltzoglou A, Papadopoulos T A, Briscoe J, Drivas C, Seintis K, Fakis M, Palilis L C, Georga S N, Krontiras C A, Kennou S, Falaras P, Boukos N, Davazoglou D, Argitis P and Vasilopoulou M 2017 Improved Stability of Polymer Solar Cells in Ambient Air via Atomic Layer Deposition of Ultrathin Dielectric Layers *Adv. Mater. Interfaces* **4** 12

[186] Lee J H, Shin J H, Song J Y, Wang W F, Schlaf R, Kim K J and Yi Y 2012 Interface Formation Between ZnO Nanorod Arrays and Polymers (PCBM and P3HT) for Organic Solar Cells *J. Phys. Chem. C* **116** 26342-8
[187] Chan M H, Chen J Y, Lin T Y and Chen Y F 2012 Direct evidence of type II band alignment in ZnO nanorods/poly (3-hexylthiophene) heterostructures *Appl. Phys. Lett.* **100** 021912
[188] Hames Y, Alpaslan Z, Kosemen A, San S E and Yerli Y 2010 Electrochemically grown ZnO nanorods for hybrid solar cell applications *Sol. Energy* **84** 426-31
[189] Elumalai N K, Jin T M, Chellappan V, Jose R, Palaniswamy S K, Jayaraman S, Raut H K and Ramakrishna S 2013 Electrospun ZnO Nanowire Plantations in the Electron Transport Layer for High-Efficiency Inverted Organic Solar Cells *ACS Appl. Mater. Interfaces* **5** 9396-404
[190] Liu J P, Wang S S, Bian Z Q, Shan M and Huang C H 2009 Organic/inorganic hybrid solar cells with vertically oriented ZnO nanowires *Appl. Phys. Lett.* **94** 173107
[191] Hu Z Y, Zhang J J, Liu Y, Li Y N, Zhang X D and Zhao Y 2011 Efficiency enhancement of inverted organic photovoltaic devices with ZnO nanopillars fabricated on FTO glass substrates *Synth. Met.* **161** 2174-8
[192] Reinhard M, Conradt J, Braun M, Colsmann A, Lemmer U and Kalt H 2012 Zinc oxide nanorod arrays hydrothermally grown on a highly conductive polymer for inverted polymer solar cells *Synth. Met.* **162** 1582-6
[193] Kim S H, Park S H, Il Lee K, Kim S M, Cho J W and Ieee 2010 *35th Ieee Photovoltaic Specialists Conference,* (New York: Ieee) pp 1636-8
[194] Huang J S, Chou C Y, Liu M Y, Tsai K H, Lin W H and Lin C F 2009 Solution-processed vanadium oxide as an anode interlayer for inverted polymer solar cells hybridized with ZnO nanorods *Org. Electron.* **10** 1060-5
[195] Takanezawa K, Tajima K and Hashimoto K 2008 Efficiency enhancement of polymer photovoltaic devices hybridized with ZnO nanorod arrays by the introduction of a vanadium oxide buffer layer *Appl. Phys. Lett.* **93** 3
[196] Wang M J, Li Y A, Huang H H, Peterson E D, Nie W Y, Zhou W, Zeng W, Huang W X, Fang G J, Sun N H, Zhao X Z and Carroll D L 2011 Thickness dependence of the MoO_3 blocking layers on ZnO nanorod-inverted organic photovoltaic devices *Appl. Phys. Lett.* **98** 103305
[197] Unalan H E, Hiralal P, Kuo D, Parekh B, Amaratunga G and Chhowalla M 2008 Flexible organic photovoltaics from zinc oxide nanowires grown on transparent and conducting single walled carbon nanotube thin films *J. Mater. Chem.* **18** 5909-12
[198] Tong F, Kim K, Martinez D, Thapa R, Ahyi A, Williams J, Kim D J, Lee S, Lim E, Lee K K and Park M 2012 Flexible organic/inorganic hybrid solar cells based on conjugated polymer and ZnO nanorod array *Semicond. Sci. Technol.* **27** 5
[199] Greene L E, Law M, Tan D H, Montano M, Goldberger J, Somorjai G and Yang P D 2005 General route to vertical ZnO nanowire arrays using textured ZnO seeds *Nano Lett.* **5** 1231-6
[200] Guillemin S, Consonni V, Appert E, Puyoo E, Rapenne L and Roussel H 2012 Critical Nucleation Effects on the Structural Relationship Between ZnO Seed Layer and Nanowires *J. Phys. Chem. C* **116** 25106-11
[201] Guillemin S, Appert E, Roussel H, Doisneau B, Parize R, Boudou T, Bremond G and Consonni V 2015 Controlling the Structural Properties of Single Step, Dip Coated ZnO Seed Layers for Growing Perfectly Aligned Nanowire Arrays *J. Phys. Chem. C* **119** 21694-703
[202] Cheng J J, Nicaise S M, Berggren K K and Gradecak S 2016 Dimensional Tailoring of Hydrothermally Grown Zinc Oxide Nanowire Arrays *Nano Lett.* **16** 753-9
[203] Parize R, Garnier J, Chaix-Pluchery O, Verrier C, Appert E and Consonni V 2016 Effects of Hexamethylenetetramine on the Nucleation and Radial Growth of ZnO Nanowires by Chemical Bath Deposition *J. Phys. Chem. C* **120** 5242-50
[204] Verrier C, Appert E, Chaix-Pluchery O, Rapenne L, Rafhay Q, Kaminski-Cachopo A and Consonni V 2017 Effects of the pH on the Formation and Doping Mechanisms of ZnO Nanowires Using Aluminum Nitrate and Ammonia *Inorg. Chem.* **56** 13111-22
[205] Peiro A M, Ravirajan P, Govender K, Boyle D S, O'Brien P, Bradley D D C, Nelson J and Durrant J R 2006 Hybrid polymer/metal oxide solar cells based on ZnO columnar structures *J. Mater. Chem.* **16** 2088-96
[206] Baeten L, Conings B, D'Haen J, De Dobbelaere C, Hardy A, Manca J V and Van Bael M K 2012 Tuning the Dimensions of ZnO Nanorod Arrays for Application in Hybrid Photovoltaics *ChemPhysChem* **13** 2777-83

[207] Whittaker-Brooks L, Mativetsky J M, Woll A, Smilgies D and Loo Y L 2013 Sputtered ZnO seed layer enhances photovoltaic behavior in hybrid ZnO/P3HT solar cells *Org. Electron.* **14** 3477-83
[208] Lee K H, Kumar B, Park H J and Kim S W 2010 Optimization of an Electron Transport Layer to Enhance the Power Conversion Efficiency of Flexible Inverted Organic Solar Cells *Nanoscale Res. Lett.* **5** 1908-12
[209] Hu Z Y, Zhang J J, Liu Y, Hao Z H, Zhang X D and Zhao Y 2011 Influence of ZnO interlayer on the performance of inverted organic photovoltaic device *Sol. Energy Mater. Sol. Cells* **95** 2126-30
[210] Ty J T D and Yanagi H 2015 Electrochemical deposition of zinc oxide nanorods for hybrid solar cells *Jpn. J. Appl. Phys.* **54** 5
[211] Takanezawa K, Hirota K, Wei Q S, Tajima K and Hashimoto K 2007 Efficient charge collection with ZnO nanorod array in hybrid photovoltaic devices *J. Phys. Chem. C* **111** 7218-23
[212] Takanezawa K, Tajima K and Hashimoto K 2008 Charge Separation Interfaces in Polymer Photovoltaic Devices Hybridized with ZnO Nanorod Arrays *Jpn. J. Appl. Phys.* **47** 8049-53
[213] Gonzalez-Valls I, Angmo D, Gevorgyan S A, Reparaz J S, Krebs F C and Lira-Cantu M 2013 Comparison of two types of vertically aligned ZnO NRs for highly efficient polymer solar cells *J. Polym. Sci. Pt. B-Polym. Phys.* **51** 272-80
[214] Ogawa Y, White M S, Sun L N, Scharber M C, Sariciftci N S and Yoshida T 2014 Substrate-Oriented Nanorod Scaffolds in PolymerFullerene Bulk Heterojunction Solar Cells *ChemPhysChem* **15** 1070-5
[215] Olson D C, Shaheen S E, Collins R T and Ginley D S 2007 The effect of atmosphere and ZnO morphology on the performance of hybrid poly(3-hexylthiophene)/ZnO nanofiber photovoltaic devices *J. Phys. Chem. C* **111** 16670-8
[216] Guo Y and Geng H W 2011 Performance of polymer/ZnO hybrid photovoltaic devices determined by reaction time for oriented ZnO nanorod growth *Thin Solid Films* **519** 2349-54
[217] Baeten L, Conings B, Boyen H G, D'Haen J, Hardy A, D'Olieslaeger M, Manca J V and Van Bael M K 2011 Towards Efficient Hybrid Solar Cells Based on Fully Polymer Infiltrated ZnO Nanorod Arrays *Adv. Mater.* **23** 2802-5
[218] Wu F, Shen W, Cui Q, Bi D Q, Yue W J, Qu Q Y and Wang M T 2010 Dynamic Characterization of Hybrid Solar Cells Based on Polymer and Aligned ZnO Nanorods by Intensity Modulated Photocurrent Spectroscopy *J. Phys. Chem. C* **114** 20225-35
[219] Conings B, Baeten L, Boyen H G, D'Haen J, Van Bael M K and Manca J V 2012 Relation between Morphology and Recombination Kinetics in Nanostructured Hybrid Solar Cells *J. Phys. Chem. C* **116** 14237-42
[220] Lee Y J, Lloyd M T, Olson D C, Grubbs R K, Lu P, Davis R J, Voigt J A and Hsu J W P 2009 Optimization of ZnO Nanorod Array Morphology for Hybrid Photovoltaic Devices *J. Phys. Chem. C* **113** 15778-82
[221] Yun D Q, Xia X Y, Zhang S, Bian Z Q, Liu R H and Huang C H 2011 ZnO nanorod arrays with different densities in hybrid photovoltaic devices: Fabrication and the density effect on performance *Chem. Phys. Lett.* **516** 92-5
[222] Ho Y C, Ho P Y, Lee H C, Chang S K, Hong Y R and Lin C F 2015 Enhancing performance of inverted polymer solar cells using two-growth ZnO nanorods *Sol. Energy Mater. Sol. Cells* **132** 570-7
[223] Ruankham P, Sagawa T, Sakaguchi H and Yoshikawa S 2011 Vertically aligned ZnO nanorods doped with lithium for polymer solar cells: defect related photovoltaic properties *J. Mater. Chem.* **21** 9710-5
[224] Malek M F, Sahdan M Z, Mamat M H, Musa M Z, Khusaimi Z, Husairi S S, Sin N D M and Rusop M 2013 A novel fabrication of MEH-PPV/Al:ZnO nanorod arrays based ordered bulk heterojunction hybrid solar cells *Appl. Surf. Sci.* **275** 75-83
[225] Ginting R T, Yap C C, Yahaya M and Salleh M M 2014 Improvement of inverted type organic solar cells performance by incorporating Mg dopant into hydrothermally grown ZnO nanorod arrays *J. Alloys Compd* **585** 696-702
[226] Ginting R T, Yap C C, Yahaya M and Salleh M M 2014 Solution-Processed Ga-Doped ZnO Nanorod Arrays as Electron Acceptors in Organic Solar Cells *ACS Appl. Mater. Interfaces* **6** 5308-18
[227] Ginting R T, Lee H B, Tan S T, Tan C H, Jumali M H H, Yap C C, Kang J W and Yahaya M 2016 A Simple Approach Low-Temperature Solution Process for Preparation of Bismuth-Doped ZnO Nanorods and Its Application in Hybrid Solar Cells *J. Phys. Chem. C* **120** 771-80
[228] Olson D C, Lee Y J, White M S, Kopidakis N, Shaheen S E, Ginley D S, Voigt J A and Hsu J W P 2007 Effect of polymer processing on the performance of poly(3-hexylthiophene)/ZnO nanorod photovoltaic devices *J. Phys. Chem. C* **111** 16640-5
[229] Baeten L, Conings B, D'Haen J, Hardy A, Manca J V and Van Bael M K 2012 Fully water-processable metal oxide nanorods/polymer hybrid solar cells *Sol. Energy Mater. Sol. Cells* **107** 230-5

[230] Olson D C, Lee Y J, White M S, Kopidakis N, Shaheen S E, Ginley D S, Voigt J A and Hsu J W P 2008 Effect of ZnO processing on the photovoltage of ZnO/poly(3-hexylthiophene) solar cells *J. Phys. Chem. C* **112** 9544-7
[231] Chou C Y, Huang J S, Wu C H, Lee C Y and Lin C F 2009 Lengthening the polymer solidification time to improve the performance of polymer/ZnO nanorod hybrid solar cells *Sol. Energy Mater. Sol. Cells* **93** 1608-12
[232] Sung Y M, Hsu F C, Chen C T, Su W F and Chen Y F 2012 Enhanced photocurrent and stability of inverted polymer/ZnO-nanorod solar cells by 3-hydroxyflavone additive *Sol. Energy Mater. Sol. Cells* **98** 103-9
[233] Leow C, Ohnishi T and Matsumura M 2015 Removal of organic contaminants from the surface of ZnO nanorods for organic/inorganic hybrid photovoltaics by using photocatalytic reaction *RSC Adv.* **5** 6232-7
[234] Iza D C, Munoz-Rojas D, Jia Q X, Swartzentruber B and MacManus-Driscoll J L 2012 Tuning of defects in ZnO nanorod arrays used in bulk heterojunction solar cells *Nanoscale Res. Lett.* **7** 655
[235] Greene L E, Law M, Yuhas B D and Yang P D 2007 ZnO-TiO_2 core-shell nanorod/P3HT solar cells *J. Phys. Chem. C* **111** 18451-6
[236] Atienzar P, Ishwara T, Illy B N, Ryan M P, O'Regan B C, Durrant J R and Nelson J 2010 Control of Photocurrent Generation in Polymer/ZnO Nanorod Solar Cells by Using a Solution-Processed TiO2 Overlayer *J. Phys. Chem. Lett.* **1** 708-13
[237] Lee Y J, Davis R J, Lloyd M T, Provencio P P, Prasankumar R P and Hsu J W P 2010 Open-Circuit Voltage Improvement in Hybrid ZnO-Polymer Photovoltaic Devices With Oxide Engineering *IEEE J. Sel. Top. Quantum Electron.* **16** 1587-94
[238] Uhlrich J J, Franking R, Hamers R J and Kuech T F 2009 Sulfide Treatment of ZnO Single Crystals and Nanorods and the Effect on P3HT-ZnO Photovoltaic Device Properties *J. Phys. Chem. C* **113** 21147-54
[239] Ajuria J, Etxebarria I, Azaceta E, Tena-Zaera R, Fernandez-Montcada N, Palomares E and Pacios R 2011 Novel ZnO nanostructured electrodes for higher power conversion efficiencies in polymeric solar cells *Phys. Chem. Chem. Phys.* **13** 20871-6
[240] Ravirajan P, Peiro A M, Nazeeruddin M K, Graetzel M, Bradley D D C, Durrant J R and Nelson J 2006 Hybrid polymer/zinc oxide photovoltaic devices with vertically oriented ZnO nanorods and an amphiphilic molecular interface layer *J. Phys. Chem. B* **110** 7635-9
[241] Ruankham P, Yoshikawa S and Sagawa T 2013 Effects of the morphology of nanostructured ZnO and interface modification on the device configuration and charge transport of ZnO/polymer hybrid solar cells *Phys. Chem. Chem. Phys.* **15** 9516-22
[242] Thitima R, Patcharee C, Takashi S and Susumu Y 2009 Efficient electron transfers in ZnO nanorod arrays with N719 dye for hybrid solar cells *Solid-State Electron.* **53** 176-80
[243] Ginting R T, Yap C C, Yahaya M and Salleh M M 2013 Influence of poly(2-methoxy-5-(2 '-ethyl)-hexyloxy-p-phenylene vinylene):(6,6)-phenyl C61 butyric acid methyl ester blend ratio on the performance of inverted type organic solar cells based on Eosin-Y-coated ZnO nanorod arrays *Thin Solid Films* **536** 286-90
[244] Lim E L, Yap C C, Yahaya M and Salleh M M 2013 Enhancement of ZnO nanorod arrays-based inverted type hybrid organic solar cell using spin-coated Eosin-Y *Semicond. Sci. Technol.* **28** 6
[245] Lim E L, Yap C C, Yahaya M and Salleh M M 2013 *3rd Isesco International Workshop and Conference on Nanotechnology 2012,* ed A A Umar*, et al.* (Bristol: Iop Publishing Ltd)
[246] Huang J S, Chou C Y and Lin C F 2010 Enhancing performance of organic-inorganic hybrid solar cells using a fullerene interlayer from all-solution processing *Sol. Energy Mater. Sol. Cells* **94** 182-6
[247] Chen C T, Hsu F C, Kuan S W and Chen Y F 2011 The effect of C-60 on the ZnO-nanorod surface in organic-inorganic hybrid photovoltaics *Sol. Energy Mater. Sol. Cells* **95** 740-4
[248] Riedel W, Wiesner S, Greiner D, Hinrichs V, Rusu M and Lux-Steiner M C 2014 Hybrid solar cells with ZnO-nanorods and dry processed small molecule absorber *Appl. Phys. Lett.* **104** 173503
[249] Zhong P, Ma X H and Xi H 2018 Passivating ZnO Surface States by C_{60} Pyrrolidine Tris-Acid for Hybrid Solar Cells Based on Poly(3-hexylthiophene)/ZnO Nanorod Arrays *Polymers* **10** 4
[250] Lee T H, Sue H J and Cheng X 2011 ZnO and conjugated polymer bulk heterojunction solar cells containing ZnO nanorod photoanode *Nanotechnology* **22** 285401
[251] Chen C T, Hsu F C, Sung Y M, Liao H C, Yen W C, Su W F and Chen Y F 2012 Effects of metal-free conjugated oligomer as a surface modifier in hybrid polymer/ZnO solar cells *Sol. Energy Mater. Sol. Cells* **107** 69-74

[252] Whittaker-Brooks L, McClain W E, Schwartz J and Loo Y L 2014 Donor-Acceptor Interfacial Interactions Dominate Device Performance in Hybrid P3HT-ZnO Nanowire-Array Solar Cells *Adv. Energy Mater.* **4** 1400585
[253] Tang S S, Tang N, Meng X Q, Huang S H and Hao Y F 2016 Enhanced power efficiency of ZnO based organic/inorganic solar cells by surface modification *Physica E* **83** 398-404
[254] Ben Dkhil S, Gaceur M, Dachraoui W, Hannani D, Fall S, Brunel F, Wang M, Poize G, Mawyin J, Shupyk I, Martini C, Shilova E, Fages F, Ishwara T, Nelson J, Watanabe T, Yoshimoto N, Margeat O, Videlot-Ackermann C and Ackermann J 2017 P-type semiconductor surfactant modified zinc oxide nanorods for hybrid bulk heterojunction solar cells *Sol. Energy Mater. Sol. Cells* **159** 608-16
[255] Yang Y, Guo W X, Zhang Y, Ding Y, Wang X and Wang Z L 2011 Piezotronic Effect on the Output Voltage of P3HT/ZnO Micro/Nanowire Heterojunction Solar Cells *Nano Lett.* **11** 4812-7
[256] Shoaee S, Briscoe J, Durrant J R and Dunn S 2014 Acoustic Enhancement of Polymer/ZnO Nanorod Photovoltaic Device Performance *Adv. Mater.* **26** 263-8
[257] Zhang K W, Wang Z L and Yang Y 2016 Enhanced P3HT/ZnO Nanowire Array Solar Cells by Pyro-phototronic Effect *ACS Nano* **10** 10331-8
[258] Briseno A L, Holcombe T W, Boukai A I, Garnett E C, Shelton S W, Frechet J J M and Yang P D 2010 Oligo- and Polythiophene/ZnO Hybrid Nanowire Solar Cells *Nano Lett.* **10** 334-40
[259] Iza D C, Munoz-Rojas D, Musselman K P, Weickert J, Jakowetz A C, Sun H Y, Ren X, Hoye R L Z, Lee J H, Wang H Y, Schmidt-Mende L and MacManus-Driscoll J L 2013 Nanostructured conformal hybrid solar cells: a promising architecture towards complete charge collection and light absorption *Nanoscale Res. Lett.* **8** 359
[260] Ambade S B, Ambade R B, Lee W, Mane R S, Yoon S C and Lee S H 2014 Development of highly transparent seedless ZnO nanorods engineered for inverted polymer solar cells *Nanoscale* **6** 12130-41
[261] Ambade S B, Ambade R B, Eom S H, Baek M J, Bagde S S, Mane R S and Lee S H 2016 Co-functionalized organic/inorganic hybrid ZnO nanorods as electron transporting layers for inverted organic solar cells *Nanoscale* **8** 5024-36
[262] Ambade S B, Ambade R B, Bagde S S and Lee S H 2016 Work-Function and Surface Energy Tunable Cyanoacrylic Acid Small-Molecule Derivative Interlayer on Planar ZnO Nanorods for Improved Organic Photovoltaic Performance *ACS Appl. Mater. Interfaces* **8** 35270-80
[263] Gratzel M 2003 Dye-sensitized solar cells *J. Photochem. Photobiol. C-Photochem. Rev.* **4** 145-53
[264] Redmond G, Fitzmaurice D and Graetzel M 1994 Visible-light sensitization by cis-bis(thiocyanato)bis(2,2'-bipyridyl-4,4'-dicarboxylato)ruthenium(II) of a transparent nanocrystalline ZnO film prepared by sol-gel techniques *Chem. Mater.* **6** 686-91
[265] Saito M and Fujihara S 2008 Large photocurrent generation in dye-sensitized ZnO solar cells *Energy Environ. Sci.* **1** 280-3
[266] Benkstein K D, Kopidakis N, van de Lagemaat J and Frank A J 2003 Influence of the percolation network geometry on electron transport in dye-sensitized titanium dioxide solar cells *J. Phys. Chem. B* **107** 7759-67
[267] Hagfeldt A and Gratzel M 1995 Light-induced redox reactions in nanocrystalline systems *Chem. Rev.* **95** 49-68
[268] Wang Z L 2004 Nanostructures of zinc oxide *Mater. Today* **7** 26-33
[269] Law M, Greene L E, Radenovic A, Kuykendall T, Liphardt J and Yang P D 2006 ZnO-Al_2O_3 and ZnO-TiO_2 core-shell nanowire dye-sensitized solar cells *J. Phys. Chem. B* **110** 22652-63
[270] Baxter J B, Walker A M, van Ommering K and Aydil E S 2006 Synthesis and characterization of ZnO nanowires and their integration into dye-sensitized solar cells *Nanotechnology* **17** S304-S12
[271] Jiang C Y, Sun X W, Lo G Q, Kwong D L and Wang J X 2007 Improved dye-sensitized solar cells with a ZnO-nanoflower photoanode *Appl. Phys. Lett.* **90** 263501
[272] Baxter J B and Aydil E S 2006 Dye-sensitized solar cells based on semiconductor morphologies with ZnO nanowires *Sol. Energy Mater. Sol. Cells* **90** 607-22
[273] Gao Y F, Nagai M, Chang T C and Shyue J J 2007 Solution-derived ZnO nanowire array film as photoelectrode in dye-sensitized solar cells *Cryst. Growth Des.* **7** 2467-71
[274] Karst N, Rey G, Doisneau B, Roussel H, Deshayes R, Consonni V, Ternon C and Bellet D 2011 Fabrication and characterization of a composite ZnO semiconductor as electron transporting layer in dye-sensitized solar cells *Mater. Sci. Eng. B* **176** 653-9
[275] Dwivedi C and Dutta V 2012 Vertically aligned ZnO nanorods via self-assembled spray pyrolyzed nanoparticles for dye-sensitized solar cells *Adv. Nat. Sci. Nanosci.* **3** 015011

[276] Ku C H and Wu J J 2007 Electron transport properties in ZnO nanowire array/nanoparticle composite dye-sensitized solar cells *Appl. Phys. Lett.* **91** 093117
[277] Yodyingyong S, Zhang Q F, Park K, Dandeneau C S, Zhou X Y, Triampo D and Cao G Z 2010 ZnO nanoparticles and nanowire array hybrid photoanodes for dye-sensitized solar cells *Appl. Phys. Lett.* **96** 073115
[278] Puyoo E, Rey G, Appert E, Consonni V and Bellet D 2012 Efficient Dye-Sensitized Solar Cells Made from ZnO Nanostructure Composites *J. Phys. Chem. C* **116** 18117-23
[279] Hongsith K, Hongsith N, Wongratanaphisan D, Gardchareon A, Phadungdhitidhada S and Choopun S 2015 Efficiency Enhancement of ZnO Dye-sensitized Solar Cells by Modifying Photoelectrode and Counterelectrode *Energy Procedia* **79** 360-5
[280] Guerin V M and Pauporte T 2011 From nanowires to hierarchical structures of template-free electrodeposited ZnO for efficient dye-sensitized solar cells *Energy Environ. Sci.* **4** 2971-9
[281] Keis K, Lindgren J, Lindquist S E and Hagfeldt A 2000 Studies of the adsorption process of Ru complexes in nanoporous ZnO electrodes *Langmuir* **16** 4688-94
[282] Lee K E, Gomez M A, Elouatik S and Demopoulos G P 2010 Further Understanding of the Adsorption Mechanism of N719 Sensitizer on Anatase TiO_2 Films for DSSC Applications Using Vibrational Spectroscopy and Confocal Raman Imaging *Langmuir* **26** 9575-83
[283] Chen L C, Tsai S F, Chen J H and Wang G W 2013 Preparation of Vertically Aligned ZnO/TiO_2 Core-Shell Composites for Dye-Sensitized Solar Cells *Int. J. Photoenergy* 9
[284] Lai H M, Wang Y Z, Du G P, Li W and Han W Z 2014 Dual functional YVO4:Eu^{3+},Bi^{3+}@SiO_2 submicron-sized core-shell particles for dye-sensitized solar cells: Light scattering and downconversion *Ceram. Int.* **40** 6103-8
[285] Zhao R, Zhu L P, Cai F P, Yang Z G, Gu X Q, Huang J and Cao L 2013 ZnO/TiO2 core-shell nanowire arrays for enhanced dye-sensitized solar cell efficiency *Appl. Phys. A.* **113** 67-73
[286] Richters J P, Voss T, Kim D S, Scholz R and Zacharias M 2008 Enhanced surface-excitonic emission in ZnO/Al(2)O(3) core-shell nanowires *Nanotechnology* **19** 305202
[287] Palomares E, Clifford J N, Haque S A, Lutz T and Durrant J R 2003 Control of charge recombination dynamics in dye sensitized solar cells by the use of conformally deposited metal oxide blocking layers *J. Am. Chem. Soc.* **125** 475-82
[288] O'Regan B C, Scully S, Mayer A C, Palomares E and Durrant J 2005 The effect of Al_2O_3 barrier layers in TiO_2/Dye/CuSCN photovoltaic cells explored by recombination and DOS characterization using transient photovoltage measurements *J. Phys. Chem. B* **109** 4616-23
[289] Wang M L, Huang C G, Cao Y G, Yu Q J, Deng Z H, Liu Y, Huang Z, Huang J Q, Huang Q F, Guo W and Liang J K 2009 Dye-sensitized solar cells based on nanoparticle-decorated ZnO/TiO_2 core/shell nanorod arrays *J. Phys. D-Appl. Phys.* **42** 6
[290] Prabakar K, Son M, Kim W Y and Kim H 2011 TiO2 thin film encapsulated ZnO nanorod and nanoflower dye sensitized solar cells *Mater. Chem. Phys.* **125** 12-4
[291] Irannejad A, Janghorban K, Tan O K, Huang H, Lim C K, Tan P Y, Fang X, Chua C S, Maleksaeedi S, Hejazi S M H, Shahjamali M M and Ghaffari M 2011 Effect of the TiO_2 shell thickness on the dye-sensitized solar cells with ZnO-TiO_2 core-shell nanorod electrodes *Electrochim. Acta* **58** 19-24
[292] Feng Y M, Ji X X, Duan J X, Zhu J H, Jiang J, Ding H, Meng G X, Ding R M, Liu J P, Hu A Z and Huang X T 2012 Synthesis of ZnO@TiO_2 core-shell long nanowire arrays and their application on dye-sensitized solar cells *J. Solid State Chem.* **190** 303-8
[293] Goh G K L, Le H Q, Huang T J and Hui B T T 2014 Low temperature grown ZnO@TiO_2 core shell nanorod arrays for dye sensitized solar cell application *J. Solid State Chem.* **214** 17-23
[294] Xu C K, Wu J M, Desai U V and Gao D 2011 Multilayer Assembly of Nanowire Arrays for Dye-Sensitized Solar Cells *J. Am. Chem. Soc.* **133** 8122-5
[295] Plank N O V, Snaith H J, Ducati C, Bendall J S, Schmidt-Mende L and Welland M E 2008 A simple low temperature synthesis route for ZnO-MgO core-shell nanowires *Nanotechnology* **19** 465603
[296] Chung J, Myoung J, Oh J and Lim S 2010 Synthesis of a ZnS Shell on the ZnO Nanowire and Its Effect on the Nanowire-Based Dye-Sensitized Solar Cells *J. Phys. Chem. C* **114** 21360-5
[297] Guillen E, Azaceta E, Vega-Poot A, Idigoras J, Echeberria J, Anta J A and Tena-Zaera R 2013 ZnO/ZnO Core-Shell Nanowire Array Electrodes: Blocking of Recombination and Impressive Enhancement of Photovoltage in Dye-Sensitized Solar Cells *J. Phys. Chem. C* **117** 13365-73

[298] Zhou Y, Xia C, Hu X Y, Huang W, Aref A A, Wang B X, Liu Z J, Sun Y M, Zhou W and Tang Y W 2014 Dye-sensitized solar cells based on nanoparticle-decorated ZnO/SnO_2 core/shell nanoneedle arrays *Appl. Surf. Sci.* **292** 111-6
[299] Jung K, Lim T, Li Y and Martinez-Morales A A 2017 ZnO-CuO core-shell heterostructure for improving the efficiency of ZnO-based dye-sensitized solar cells *MRS Adv.* **2** 857-62
[300] Horiuchi H, Katoh R, Hara K, Yanagida M, Murata S, Arakawa H and Tachiya M 2003 Electron injection efficiency from excited N3 into nanocrystalline ZnO films: Effect of (N_3-Zn^{2+}) aggregate formation *J. Phys. Chem. B* **107** 2570-4
[301] Westermark K, Rensmo H, Siegbahn H, Keis K, Hagfeldt A, Ojamae L and Persson P 2002 PES studies of Ru(dcbpyH(2))(2)(NCS)(2) adsorption on nanostructured ZnO for solar cell applications *J. Phys. Chem. B* **106** 10102-7
[302] Chou T P, Zhang Q F and Cao G Z 2007 Effects of dye loading conditions on the energy conversion efficiency of ZnO and TiO_2 dye-sensitized solar cells *J. Phys. Chem. C* **111** 18804-11
[303] Magne C, Moehl T, Urien M, Gratzel M and Pauporte T 2013 Effects of ZnO film growth route and nanostructure on electron transport and recombination in dye-sensitized solar cells *J. Mater. Chem. A* **1** 2079-88
[304] Magne C, Urien M, Ciofini I, Tugsuz T and Pauporte T 2012 Amphiphilic acids as co-adsorbents of metal-free organic dyes for the efficient sensitization of nanostructured photoelectrode *RSC Adv.* **2** 11836-42
[305] Kojima A, Teshima K, Shirai Y and Miyasaka T 2009 Organometal Halide Perovskites as Visible-Light Sensitizers for Photovoltaic Cells *J. Am. Chem. Soc.* **131** 6050-1
[306] Qin P, Tanaka S, Ito S, Tetreault N, Manabe K, Nishino H, Nazeeruddin M K and Gratzel M 2014 Inorganic hole conductor-based lead halide perovskite solar cells with 12.4% conversion efficiency *Nat. Commun.* **5** 3834
[307] Fan Z, Sun K and Wang J 2015 Perovskites for photovoltaics: a combined review of organic-inorganic halide perovskites and ferroelectric oxide perovskites *J. Mater. Chem. A* **3** 18809-28
[308] https://www.nrel.gov/pv/assets/pdfs/pv-efficiencies-07-17-2018.pdf
[309] Leijtens T, Lauber B, Eperon G E, Stranks S D and Snaith H J 2014 The Importance of Perovskite Pore Filling in Organometal Mixed Halide Sensitized TiO_2-Based Solar Cells *J. Phys. Chem. Lett.* **5** 1096-102
[310] Stranks S D, Eperon G E, Grancini G, Menelaou C, Alcocer M J P, Leijtens T, Herz L M, Petrozza A and Snaith H J 2013 Electron-Hole Diffusion Lengths Exceeding 1 Micrometer in an Organometal Trihalide Perovskite Absorber *Science* **342** 341-4
[311] Ball J M, Lee M M, Hey A and Snaith H J 2013 Low-temperature processed meso-superstructured to thin-film perovskite solar cells *Energy Environ. Sci.* **6** 1739-43
[312] Lee M M, Teuscher J, Miyasaka T, Murakami T N and Snaith H J 2012 Efficient Hybrid Solar Cells Based on Meso-Superstructured Organometal Halide Perovskites *Science* **338** 643-7
[313] Liu D Y and Kelly T L 2014 Perovskite solar cells with a planar heterojunction structure prepared using room-temperature solution processing techniques *Nat. Photonics* **8** 133-8
[314] Son D Y, Im J H, Kim H S and Park N G 2014 11% Efficient Perovskite Solar Cell Based on ZnO Nanorods: An Effective Charge Collection System *J. Phys. Chem. C* **118** 16567-73
[315] Kumar M H, Yantara N, Dharani S, Graetzel M, Mhaisalkar S, Boix P P and Mathews N 2013 Flexible, low-temperature, solution processed ZnO-based perovskite solid state solar cells *Chem. Commun.* **49** 11089-91
[316] Son D Y, Bae K H, Kim H S and Park N G 2015 Effects of Seed Layer on Growth of ZnO Nanorod and Performance of Perovskite Solar Cell *J. Phys. Chem. C* **119** 10321-8
[317] Wang B X, Liu T F, Zhou Y B, Chen X, Yuan X B, Yang Y Y, Liu W P, Wang J M, Han H W and Tang Y W 2016 Hole-conductor-free perovskite solar cells with carbon counter electrodes based on ZnO nanorod arrays *Phys. Chem. Chem. Phys.* **18** 27078-82
[318] Dong J, Zhao Y H, Shi J J, Wei H Y, Xiao J Y, Xu X, Luo J H, Xu J, Li D M, Luo Y H and Meng Q B 2014 Impressive enhancement in the cell performance of ZnO nanorod-based perovskite solar cells with Al-doped ZnO interfacial modification *Chem. Commun.* **50** 13381-4
[319] Zhang J, Barboux P and Pauporte T 2014 Electrochemical Design of Nanostructured ZnO Charge Carrier Layers for Efficient Solid-State Perovskite-Sensitized Solar Cells *Adv. Energy Mater.* **4** 1400932
[320] Mahmood K, Swain B S and Amassian A 2015 16.1% Efficient Hysteresis-Free Mesostructured Perovskite Solar Cells Based on Synergistically Improved ZnO Nanorod Arrays *Adv. Energy Mater.* **5** 1500568
[321] Zhang J and Pauporte T 2015 Effects of Oxide Contact Layer on the Preparation and Properties of CH(3)NH(3)Pbl(3) for Perovskite Solar Cell Application *J. Phys. Chem. C* **119** 14919-28

[322] Yang J L, Siempelkamp B D, Mosconi E, De Angelis F and Kelly T L 2015 Origin of the Thermal Instability in $CH_3NH_3PbI_3$ Thin Films Deposited on ZnO *Chem. Mater.* **27** 4229-36
[323] Yang F, Kang D W and Kim Y S 2017 Improved interface of ZnO/CH3NH3PbI3 by a dynamic spin-coating process for efficient perovskite solar cells *RSC Adv.* **7** 19030-8
[324] Song J X, Liu L J, Wang X F, Chen G, Tian W J and Miyasaka T 2017 Highly efficient and stable low-temperature processed ZnO solar cells with triple cation perovskite absorber *J. Mater. Chem. A* **5** 13439-47
[325] Guo Y, Kang L L, Zhu M H, Zhang Y, Li X and Xu P 2018 A strategy toward air-stable and high-performance ZnO-based perovskite solar cells fabricated under ambient conditions *Chem. Eng. J.* **336** 732-40
[326] Cao J, Wu B H, Chen R H, Wu Y Y Q, Hui Y, Mao B W and Zheng N F 2018 Efficient, Hysteresis-Free, and Stable Perovskite Solar Cells with ZnO as Electron-Transport Layer: Effect of Surface Passivation *Adv. Mater.* **30** 1705596